

# **3D SEISMIC GEOMORPHOLOGY OF SUBMARINE CHANNEL-LEVEE SYSTEMS IN SALT-RELATED SLOPE SETTING: A CASE STUDY FROM THE WESTERN DEEPWATER EGYPT**

**Amando Lasabuda**

Master Thesis in Petroleum Geoscience



Department of Earth Science

University of Bergen

June, 2013

## ABSTRACT

High resolution 3D seismic dataset has been used to examine gravity-driven deposits from the Plesitocene to present-day in the structurally complex area of the western Nile deepwater. The underlying Messinian salt and its associated faults and the existence of fluid-migrated features generated local seabed topography that affected sedimentation and seismic facies distribution.

Seismic interpretation combined with planform analysis of attribute maps were utilized to define five seismic facies which are distinguished by amplitude strength, reflections, and geometry. The observation of the temporal and spatial relationship of five seismic units using isochron map analysis offers an insight into seismic stratigraphy development which can be described in three main phases. The first phase is characterized by the deposition of two main mass transport deposits (seismic unit 1 and 2). The second phase is defined by the development of channelized-fan deposit (seismic unit 3). The final phase is characterized by the deposition of near-seabed MTD and present-day channel-levee system (seismic unit 4) and the development of major mud diapirs (seismic unit 5).

Spectrally decomposed and colour-blended seismic volume analysis combined with seismic facies interpretation in seismic cross-section have been useful to morphologically investigate and quantify three submarine channels and their associated elements (e.g. thalweg and erosional depth longitudinal profile, levee width and thickness). The results revealed an architectural element variation and the channel pathways with respect to local seabed topography. Increases in sinuosity are related to decreases in channel axis gradient and followed by evidence of channel aggradation. Levee thickness development shows an overall decrease in thickness and width downslope with local variations due to structural bathymetry changes (e.g. thickness increase towards the hanging wall of the main fault).

Overall a change downslope from degradational to aggradational following equilibrium profile is observed. This is evidenced by a deeply incised channel erosional depth in the upperslope and increasing in sinuosity in the lower slope. Sinuous form is observed when the channel experiences a shallow gradient and availability of accommodation space followed by the development of lateral accretion packages (LAPs). Local structural growth (e.g. minibasin and anticline) has a big influence on the channel path geometry.

Submarine channel deposit is often a prominent reservoir target in many deepwater explorations around the world. A near-seafloor study with a higher seismic resolution may give an analogue to image turbiditic reservoir architecture. Therefore, this study improves the understanding in the interaction of sedimentation and structural variations which can be applied to hydrocarbon exploration to predict control and distribution of deepwater turbiditic reservoirs.



## Acknowledgement

None of this thesis would have been possible without support from my primary advisor, Professor Rob Gawthorpe. I appreciate his guidance and continued believe in my ability to complete this study.

I would like to acknowledge the contributions of my second supervisor Kristina Bakke from Statoil Bergen for her advice and providing the data.

Support for this thesis was provided by 3D seismic laboratory in University of Bergen for the Schlumberger's Petrel and ffA Geoteric softwares.

Mas Fachri and David are thanked for their constructive reviews and comments which greatly improved this thesis.

I am especially grateful to my parents, Said and Erna Lasabuda, who always made education top priority. My brother and sister, Kiki and Ami Lasabuda and the big family in Indonesia are thanked for their support and pray for me to complete this study.

My gratitude also extends to the awesome Seismic-lab gang, Remi Ersland, Vegard Hausken, Thomas Kristensen, Evangelos Kaikas, and Andreas Hovland for the research discussion, camaraderie, and cheerfulness during the tough time in the thesis-writing period.

I appreciate the help from Christian Rønnevik for the thesis layout. Njål Solberg Greiner, Victor Våga, and Vegard Snusman are thanked for the Friday's porridge chats. I am especially thankful to Coralie Quadri for the coffee break.

Markeveien family Wilud Wulandari and Andria Utama, RT-Bergen community, and all my GEO colleagues are thanked for creating my amazing life in Norway.

Bergen, June 2013

Amando Lasabuda

# CONTENTS

1. INTRODUCTION.....	1
1.1. Aims and objectives.....	1
1.2. Thesis layout.....	1
1.3. Study area.....	2
1.4. Dataset and Methods.....	3
1.4.1. Dataset.....	3
1.4.2. Methods.....	4
1.4.2.1. Quantification.....	4
1.4.2.2. Seismic stratigraphy interpretation.....	4
1.4.2.3. Surface-based seismic attributes.....	5
2. BACKGROUND.....	7
2.1. Tectonostratigraphy of North Africa and Nile Deep Sea Fan (NDSF).....	7
2.1.1. The Messinian salinity crisis.....	11
2.2. Seismic geomorphology and terminology for idealized submarine channel-levee system and other elements.....	12
2.3. Salt tectonics.....	15
2.4. Deepwater exploration.....	17
3. SEISMIC STRATIGRAPHY ANALYSIS.....	19
3.1. Seismic Facies.....	19
3.1.1. Seismic facies 1 – Channel and channel-fill deposit.....	19
3.1.2. Seismic facies 2 – Levee deposit.....	20
3.1.3. Seismic facies 3 – Mass transport deposit.....	20
3.1.4. Seismic facies 4 - Fan lobes deposit.....	21
3.1.5. Seismic facies 5 - Mud diapirs.....	22
3.2. Seismic Units.....	24
3.2.1. Seismic unit 1 – Transparent debris flow (TDF).....	24
3.2.2. Seismic unit 2 – Buried mass transport deposit (BMTD).....	25
3.2.3. Channel-levee complex and fan lobes.....	25
3.2.4. Seismic unit 4 – Present day channel-levee system and near-seabed mass transport deposit (NSMTD).....	26
3.2.5. Seismic unit 5 – Mud diapirs.....	27
3.3. Seismic Geomorphology.....	42
3.3.1. Channel-levee system A.....	42

3.3.1.1. Channel-levee system development within the minibasin.....	49
3.3.2. Channel-levee system B.....	53
3.3.3. Channel-levee system C.....	57
3.3.4. Mass Transport Deposit (MTD).....	62
4. DISCUSSION.....	66
4.1. Structural controls of seismic units development.....	66
4.2. Sinuous submarine channel-levee system.....	69
4.3. Channel avulsion.....	72
4.4. Structural influence on submarine channel-levee system.....	73
4.4.1. Case I: Fault growth influences to channel-levee system.....	74
4.4.2. Case II: Channel-levee system response to anticlines and mud diapirs.....	76
4.5. Slope gradient profile linked to development of channel-levee systems.....	78
5. CONCLUSION.....	79
REFERENCES.....	81

# 1. INTRODUCTION

## 1.1. Aim and Objectives

The aim of this thesis is to study depositional elements of turbiditic systems and their response to structural changes in deepwater setting.

The specific objectives are:

- a. Quantify the submarine channel-levee systems and other depositional elements at Pleistocene to present-day period in the western Nile Deep Sea Fan (NDSF).
- b. Discuss factors that may influence the development of channel-levee systems
- c. Examine spatial and temporal distribution of turbiditic depositional elements.

High resolution near-seafloor 3D seismic data offers insights into stratal architectural information and depositional process. This study approach has been used to confidently identify depositional elements in near-seafloor setting which offers analogues to the same features in the reservoir level or deeper zone. Investigations on stratal stacking patterns, gradient changes, and sediment accommodation were carried out to enhance the geological understanding of the NDSF and contribute to further hydrocarbon exploration in the Western Nile Deepwater.

## 1.2. Thesis Layout

This thesis is organized into five chapters. Chapter 1 gives the big picture of the project itself. It provides information about the location of the study area, the data that had been used, and the methodology that had been applied to quantify the seismic interpretation and attributes process. Chapter 2 describes the regional geology of the study area focusing on deepwater depositional environment and salt-related structures. Deepwater hydrocarbon exploration in the study area is briefly discussed at the end of this chapter.

Chapter 3 provides the main results and observations of this study. It provides the measurements and outlines the interpretation of stratigraphic units and facies. Chapter 4 elaborates on the findings using relevant theories and connects the missing puzzle by combining concepts from other literature or previous works. Finally, chapter 5 concludes the study and shows how the approach can be implemented along with possible solutions related to the NDSF hydrocarbon exploration.

### 1.3. Study Area

The study area is located in the western flank of the Egyptian deepwater, in the Eastern Mediterranean, which has experienced prolonged hydrocarbon exploration activities (Fig. 1.1). Over the past decades, Aal et al. (2000) estimates that 4.0 BBOE, containing mostly gas and condensate, has been discovered in the Nile Delta. Most of these discoveries were made in the eastern part of offshore Egypt in the deepwater Levantine emerging basin or in near-shelf offshore Egypt in the Nile Delta mature basin (Tari et al., 2012a). The oil and gas industry has recently tended to move its exploration activity to the ultra deepwater areas which have a water depth of 2500-3000 m, which is similar to the depth range in the study area.

Approximately 42 TCF gas has been designated as proven reserves and about 50 TCF has yet to be found in the Nile Delta (Boucher et al., 2004). One of the hydrocarbon exploration challenges is the limited availability of well data where only one deepwater well, i.e. Kiwi-1, has been drilled in the western ultra deepwater area with a water depth of approximately 2700 m (Tari et al., 2012b). Therefore, this study area is both interesting and also provides a challenging investigation.

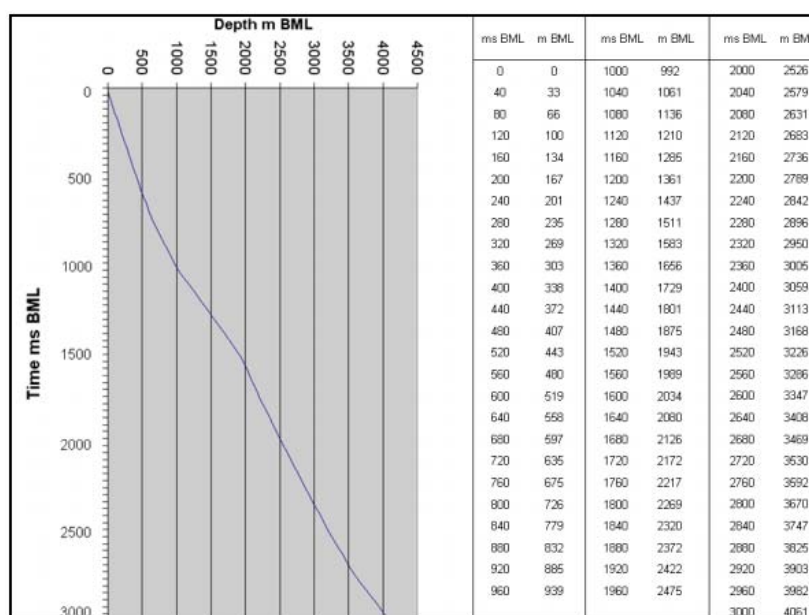


**Fig. 1.1.** Map showing an approximate location of the study area (the red square) and the surrounding region. (www.maps.google.com, downloaded 2013)

## 1.4. Dataset and Methods

### 1.4.1. Dataset

The 3D seismic data, which was supplied by Statoil from Block 9 - El Dabaa covers an area of approximately 35 km long and 27 km wide in the western offshore Egypt. This 3D seismic data is of high resolution data with an inline spacing of 12.5 m and cross-line spacing of 6.25 m. The full recorded length was 3000 ms with a sample rate of 2 ms. All interpretations were directly conducted from this seismic data.



**Table 1.1.** – Time-to-depth conversion (Statoil report, 2012)

There is no well data used in the study area. Statoil converted the TWT data to depth and result of this is shown in Table 1. The seismic resolution may vary with depth, depending on frequency content and seismic velocity. Tuning thicknesses as results of  $\lambda/4$  are described in table 1.2. The seismic data is displayed as zero phases with normal SEG polarity. Statoil (2012) reported that the seafloor has a velocity of 1520 m/s and the top Pliocene has a velocity of 1800 m/s. Therefore, the top late Pleistocene is assumed to contain a velocity of c. 1600 m/s and will be used in all calculations to convert TWT measurements to depth.

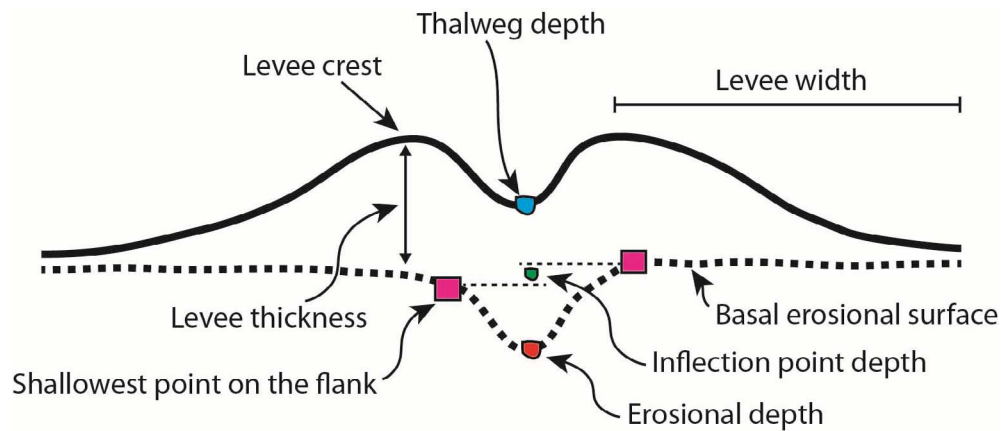
Position	TWT (ms)	Velocity (m/s)	Frequency (Hz)	Resolution (m)
Seabed	3400	1520	125	3
Top Pliocene	3900	1800	60	8
Top Salt	4300	4400	35	30

**Table 1.2.** – Seismic resolution (Statoil report, 2012)

### 1.4.2. Methods

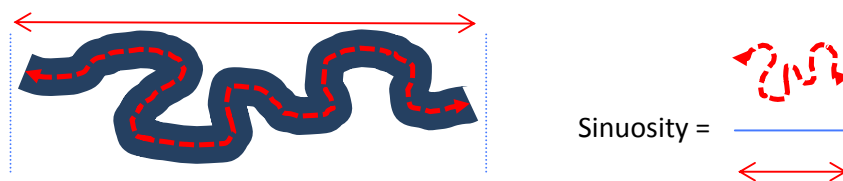
#### 1.4.2.1. Quantification

The channel-levee system measurement was carried out using quantification illustration (shown in Fig. 1.2). The channel erosional depth is marked as the lowest point within the Basal Erosional Surface (BES) and is not necessary located in the BES centre. The inflection point depth is the average depth between the two shallowest points on the flank of BES. The levee crest is defined as the highest point whereas the levee length is defined as the horizontal distance from the crest to the levee pinch out.



**Fig. 1.2.** The components of channel-levee system measurement.  
(modified from Catterall et al., 2010).

The channel sinuosity is measured by dividing the actual length of the channel by the shortest distance between the initial points (Fig. 3). The higher sinuosity of the channel-levee system shows a higher value.



**Fig. 1.3.** Channel sinuosity measurement

#### 1.4.2.2. Seismic Stratigraphy Interpretation

3D Seismic interpretation was conducted using Schlumberger's Petrel software. The seismic cube was commonly interpreted every 16-128 line both in-line and cross-line based on necessity. Seismic horizons were picked using the guided-tracking mode to ensure they were placed in the desired exact points. In order to generate surface, the mapped horizons were displayed in a 2D window and the entire interpretation was finalized using paintbrush or 3D auto-track plug-in in Petrel.

The Isochron maps were produced to observe thickness variation. The amplitude attribute map was prepared to view the distribution of seismic amplitude strength and is represented by colour gradation. The attribute variance map is another powerful tool to highlight the structures or the unseen geological features by ordinary seismic slice. Another technique is to combine those maps to boost the shape and strengthen the visualization. All the processes that were implemented during the attribute maps generation was QC-ed by a specified parameter as well as seen in 3D window to ensure the maps quality.

At least 5 regional horizons were interpreted above the Pliocene-aged deposits, the top Pliocene, K, L, M, and the seafloor horizon respectively. The horizons were picked either between a peak or a trough (z-crossing) or between a trough or a peak. Deepwater sediment is commonly deposited as a series of events, therefore the zero-crossing horizon picking method effectively separates these units and local features.

Seismic stratigraphy interpretation has been used to locate deepwater features as it shows various reflections in seismic cross sections. Seismic facies description and classification plays an important role in determining unit and distribution. There are at least 5 seismic facies and 5 seismic units identified in this study. Three channel-levee systems and mass transport deposit were morphologically described and quantified directly from seismic data.

#### **1.4.2.3. Surface Based Seismic Attributes**

Tuning thickness is one of the main constraints in the seismic-based method. The seismic resolution might be a key aspect for observing geomorphology within seismic data that somehow can limit the interpreter. Levee pinch out to determine the channel-levee system boundary and distributary small channel within frontal splays or crevasse splays can be challenging features to display. Therefore, seismic visualization becomes important and challenging when investigating geological deposits.

Seismic attributes extraction has been a prominent method to qualitatively and quantitatively map geological features and understand its processes (Chopra and Marfurt, 2008). Unquestionably, this technique has been one of the prominent methods used in the oil and gas exploration industry. Spectral decomposition is a method that can effectively decompose frequency content directly from the seismic and is adopted to significantly delineate below-resolution geo-bodies (Chakraborty and Okaya, 1995). This technique uses fourier-based transform and deconvolution that can efficiently switch from the time domain to the frequency domain. The amplitude spectra can delineate temporal bed thickness variability while the phase spectra which is sensitive to subtle perturbation can outline lateral geologic discontinuities (Partyka et al., 1999). The resulting tuning cube can be visualized in



frequency slices which contain the best dominant frequency rather than showing full-bandwidth energy and phase extractions.

The RGB colour blend method which is derived mainly from red-green-blue colouring composition, is a robust approach for imaging (Henderson et al., 2008). The concept behind this mixture is that the intensity of each RGB colour represents the frequency content. The light and dark colour RGB blend is a way to visualize the result of spectral decomposition analysis. To simplify, McArdle and Ackers (2012) summaries that if one frequency dominates, so will the assigned frequency colour in the RGB blend result. If there is a strong and equal signal from three associated decomposition frequencies, the white colour will appear. And last but not least, if there is no resulting response from any of the colours, the black colour will appear.

Spectral decomposition, which implemented the RGB colour blend technique, was conducted by using GeoTeric software from ffa. The workflow was commonly completed by initially defining the Region of Interest (ROI) which shows the main desired area or geological features. Spectrum analysis is used to determine minimum and maximum frequencies, bandwidth, and the number of bins and QC-ed by finding the most fitting spectrum within the seismic frequency spectrum. The best 3 frequencies are assigned and 3 cubes from 3 different central frequencies with overlapping bandwidth are created. Eventually, the final cubes are colour blended and the resulting variation in frequency and amplitude is associated with a variation in colour and intensity (McArdle and Ackers, 2012).

## 2. BACKGROUND

### 2.1. Tectonostratigraphy of North Africa and The Nile Deep Sea Fan (NDSF)

Eastern Mediterranean resulted from complex, thick-skinned, crustal-scale tectonics driven by the interaction of three main plates: the Eurasian, African, and Arabian and other microplates (Fig.2.1) (Garziglia et al., 2008; Loncke et al., 2006; Mascle et al., 2000). The African plate has been subducted under the Eurasian plate since the late Cretaceous at a rate of almost 40 mm/year (Aal et al., 2000). In the eastern part, the Arabian plate moved northwards and triggered the Dead Sea shear zone with respect to Levantine-Sinai microplate. To the south, the Suez-Red Sea rift has separated the Sinai and African plates. The eastern and northern Anatolian fault zone is still active and has strike-slip motion in its north part relative to the Arabian and Anatolian plate. To the northwest, the rapidly moving Aegean-Anatolian plate marks the southern transform zone boundary along the Hellenic and Cyprus arc. All these relative plate movements reveal the regional plate tectonic activity in the area surrounding the eastern Mediterranean.

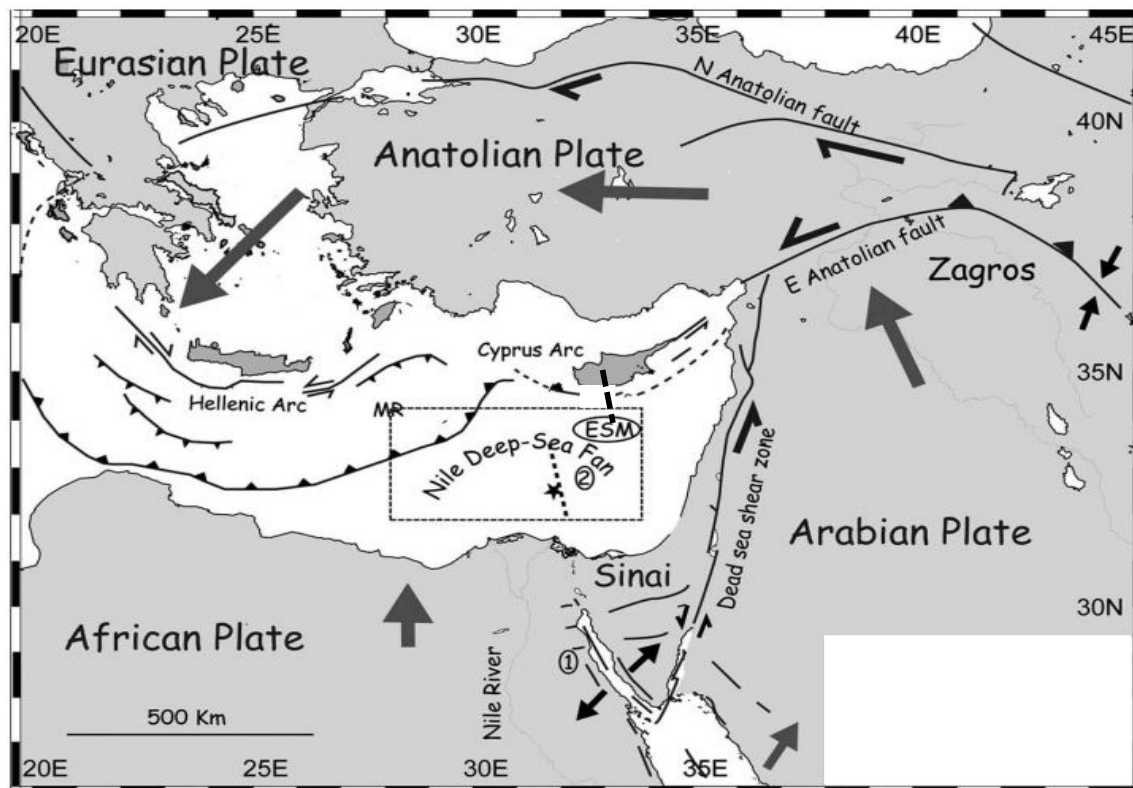
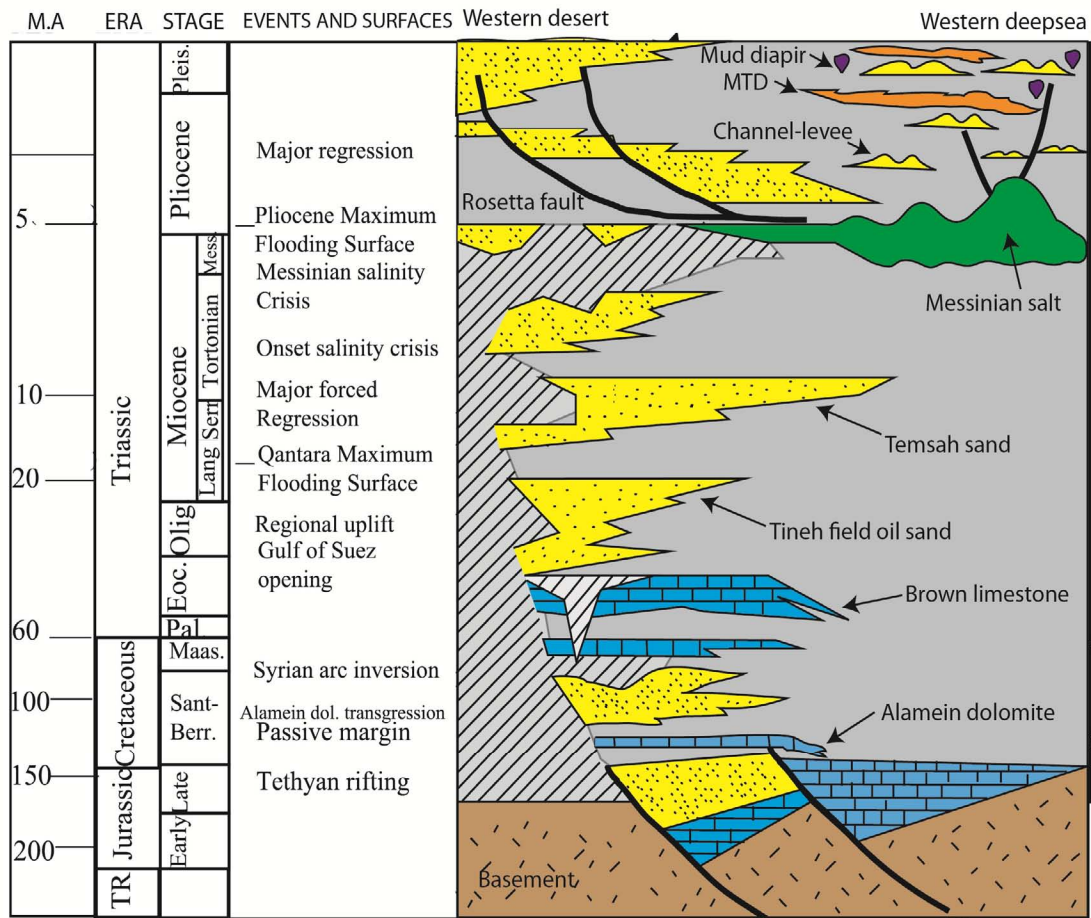


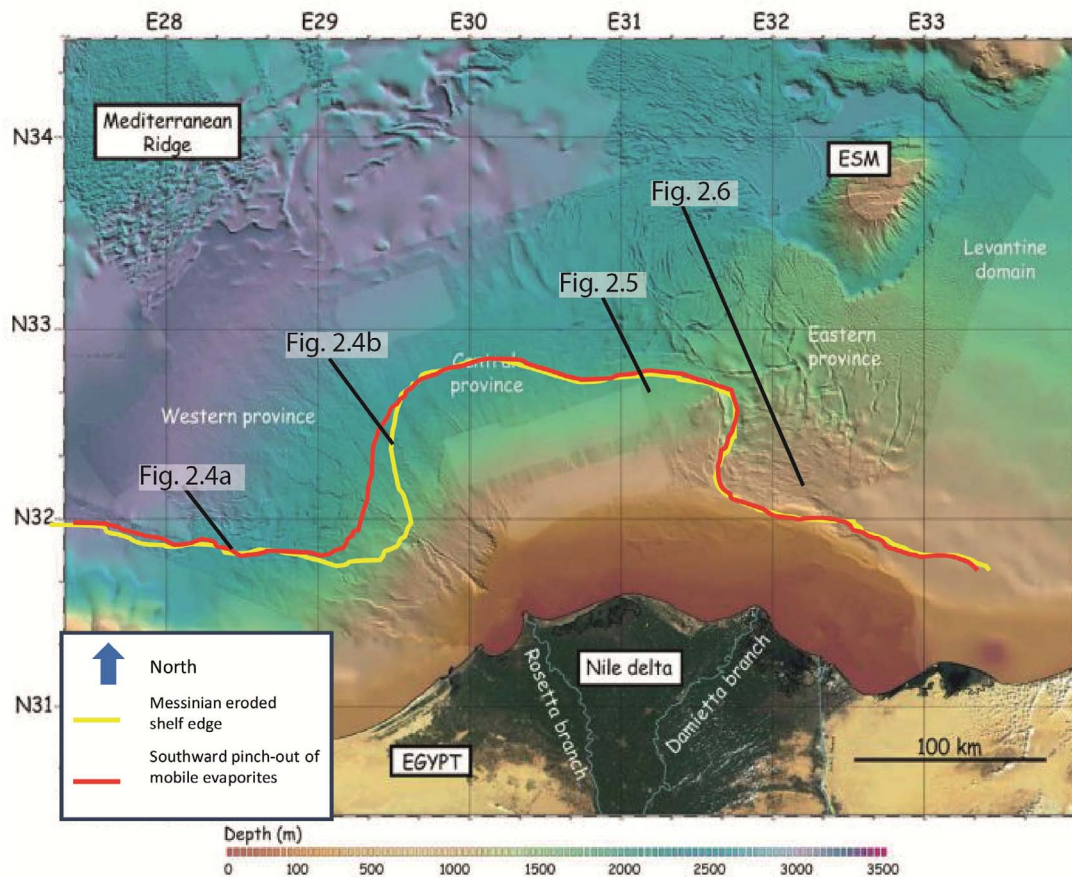
Fig. 2.1. Geodynamics of The Eastern Mediterranean (Loncke et al., 2006).



**Fig. 2.2.** The stratigraphy column describing main elements, key tectonic events, and major surfaces from the eastern desert to the western NDSF. Note there are limited core data and literatures available describing lithology of the western deepwater Egypt and therefore the stratigraphic column above is dominated by lithology name from the western land of Egypt. (modified from Dolson et al, 2005)

Key events have been investigated by Dolson et al. (2005) from the Jurassic period up until the present time (Fig. 2.2). Tethyan rifting occurred in the late Jurassic period and was followed by the Cretaceous passive margin which marked the major pre-messinian fault system. The opening of the Gulf of Suez during the late Eocene and the early Oligocene caused Egypt to tilt northwards. This event generated highly sediment supply to the deep basin through an eroded canyon. The Nile Delta region has experienced episodic relative sea-level rises and falls. The key transgression occurred during the lower Miocene period and was followed by a major forced regression that marked the onset of the Messinian salinity crisis. These consecutive events were ended by the Pliocene transgression and were followed by a major regression during the mid-Pliocene period that resulted in abundant channel-levee systems development and significant gravity-driven sediment deposition in the Plio-Pleistocene period.

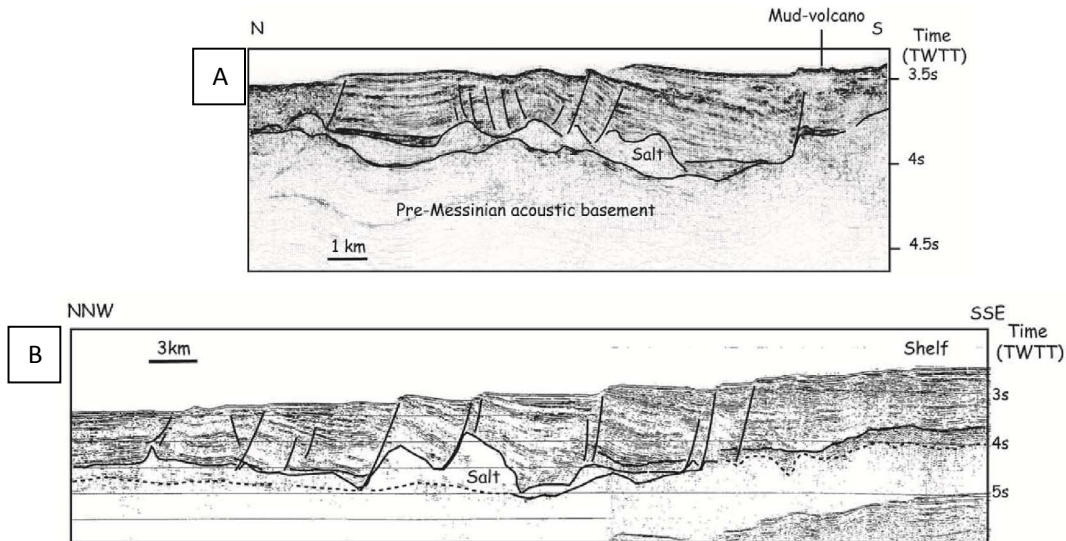
The Nile Deep Sea Fan (NDFS) is located in the northern part of Egypt and is bounded by the Mediterranean ridge in the western margin and the Eratosthenes sea mount in the easternmost part (Fig. 2.2) (Loncke et al., 2006). The NDSF sediment filled the upper part of the Egyptian passive margin which was formed from the Jurassic up to the Cretaceous period. This generated a thick overburden that covered an area of up to 100.000 km<sup>2</sup> (Loncke et al., 2006).



**Fig. 2.3.** The NDSF area (Loncke et al., 2006). Red line marks the southward pinch-out of the Messinian salt. Yellow line shows the Egyptian shelf edge that separates platform and deep basin.

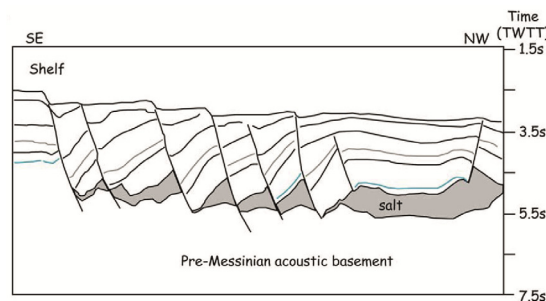
The NDSF comprises of 3 main provinces: the western, central, and eastern province. Each province has different features and deformation styles. The Western province is characterized by numerous channel-levee systems, normal faults growth, folds and abundant mud diapirs (Fig. 2.4A and B). In the western part of this province, sets of salt-related normal faults have developed which has resulted in tilted thick Plio-Quaternary sediments (Fig. 2.4A). A series of turtle-back anticlines have developed above the Messinian salt. In the shallow depth, mud diapirs have commonly overlain the sediment and reached

the seafloor. To the eastern side of the western province, structures commonly show a series of big regional normal fault growth in association with salt activity (Fig. 2.4B). The Rosetta trend is identified as a left-lateral oblique slip in the most upper slope of the western province with a NW-SE orientation. Gas chimneys are observed in specific locations in the platform/upper-slope domains within the western NDSF. It is often documented in a non-deformed area where there is no salt activity. Thus, it can be observed that these features, as indicated by (Loncke et al., 2004), are infected from different sources when compared to mud diapirs.



**Fig. 2.4.** A: The western part of the western province  
B: The eastern part of the western province (Loncke et al., 2006)

The central province has less channel-levee systems, a significant amount of normal faults, and rollover anticlines (Fig. 2.5). The channel-levee systems within this province are inferred to be eroded/dislocated by recent debris flow (Loncke et al., 2006). Adjacent to the shelf, sets of normal faults have highly affected the area. Further in the deeper part, the underlying salt has reduced its movement resulting in a stable area where no significant faults have been found.



**Fig. 2.5.** The main structures within the central province of NDSF (Aal et al., 2000)



The major faults within the eastern province are influenced by the Tamsah trend which has a NW-SE right-lateral oblique slip orientation. Long section of the eastern province provides a regional picture of salt tectonic development (Fig. 2.6). The upper section is characterized by a series of normal faults in association with upslope extension due to salt tectonic (Fig. 2.6, box 1). In the middle part, structures commonly exhibit salt-related graben and less deformed packages (Fig. 2.6, box 2 and 3). To the distal part, the area is characterized by fold growth and a series of reverse faults in accordance to a compressional regime of salt tectonic (Fig. 2.6, box 4).

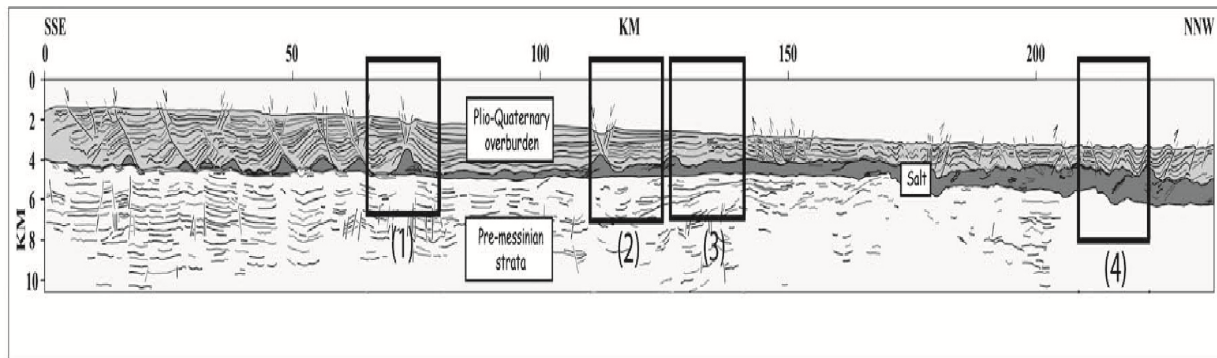


Fig. 2.6. Cross-section showing deformation style of the eastern province (Loncke et al., 2006)

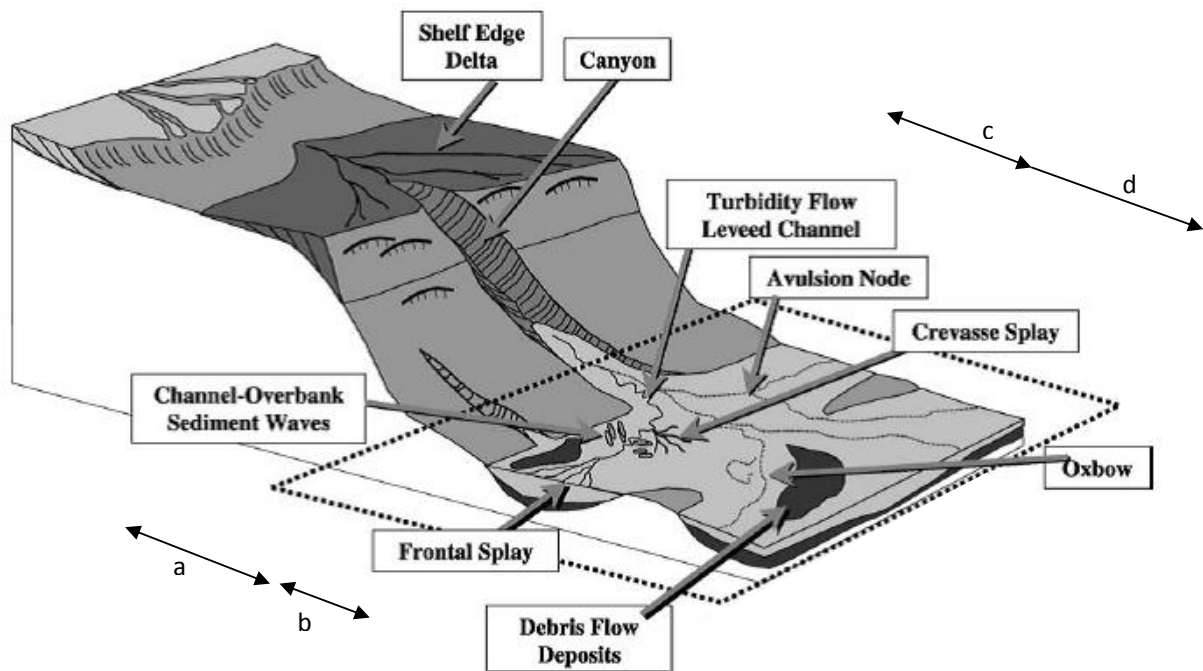
### 2.1.1. The Messinian salinity crisis

The Messinian salinity crisis during the late Miocene period has affected the deposition of evaporites that covers most of the Mediterranean area (Hsü et al., 1973; Kellner et al., 2009; Ryan, 1978; Sestini, 1989). The Mediterranean area has been investigated by Hsü et al. (1973), who was found out that some 6 million years ago it was a desiccated deep basin. This assumption was based on evidence from several drilling results. The cores show Nodular and “chicken wire” anhydrite which indicate that the Mediterranean area was deposited under hot and arid coastal flats. A trace of halite also confirms that it had an ancient Aeolian environment. The Mediterranean area is seen as a closed isolated basin based on the distribution of the evaporites. During major regression, the surrounding Mediterranean area has been subjected to erosion as resulted of a lot of river channel development that may extend down to a deeper basin.

The interaction between the overburden sediment and the underlain evaporites has shown a close relationship. The overlain sediment has been deformed by the salt-related tectonic and, hence, created a complex area. The mobile evaporites have contributed to the tectonic evolution of the upper Miocene sediments which has triggered regional gravity sliding and spreading processes (Vendeville, 2005).

## 2.2. Seismic geomorphology and terminology for idealized submarine channel-levee system and other elements.

3D Seismic has been extensively used in the industry and seismic geomorphology has been found to be powerful to image subsurface geological structures and provide valuable insights regarding depositional elements. Seismic geomorphology is defined as the application of analytical techniques pertaining to the study of landform and to the analysis of ancient, buried geomorphological surfaces as imaged by 3D seismic data (Posamentier et al., 2007). The technique that may be applied is horizon-based or volume-based attribute mapping



**Fig. 2.7.** Model showing the idealized component within deepwater slope settings. Note a,b,c, and d (see text) pointing out the deepwater main environments. (modified from Posamentier, 2003) .

Common deepwater development as suggested by Steffens et al. (2004), in the upper part is characterized by canyon formation with highly erosive processes and sediment bypass. Basal debrite and gravity-driven deposits associated with a turbidity current or debris flow are identified to cover the extensive area towards the basin floor. These deposits often show overlain channelized packages and other related features.

Numerous proposes for deepwater deposits have been published in various journals. The five key deepwater elements suggested by Posamentier and Kolla (2003) are:

1. *The channel-levee system* can be preserved in a single unit or in multiple channel stories. It may show high sinuosity and with evidence of accretion packages both in the inner bend or outer bend. Stacking channel-levee systems can be described by

cut-and-fill process and is grown as aggradation and lateral migration (Kolla et al., 2007). Studies relating to submarine channel-levee system of various basins around the world are abundant.

2. *Channel-overbank sediment waves and levee deposits* are commonly found in a major submarine channel-levee system. Levees are defined as narrow convex-up confining ridges adjacent to channels, whereas the concave-up wedges extending laterally away from the channel are defined as overbank deposits (Normark et al., 1993). Levees are commonly wider than channel itself and can be present with or without sediment waves.
3. *Frontal-splay* is a termination for distributary-channel pattern that is commonly located at the end of channel-levee system. Frontal splay has a bigger dimension than crevasse splay.
4. *Crevasse-splay* is formed when channelized turbidity flows breach the adjacent levee. It tends to cover a wider area than overbanks splay.
5. *Debris-flow channels, lobes, and sheets*. Debris flow channels, in some cases, are associated with levees when sinuosity tends to be lower than the turbiditic channel-levee system. Debris-flow sheets can be very extensive and can reach a basin floor. Debris-flow lobes commonly tend to be elongated and narrow, but in some areas cover a broad area.

General terminology for 4 main environments related to the turbiditic system as suggested by Normark et al. (1993) such as (see Fig 2.7) are:

- a. *Shelf edges* show large-scale erosional features, for example a canyon (Fig 2.7, point a).
- b. Basin margin zones display a variety of elements depending on the basin slope settings (Fig 2.7, point b).
- c. *Proximal basin zones* commonly exhibit stacking of sheet-like sand-rich deposits (Fig 2.7, point c).
- d. *Distal basin zones* are characterized by finer grained and thin-bedded sandstones (Fig 2.7, point d).

The process involved within the slope system is strongly related to the gravity-driven mechanism (Fig. 2.8). Slope failure is one of the causes of sediment that generates debris and turbidity flow downslope. Debris slide is categorized as a relatively coherent mass and exhibits translational or rotational movement but shows minor internal structures. Other gravity flow types which involve more avalanche degrees and shows more internal deformation is known as slump.



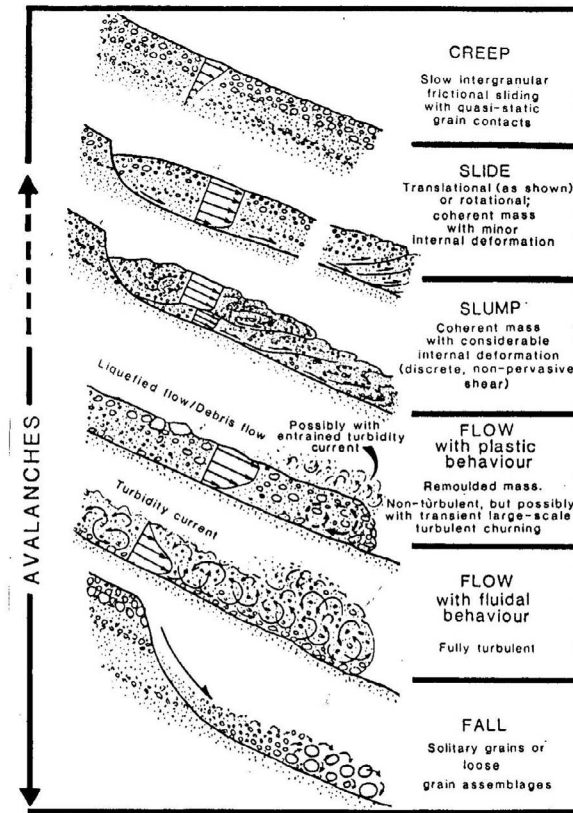


Fig. 2.8. Diagram showing spectrum of subaqueous debris mass-movement processes (Nemec 1989).

Debris flow is termed as gravity-driven flow with plastic behavior that can occur in subaerial or subaqueous conditions. This flow can be distinguished as cohesive or cohesionless (non-cohesive) debris flow. The cohesive debris flow is determined when it involves mainly or only cohesive yield strength while the cohesionless debris flow is classified when it experiences mainly or only frictional yield strength (Nemec, 2009). Debris flow destructive abilities arise because of the combination of extreme mobility and large momentum and are therefore often found to erode the underlying strata.

In the outcrops, the debris-flow deposits show very poorly sorted succession (Leeder, 2011). Normal-graded debris flow deposits are attributed to the cumulative effects of sustained deposition from a travelling debris flow (Leeder, 2011). Meanwhile, the inverse grading debris-flow deposits may occur in different mechanisms: i) High-rate grain collision pushes upward the coarser clasts by dispersive pressure and/or pushed downward the finer grain. ii) Another process could be due to strong shear in the lower part which progressively decreases to the upper succession. Debris flow which descends a relatively steep slope will experience acceleration and intense shearing against ambient water. This debris-flow will erode the underlying surface while the top part will generate turbidity currents. When the debris flow descends a relatively gentle slope, it will show little or no mixing.

Turbidity currents are commonly used for fluidal flows under a subaqueous condition. This current may originate from different processes, such as the transformation of debris flow, the underflow of a river discharged as hyperpycnal plumes, or a very narrow shelf where a head of submarine canyon may arise and collect sediment by longshore drift (Leeder, 2011).

The acceleration state of flows as described by Kneller and Branney (1995) is whether the flow is steady or unsteady, uniform or non-uniform. If it is unsteady, the unsteadiness is waning or waxing. Moreover, if it is non-uniform, this flow could be distinguished whether accumulative or depletive.

Bouma et al. (1962) suggested a widely known model for turbidites succession which starts with massive normal grading (very coarse to coarse/medium sand) at the bottom followed by plane-parallel stratification as a product from the upper flow regime (Fig. 2.9). The next succession is a current-ripple cross-lamination (fine/very fine sand to coarse silt) overlain by parallel lamination deposit (fine silt laminae). The uppermost 'ideal' turbidites succession consists of mud.

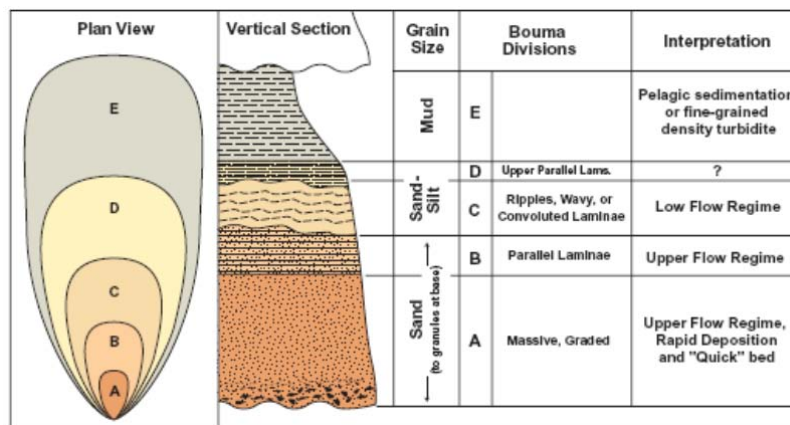


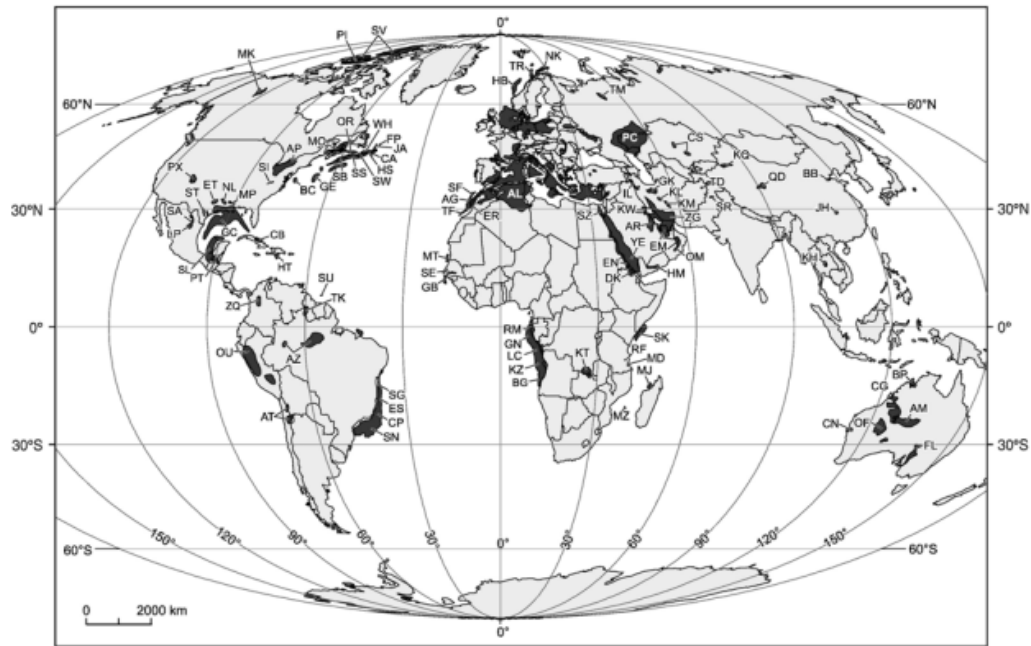
Fig. 2.9. Idealized turbiditic section modified from Bouma (1962)

### 2.3. Salt Tectonic

Salt tectonic and its related structures play an important role in shaping basin morphology around the globe (Fig 2.10, Fig. 2.11). Whenever pressurized from the overlain sediment, the salt flows and therefore affects the overburden deposits. Salt is relatively incompressible and thus makes this deposit unstable and easy to deform. Salt also has lower density and has positive buoyancy (Talbot, 1993). The main driving force of salt is differential loading that may be related to gravitational forces (Hudec and Jackson, 2007)

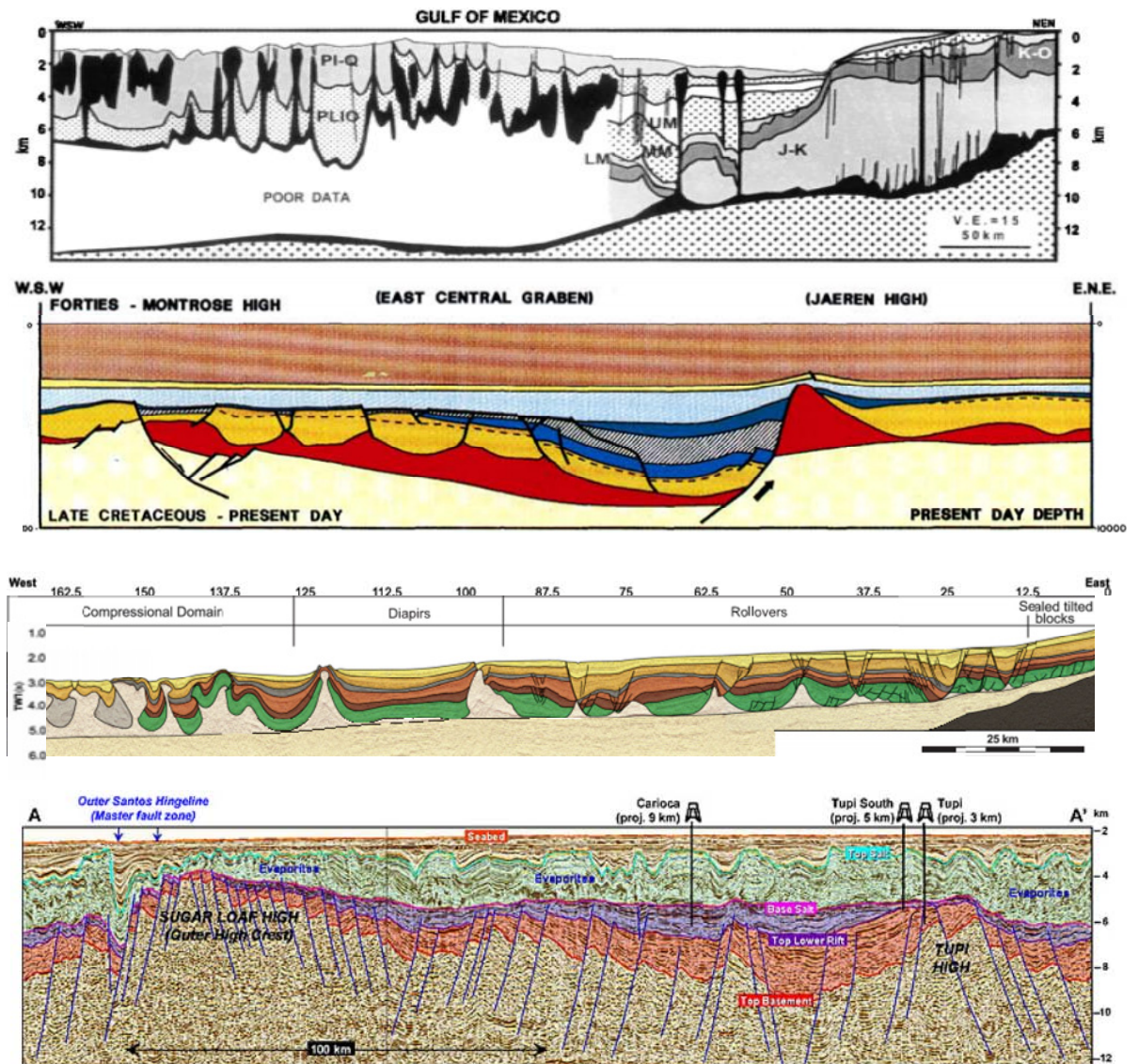
Salt basins tend to have updip extension and downdip shortening (Vendeville, 2005). The common thin-skinned structures are in passive margin display tilted blocks, roll-over complex, diapir, and compressional domain (Fort et al., 2004). Different sedimentation rates

and timing (rapid or long-rate sedimentation) influence the structural type of salt deformation. Slope angle is another factor in salt play, as the slope becomes steeper, the structure tends to build basinwards (Vendeville, 2005). However, the salt-influenced basin process and mechanism involved in this system are still being debated (Brun and Fort, 2011; Rowan et al., 2012). Numerous experiments and modeling are underway to help understand salt tectonic (Garcia et al., 2012; Gemmer et al., 2005; Rowan et al., 2012).



**Fig. 2.10.** Map showing global distribution of basins containing salt structures (Black-colored area) around the world (Hudec and Jackson, 2007).

Mobile substrates have been found to be useful in trapping and controlling reservoir distribution (Fig. 2.11). The trapping style related to salt tectonic usually corresponds to structural traps as well as combining with stratigraphic traps. Salt-related products for instance, salt sheet, salt canopy, and salt bulb are established as effective elements in trap construction. Major salt basins and mini-basins are documented to play an essential part in hydrocarbon exploration and production (Fig 2.11).



**Fig 2.11.** Images illustrating example of seismic cross-section from various salt-dominated basins all around the world. It provides insight in how salt plays important keys in basin deformation and hydrocarbon exploration. **(a)** Gulf of Mexico (Wu et al., 1990) **(b)** East Central Graben, North Sea (Penge et al., 1993) **(c)** Kwanza Basin, Angola, West Africa (Fort et al., 2004) **(d)** Arbitrary line through outer high, Santos Basin, Brazil (Gomes et al., 2009)

## 2.4. Deepwater Exploration

Deepwater exploration has expanded over the last decade (Pettingill and Weimer, 2002). Deepwater exploration was previously leveled at water depths of at least 500 m. Such exploration has recently moved even further downslope to a water depth of 2000 to 3000 m (ultra deepwater). Several recent discoveries show promising results for further development, for instance in the Gulf of Mexico, West Africa, and South America. Therefore, turbiditic study and other gravity-driven deposits have now been extensively studied.

Numerous works from scientists have been contributed significantly to enhance understanding of deepwater settings.

In deepwater setting, approximately 58 billion barrels of oil equivalent which consists of 39 million barrels of oil and 112 trillion ft<sup>3</sup> of gas has been discovered (Pettingill and Weimer, 2002). The hydrocarbon potential of the deep and ultra deepwater in the Gulf of Mexico is estimated to be up to 46 billion barrels of crude oil equivalent (Anderson et al., 2009). There are approximately 1200 to 1300 deepwater oil and gas fields around the world and there are more to come (Stow and Mayall, 2000).

The deepwater exploration rate progressively increased after many giant fields were discovered, from 10% in late 1985 to 30% in 2002. This rate is classified based on confined or non-confined settings and also with or without mobile substrate (Pettingill and Weimer, 2002). Salt tectonic plays an important part in deepwater plays. Pre-salt imaging has been improved in recent years to provide better visualization (Dewey et al., 2006; Huang et al., 2010; Malaguti et al., 2001).

Almost 90% of the recourse found in turbiditic sandstone reservoirs with porosity could be more than 30% and 1000s mD for permeability (Pettingill and Weimer, 2002). Submarine channel also emerged as one of the prominent targets to be a reservoir (Cross et al., 2009; De Ruig and Hubbard, 2006; Samuel et al., 2003). Hydrocarbon plays in Egyptian deepwater are inferred to be Pliocene turbiditic, Miocene canyon shallow marine and pre-salt limestone and turbiditic system (Aal et al., 2000). Eventually, although many researchers are working in deepwater Egypt, the exploration activity still needs more comprehensive studies to gain a better understanding of this prosperous region.

### 3. SEISMIC STRATIGRAPHY ANALYSIS

This seismic stratigraphy chapter consists of three main sections: i) seismic facies, ii) seismic stratigraphy, and iii) seismic geomorphology. Seismic facies are categorized according to their amplitude strength, reflector continuity, and geometry (Table 1). Seismic sequence analysis describes each package that is bounded by a specific bounding surface. Seismic sequence boundaries represent major changes in seismic facies and/or are marked by systematic reflector terminations. Seismic geomorphology combines traditional seismic facies analysis with planform analysis of seismic attributes to understand the geomorphology and sedimentology of the depositional system in the study area.

#### 3.1. Seismic Facies

Five seismic facies have been identified within the study area (Table 1). All of these facies will be described and interpreted in the following sections.

##### 3.1.1. Seismic facies 1 (SF1) - Channel and channel-fill deposits

Seismic facies 1 is characterized by a general U-shaped external geometry of up to c. 125 ms TWT (200 m) deep and 700 m wide that cuts down into, and truncates older reflections. This seismic facies 1 consists of low to medium amplitude and high amplitude reflections (HARs) in sub-horizontal to sub-parallel or chaotic internal geometry. This seismic facies can be distinguished into SF1a and 1b. SF1a has a more continuous reflector while SF1b shows chaotic patterns. Both of these seismic facies display an irregular base and have a relatively conformable top. High amplitude reflections are commonly distributed in the lower and central parts of channel-like erosional fairways. This seismic facies commonly shows overall decreasing amplitude upwards. In the cross-section, this channel-like feature displays a localized body with the surrounding reflection on-lapping to this feature. In another area, it shows sharpened U-shaped feature surrounding by relatively transparent to low amplitude wedge-shaped form. In the RGB colour blend attribute maps, this seismic facies shows sinuous and occasional meandering features of bright amplitude that can be traced for tens of kilometres (Table 1).

SF1 in the study area is interpreted as channel axis deposit. The general U-shaped geometry represents a channel thalweg within the basal erosional surface (BES). The low to high amplitude reflections within the channel characterise the product of a relatively high energy flow that settles down the sediment inside the channel body. These channel and channel-fill facies are located along the three channel-levee systems within the study area. The mounded form above some channel axes suggests that less compactable sediment has been deposited compare to the adjacent deposits (Posamentier, 2003). Therefore,

differential compaction may be suggested to infer the lithology, sand-rich sediments could be associated with channel-fill and mud prone deposits may be associated with the levee system. From other studies where core data is available, the lower part is interpreted as having coarser-grained sediments while the upper packages have predominantly shale or mud-rich sediments (Mayall et al., 2006; Pickering et al., 1986; Pirmez et al., 1997).

### **3.1.2. Seismic facies 2 (SF2) - Levee Deposit**

Seismic facies 2 has low to moderately medium amplitude and commonly shows transparent patterns which are located adjacent to SF1. Seismic reflection continuity for this seismic facies is relatively continuous with a parallel to wavy internal form. This seismic facies display a symmetric wedge-shaped geometry with a thickness that exponentially decreases away from the centre. In some areas where faults are highly influenced the area, this seismic facies shows an asymmetric form. The thickness of SF2 can vary from c. 14 to 83 ms TWT (22 to 133 m). In RGB colour blend attribute maps, this seismic facies is presents alongside the SF1 and commonly shows wavy-like features with low amplitude strength (Table 1).

SF2 is interpreted as levee deposits which flank the submarine channel and is laid above the BES. Ideally, levee development should be symmetric and outward-thinning if there are no major disruptive tectonic influences or other submarine features disturbances. This levee facies character shows build-up layering which indicates an aggradation development from a spill-over process of turbidity current. These layered transparent reflections compared to bright HARs of channel fill deposits may infer that this seismic facies consists of mud-rich lithology. From other research where core data is available, the lithology expressed silty to fine-grained sediments (Pickering et al., 1986).

Probably, there is no significant inner levee observed in the study area due to smaller dimension of submarine channel compared with channel-levee systems analysed from other work in the Gulf of Mexico, Indus fan, Niger delta, and Offshore Trinidad Tobago (Deptuck et al., 2003; Posamentier, 2003; Wood and Mize-Spansky, 2009). Therefore, levee termination that discussed here refers to outer levee or master bounding levee (Kane et al., 2007).

### **3.1.3. Seismic facies 3 (SF3) - Mass Transport Deposit**

The most prominent signature of SF3 is that it displays chaotic internal geometry. This seismic facies shows acoustically incoherence and displays discontinuous reflection with a low to medium amplitude. This makes SF3 can be identified from the seismic cross-section (Table 1). SF3 has an irregular base and in some areas, reflects an occasional internal layering form. In the study area, major SF3 can be documented lying near the seabed and in the lower part of the succession. In attribute maps, this SF3 shows irregular form and in some case, it exhibits a scouring-like striation (Table 1).

Seismic facies 3 is interpreted as mass transport deposit (MTD). This gravity-driven feature is broadly common deposit within a deep-water settings (Damuth and Flood, 1983; Gardner et al., 2003; Pickering et al., 1986; Posamentier and Kolla, 2003). The irregular base is an indication of an erosive surface which marks the eroded underlying sediment. Mass transport deposit, which consists of major slump and debris material, has been shown to be internally deformed so it may be regarded as product of remobilized sediment (see subchapter 3.3.4). The chaotic and low amplitude reflection may indicate a heterolithic mud-rich deposit. In core, borehole-image and dipmeter studies from other studies, it is interpreted as finer-grained to muddy deposit which contains soft-sediment faulting and folding (Lopez, 2001; Samuel et al., 2003). The termination used in this study area is near-seabed mass transport deposit (NSMTD) and buried mass transport deposit (BMTD). The NSMTD lies on the top of the succession and is occasionally overlain by the present-day seabed channel particularly in central part of the study area. The BMTD is located below the channelized-fan deposit and above the regional transparent debris flow (TDF).

#### **3.1.4. Seismic facies 4 (SF4) – Fan-lobe Deposit**

Seismic facies 4 is observed to have a very low to medium amplitude strength which displays continuous reflection packages and has an extensive lateral distribution throughout the study area with a thickness of up to c. 200 ms TWT (320 m). This seismic facies exhibits relatively homogenous parallel beddings and in the eastern part of the study area, it is obviously sandwiched between NSMTD and BMTD. SF4 has an irregular top that has been eroded by NSMTD and also has a relatively conformable base. This seismic facies is occasionally disturbed by the development of mud diapirs. In some case, this seismic facies also coincide with very bright HARs. In RGB colour blend attribute maps, SF4 shows a low to bright amplitude and occasional small channelized features (Table 1).

Seismic facies 4 is interpreted as submarine fan-lobe deposit and is inferred that these thick prograding lobate sand sheets are sourced by Rosetta canyon (Migeon et al., 2010). This typical fan deposit is well documented in deep-water submarine settings worldwide (Clark and Cartwright, 2009; Cross et al., 2009; Wynn et al., 2007).

Continuous and alternating strong amplitude reflectors suggest that this seismic facies contain predominantly intercalated turbiditic sand-shale deposits which is suggested by other researchers working with core data that they encompass a range of succession from fine grained to mud-rich deposit (Kane et al., 2007; Pickering et al., 1986).



### **3.1.5. Seismic facies 5 (SF5) - Mud Diapirs**

This is considered as seismic facies due to its abundant appearance in the western NDSF. This seismic facies displays a transparent to very low amplitude and can be seen as chaotic pattern which is formed a caldera or cone-like features in seismic cross-section (Table 1). SF5 occurrence is often coincident with underneath salt-related fault. The seismic facies thickness could reach 520 ms TWT (832 m) with a diameter that may vary up to 3.6 km. From RGB colour blend attribute map, this seismic facies exhibits a circular black form (Table 1).

Seismic facies 5 is interpreted as mud diapirs and has been studied in the region from other workers. It is thought as a result of liquid-escape features (Feseker et al., 2010; Loncke et al., 2004). The underneath salt-related faults below mud diapirs are inferred to be a migration pathway for deep-seated liquefied sediments. The growth of the mud diapirs is thought to remarkably influence the development of channel-levee system and affect the structural setting among units within the study area. This will be discussed later in the following seismic unit chapter.

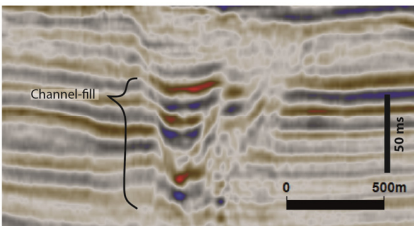

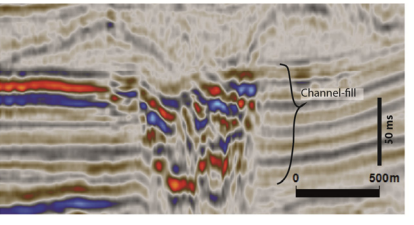
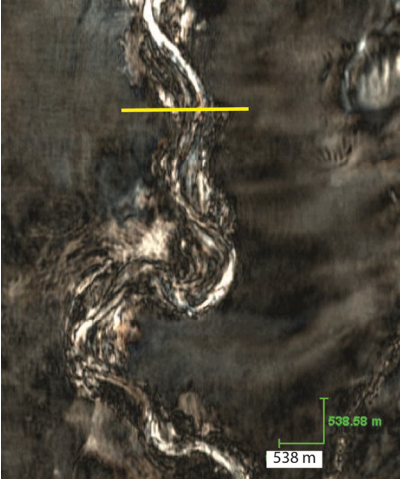
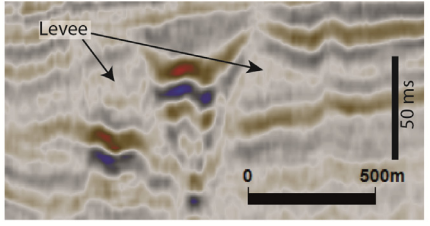
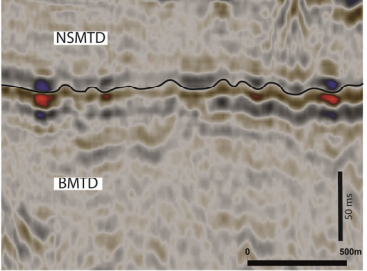

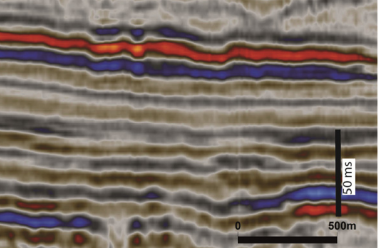
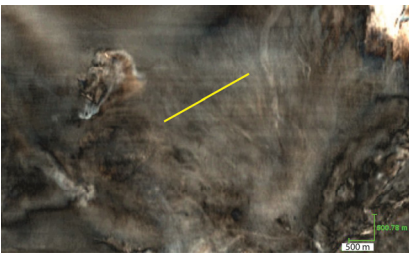
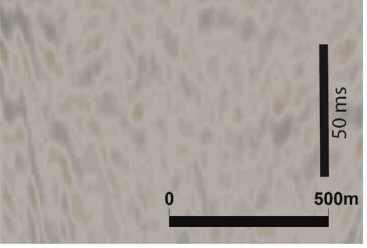
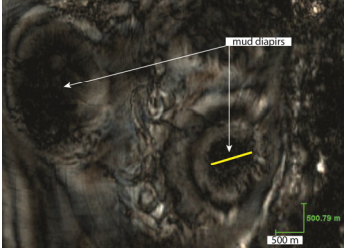
Seismic facies	Amplitude strength	Reflection continuity	Internal geometry	External geometry	Distribution	Process interpretation	Depositional element	Cross section	Plan view
1a	Low to High amplitude reflections (HARs)	Discontinuous	Sub-horizontal, parallel	U-shaped	Mostly characterized channel A. Distal reach of Channel B and C.	Turbidity flow in confined or unconfined channel-like erosional fairway.	Channel and channel-fill		
1b	HARs	Discontinuous	Chaotic	Sharped, U-shaped	Upper reach channel B and channel C	Fairly high energy turbidity flow to generate an erosive fairway for its sediment to bypass and deposit.	Channel and channel-fill		
2	Low to high	Continuous	Parallel to wavy	Wedge-like, thickness decline away from the channel axis	-Channel A: Occasionally disturbed by mud diapirs -Channel B: In upper reach, it is coincident with debrites. -Channel C: In upper reach, it is superimposed with adjacent levee from other CLS or eroded by CLS B	Overbank/spillover flow that overtop channel margin and deposited on the flank of channel.	Levee		
3	Transparent to medium	Discontinuous	Chaotic	Erosive base, sub-horizontal	- near seabed mass transport deposit (NSMTD), - buried mass transport deposit (BMTD) - regional transparent debris flow (TDF)	Subaqueous debris flow as combination of extreme mobility and large momentum. Gravity-driven flow that erode the underlying strata.	Mass Transport Deposit		
4	Transparent to medium	Continuous	Parallel	Homogenous parallel bedding	Covers most of the study area.	Turbidity flow that generate fan-lobes.	Fan lobe		
5	Transparent to low	Discontinuous	Chaotic	Caldera-like or Cone-like features	Western part of study area. Observed to be located near fault zone.	Fluid-escaped features through faults as its migration pathways. High rate of sedimentation which creates thick overburden that is pressurized uncompacted sediment, ex: mud.	Mud diapir		

Table 1. Table showing the five seismic facies characters and their appearance in the cross-section and plan view.

### 3.2. Seismic Unit

The seismic unit within the study area can be classified into 5 seismic units: transparent debris flow (TDF), buried mass transport deposit (BMTD), channelized-fan deposit, and present-day CLS and near-seabed mass transport deposit (NSMTD) (Fig. 3.1). By the end of this sub-chapter, mud diapirs will be classified as one unit because of its abundant existence. All the units are observed to be highly influenced by underlying mobile substrate, the Messinian salt (Figs. 3.2 A, B, and C). The units described here are present above Pliocene-aged deposits.

#### 3.2.1. Seismic unit 1 (SU1) - Transparent Debris Flow (TDF)

Transparent debris flow is a term that was introduced by Loncke et al. (2006). The distribution of TDF covers the entire study area and remains almost the same thickness over the whole region with a thickness of up to c. 345 ms TWT (552 m) (Fig. 3.3). It generally shows an identical appearance to SF3 (Table 1) bounded by top Pliocene horizon at the base and K horizon above. The top Pliocene horizon is interpreted in the continuous zero-crossing marking the significant change in seismic surface. SU1 exhibits an irregular base with a major onlap from underlying thick Pliocene deposit to this unit which is most likely related to erosion caused by debris flow (Fig 3.1).

The southernmost part of this seismic unit is characterised by the development of the minibasin and shows a significant syncline form which is due to overburden sediment which can reach up to 4050 ms TWT at its deepest point (Fig. 3.3, point A). The main fault zone in the centre of the study area marks a major offset in this unit (Fig. 3.3 point B). A massive mud diapir also present adjacent to the fault zone resulting in thickness reduction of this unit (Fig. 3.3, point C). The eastern part shows a relatively stable, vast, and similar thickness of about c. 200 ms TWT (320 m) with no major disturbance from the Messinian mobile substrate (Fig. 3.3 point D). The graben structure in the western part of the study area is affected the SU1 to become thinner as the overlying sediment including the mud diapir, fulfil the accommodation space (Fig. 3.3, point E). At the south-westernmost area, many mud diapirs are observed and reduced SU1 thickness due to mud diapirs late development (Fig. 3.3, point F). At the most eastern part, this seismic unit is occasionally disturbed by channel-levee development (Fig. 3.3, point G). These channel-levee systems are probably a result of a continuation from the underlying layer (Pliocene aged) towards the younger strata. In the central part, major erosion of Pliocene deposit has occurred due to the northern depocenter development which has resulted in thinner Pliocene deposit (Fig. 3.3, point H).

### 3.2.2. Seismic unit 2 (SU2) – Buried Mass Transport Deposit (BMTD)

Seismic unit 2 is laid below the L horizon which is the base of this seismic unit and above the K horizon which indicates the top of the regional TDF. The main composition of this seismic unit is characterized as mainly a transparent and chaotic reflector which is interpreted as BMTD. This SU2 is fairly identifiable from the upper layered SU3 and the underlying SU1. The contact of SU2 and 1 is occasionally separated by high amplitude reflection packages (HARPs) (see subchapter 3.3.4). The L horizon is interpreted in zero-crossing (s-cross) which marks the base of the upper layered fan lobes deposit and which has relatively continuous reflection. The K horizon is interpreted in s-crossing as well to observe the morphology of base erosional BMTD. This seismic unit is extensively distributed in the study area and is identified as having a major irregular base. The isochron map of this seismic unit shows general thinning northwards from c. 200 ms TWT (320 m) progressively decreasing to c. 24 ms TWT (38 m) (Fig. 3.4B).

The thickest part of this seismic unit is laid on the southernmost area which contains another CLS apart from the CLSs that are described in this study (Fig. 3.4, point A). Immediately adjacent to this area, minibasin exists and the BMTD shows that it has a thickness of about 174 ms TWT (278 m) (Fig. 3.4 point B). The BMTD in graben structure displays moderately thinner at about 65 ms TWT (104 m) (Fig. 3.4 point C). The north-western mud diapirs complex and the central giant mid diapir have affected the thickness of SU2 which gradually decreased towards the centre of mud diapirs (Fig 3.4, point D). However, the mud diapirs are influenced the external morphology of the BMTD following the mud diapirs form.

Within the eastern side of the study area, the BMTD exhibits occasionally layered packages (Fig. 3.4, point E, see Fig. 1). This suggests that the BMTD had been deposited over several events. Further north, in the central part, this seismic unit exhibits a significant and immediate change in depth as a result of a steep slope in association with northern depocentre development (Fig. 3.4, point F). This area shows a major depression and thick overburden sediment. The thinnest BMTD c. 10 ms TWT (16 m) is observed at the extreme north-western part of the study area (Fig. 3.4, point G). Because of the overall thickness distribution on the isochron map, this seismic unit is thought to be sourced from the southern area towards the north east.

### 3.2.3. Seismic unit 3 (SU3) – Channelized-fan deposit

Seismic unit 3 is topped by the M horizon which separates the SU3 and SU4. The L Horizon at the bottom of this unit is picked on a zero crossing that marks the reflection change from general transparent unit to medium-high amplitude of SF4 (Table 1). The upper reflection often shows an irregular top particularly in areas where overlying NSMTD is existed. The

Messinian salt has effectively contributed to the deformation of the Plio-Pleistocene deposit including this SU3. This has resulted in the central part is occasionally found being exposed as sea floor (Fig. 3.2C and 3.5, point A).

Seismic unit 3 encompasses the studied channel-levee complexes within the study area, the thick layered fan lobes deposits and the major mud diapirs. The leveed-channels within the study area are comprised of 3 channel-levee systems, A, B, and C, respectively. All the CLSs are considered part of this seismic unit as consequences of channelized-fan lobe deposit and will be described and have its details quantified in the seismic geomorphology chapter (see chapter 3.3).

Seismic unit 3 is covered the whole study area and is shown overall similar thickness except in the locations where mud diapirs are occurred (Fig. 3.5, point B). Within the central part of the minibasin, this seismic unit exhibits thicker deposits of c. 200 ms TWT (320 m) (Fig. 3.5, point C). In the area where northern depocenter is located, SU3 also has a high thickness of about 187 ms TWT (300 m) (Fig. 3.5, point D). Towards the north-westernmost area, SU3 expresses the thinnest part c. 55 ms TWT (88 m).

#### **3.2.4. Seismic unit 4 – Present-day channel-levee system and Near Seabed Mass Transport Deposit (NSMTD)**

Seismic unit 4 is bounded by the seabed and M horizon. The seabed horizon was picked in peak seismic reflector based on increasing acoustic impedance from sea water to seafloor sediment. The M horizon marks the base of NSMTD in the eastern part which is shown as an irregular surface, but appears as a parallel continuous reflection in the north-western part, which characterizes the contact between CLS B and the overlying present-day seabed channel (Fig. 3.9).

In area where SU4 contains the NSMTD, it shows mostly a transparent unit with discontinuous reflector which is the SF3 (Table 1). From the seismic-cross section, elongate HARs are occasionally present below the NSMTD in the north east part of the study area (see sub-chapter 3.3.4).

Present-day CLS is occupied most of the northern part of the study area and exhibits a relatively conformable surface to the underneath NSMTD (Fig. 3.6). In the central part, the present-day CLS shows high degree of sinuosity in confined constructional levees (Fig. 3.7). This present-day CLS captured in the study area constitutes a distal part of the whole system before it was transformed into a lobe in the Herodotus Basin (Fig. 3.6) (Migeon, et. al 2010). The darker colour on the north side within the TWT map shows that a deeper topography has resulted in accommodation space becoming available for this present-day CLS to be developed and is shown as a thick deposit within the isochron map (Fig. 3.8, point

A). To the major west part, the SU4 expresses a similar thickness of about 20 ms TWT (30m) and this is considered as the thinnest part within the study area (Fig. 3.8, point C)

From the previous study, the western NDSF is characterized by numerous channel-levee systems, giant failure scars and associated mass transport complex (Ducassou et al., 2009). At least four main channel systems were identified in the western NDSF as CLS DSF3, DSF4, DSF5, and DSF6 and are listed from older to younger age respectively (Fig. 3.5). (Migeon et al., 2010). The downstream part of channel DSF6 is reported to be 1.5 km wide, 40 m deep, and sinuosity of 2.3 at a water depth of 2900 m that are inferred to reach the Mediterranean ridge (Migeon et al., 2010).

The NSMTD spreads from south east to north east in the eastern part of the study area as the TWT map of the M horizon illustrates general base deepening northwards with a thickness of about 98 TWT (157 m) in the upper slope to 154 TWT (246 m) in the lower slope (Fig. 3.8, point B). The thinnest packages of NSMTD are associated with tilted footwall generated by the main fault in the central region and therefore, the NSMTD is only occupied almost half of the study area (Fig. 3.9). The NSMTD is also exposed as part of the seafloor topography adjacent to levee deposit of CLS B and shows a relatively transparent to low amplitude of SF3 (Table 1) (see Fig. 3.7). In some areas, the NSMTD exhibits an internally angled strong reflector that may be inferred as tilted blocks that is common deposit associated with gravity-derived sediment transport. (see sub-chapter 3.3).

Late Pleistocene remobilized sediments along salt-related structures are probably corresponded to oversteepenings in association with salt-tectonic activity (Loncke et al., 2009). As a result, Rosetta fan constitutes 30-40% of its thickness composed from the transparent deposits that refers to large slope failures. Mud diapirs have also been observed within this seismic unit.

### **3.2.5. Seismic unit 5 - Mud Diapirs**

In the eastern Mediterranean, especially within the western part, mud diapirs are abundant and are influenced seabed topography (Fig. 3.10.). This SU5 is categorized as SF5 with a caldera-like or cone-like shaped with dimension up to c. 520 ms TWT (832m) (Table 1). This seismic unit which is occurred commonly in SU3 interval is commonly laid at shallow depth and often popped up on the seafloor. Channel-levee system architecture elements are often interfered or disturbed by these features (see chapter 3.3). The occurrence of this seismic unit is often followed by underlying salt-related faults (Fig. 3.10).

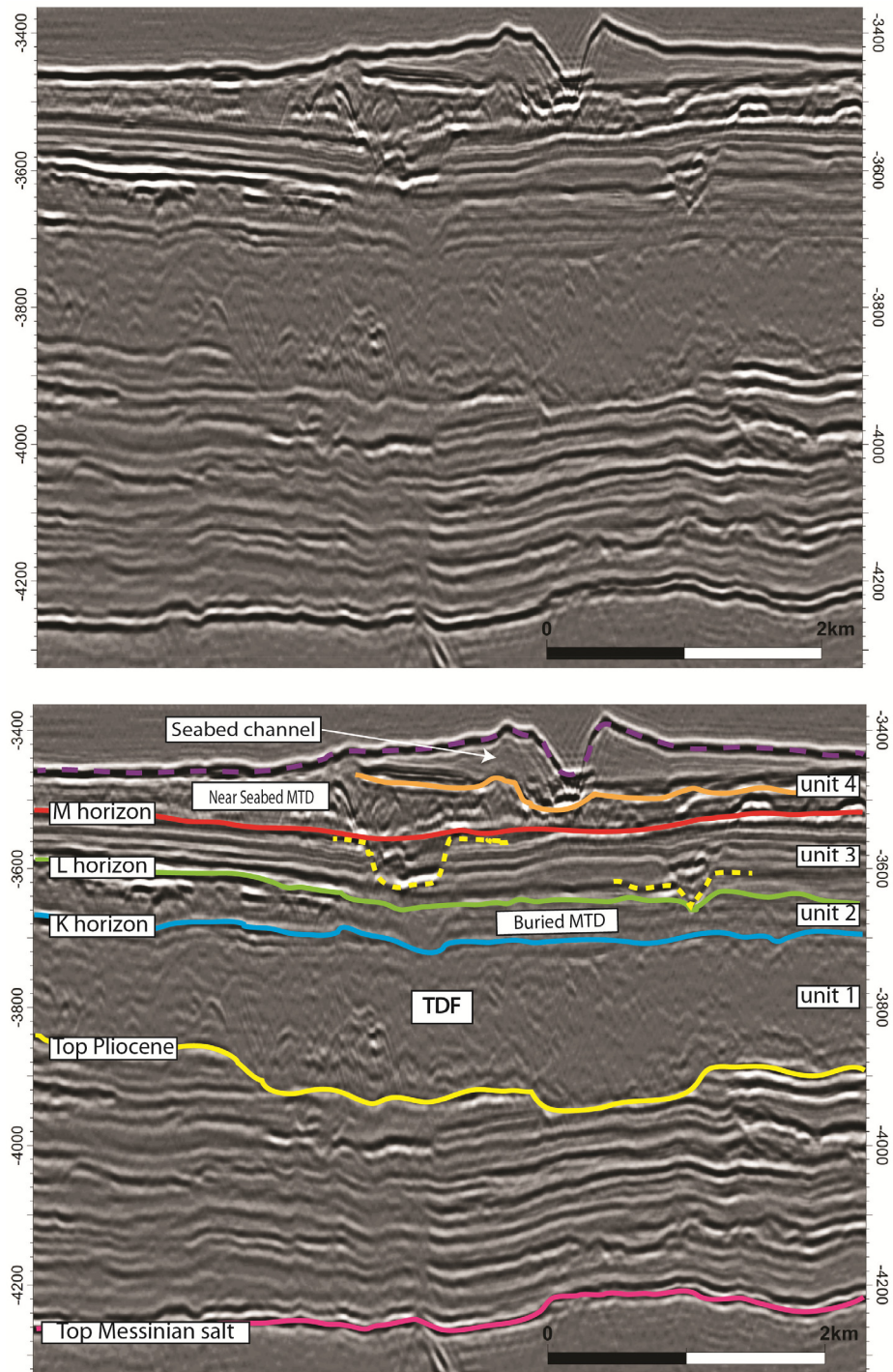
Previous studies, Camerlenghi et al. (1992) and Limonov et al. (1996) have reported that mud diapirs occurrence is even more abundant towards the Mediterranean ridge as considered as the giant accretionary complex with interplay of fault and fold of the African margin. This ridge is a product of collision in the upper part and subduction between the

African plate and the Eurasian plate in the lower part. This complex has experienced thrusting and compressional stress that pressing up the underneath fluid-rich layer. The Messinian salt itself has produced general upslope extension and downslope compression, and therefore mud diapirs have occurred mainly towards the basinward area.

Mud diapirs as defined by Kopf (2002), is fluid-rich or clay-rich sediment that is accumulated in the deep-sea and slowly migrated upwards most likely through narrow weakness zones (e.g. Fault). This deep-seated sediment is commonly released due to increasing compaction and temperature. Milkov (2000) tried to investigate mud diapirs or mud volcanoes worldwide and he came up with a suggestion that mud diapirs can be generated by two main reasons: high sedimentation rate or lateral tectonic compression with plastic clay layer present. Zitter et al. (2005) suggested that this sedimentary features are created where mixed fluid-rich fine-grained sediments often associated with fragments of rock or consolidated mud, are expelled at the earth surface or on the seafloor. As the mud migrates upwards, it disturbs the overlaying sediments and commonly interfered with the existing sediment (Fig. 3.11)

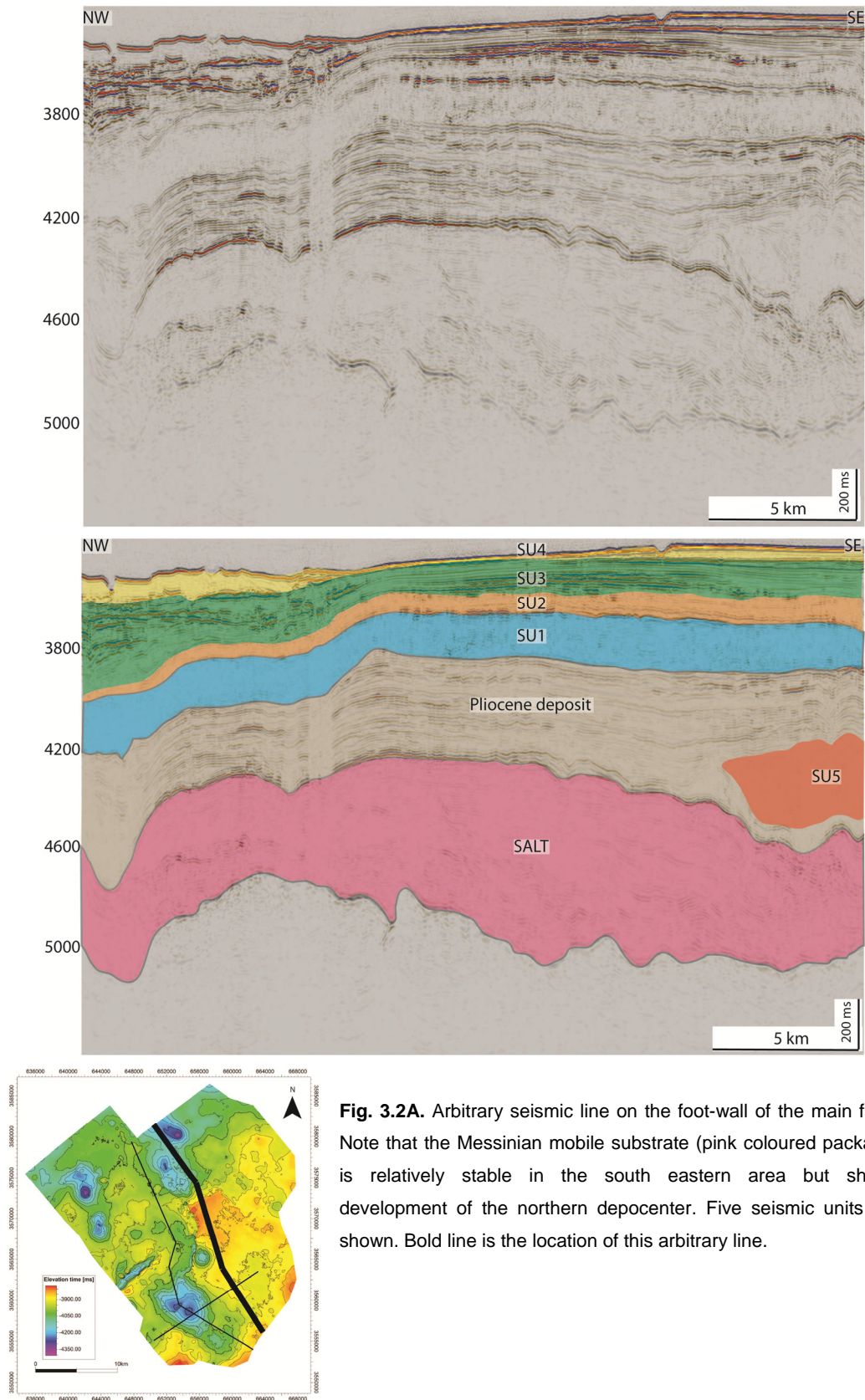
Rapid sediment loading is created under compaction condition and thus possible generates gas hydrates dissociation process. The warm fluids from a great depth migrate upwards and release large amounts of methane. In some area, local HARP can be found which has probably been caused by the gas hydrates occurrence. Gas hydrate within the peripheral of mud volcanoes is indicated to form by metasomatic process driven by a diffusion of methane and mixing with locally driven water (Kopf, 2002).



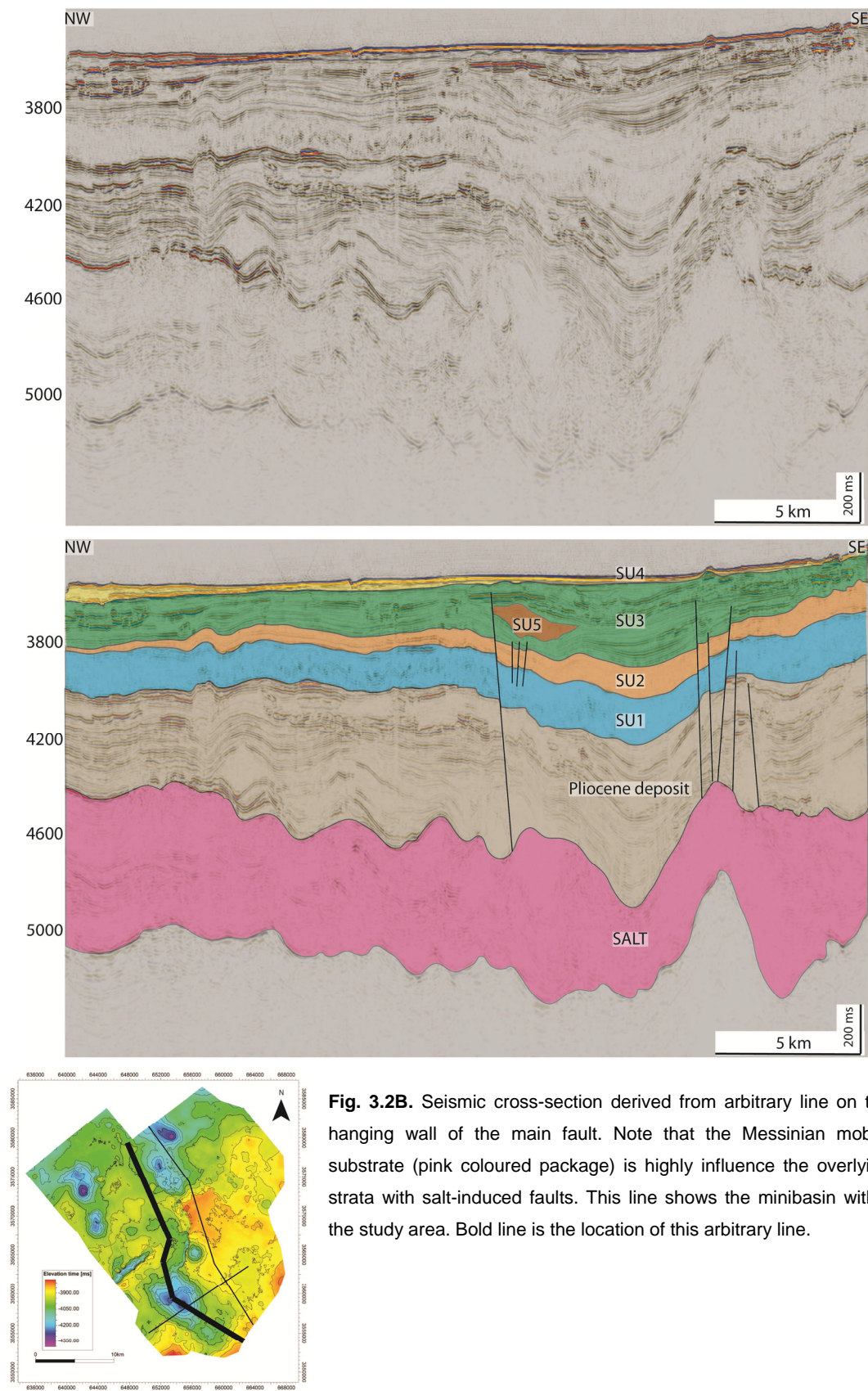


**Fig. 3.1.** Seismic cross section showing five seismic units. The focus of the study is the whole unit above Pliocene deposit which is Pleistocene in age to the present-day deposits. Note the K, L, M horizon are the key horizons as there no well control that can precisely indicate the age within the study area. Top Pliocene horizon and Top Messinian salt horizon is referred to Statoil age interpretation.



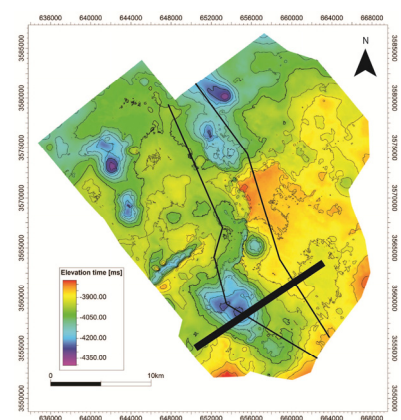
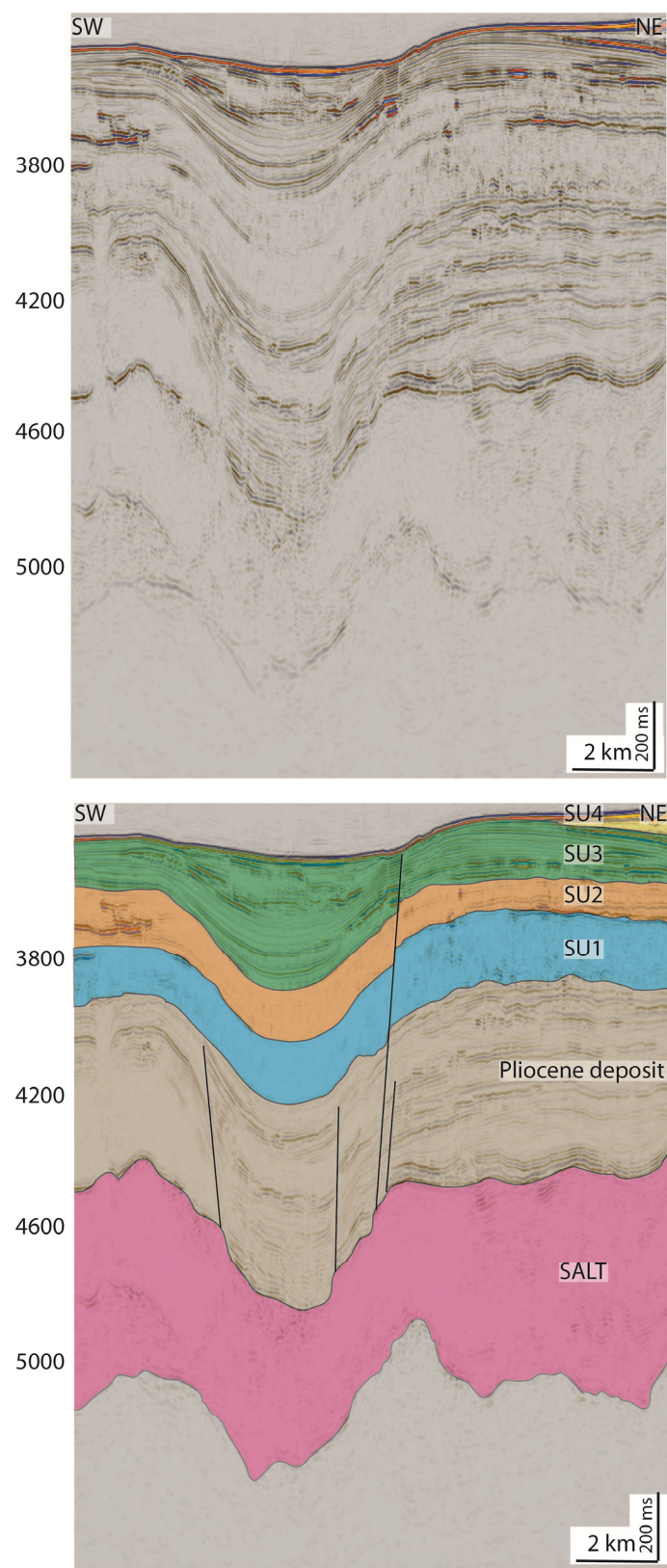


**Fig. 3.2A.** Arbitrary seismic line on the foot-wall of the main fault. Note that the Messinian mobile substrate (pink coloured package) is relatively stable in the south eastern area but shows development of the northern depocenter. Five seismic units are shown. Bold line is the location of this arbitrary line.

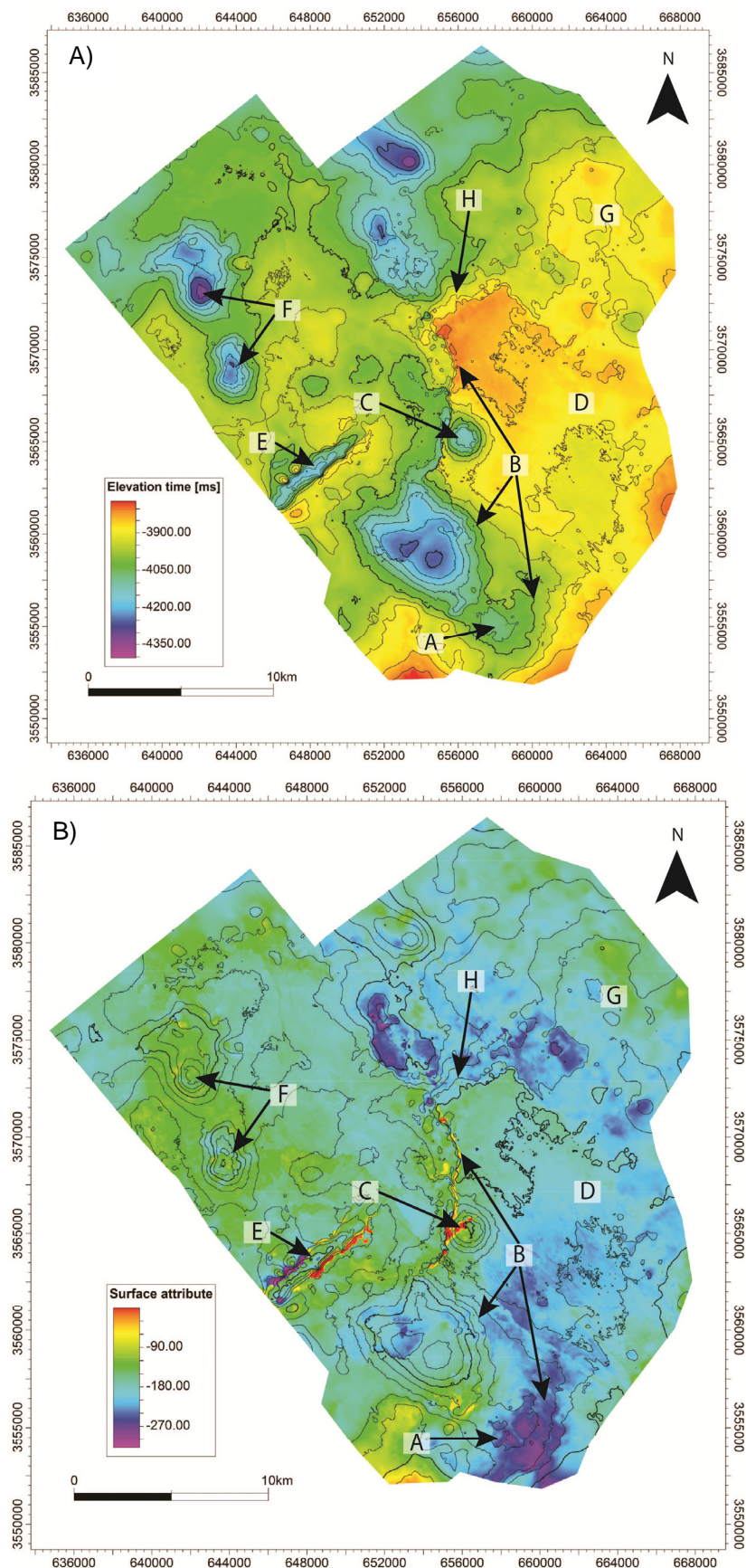


**Fig. 3.2B.** Seismic cross-section derived from arbitrary line on the hanging wall of the main fault. Note that the Messinian mobile substrate (pink coloured package) is highly influence the overlying strata with salt-induced faults. This line shows the minibasin within the study area. Bold line is the location of this arbitrary line.



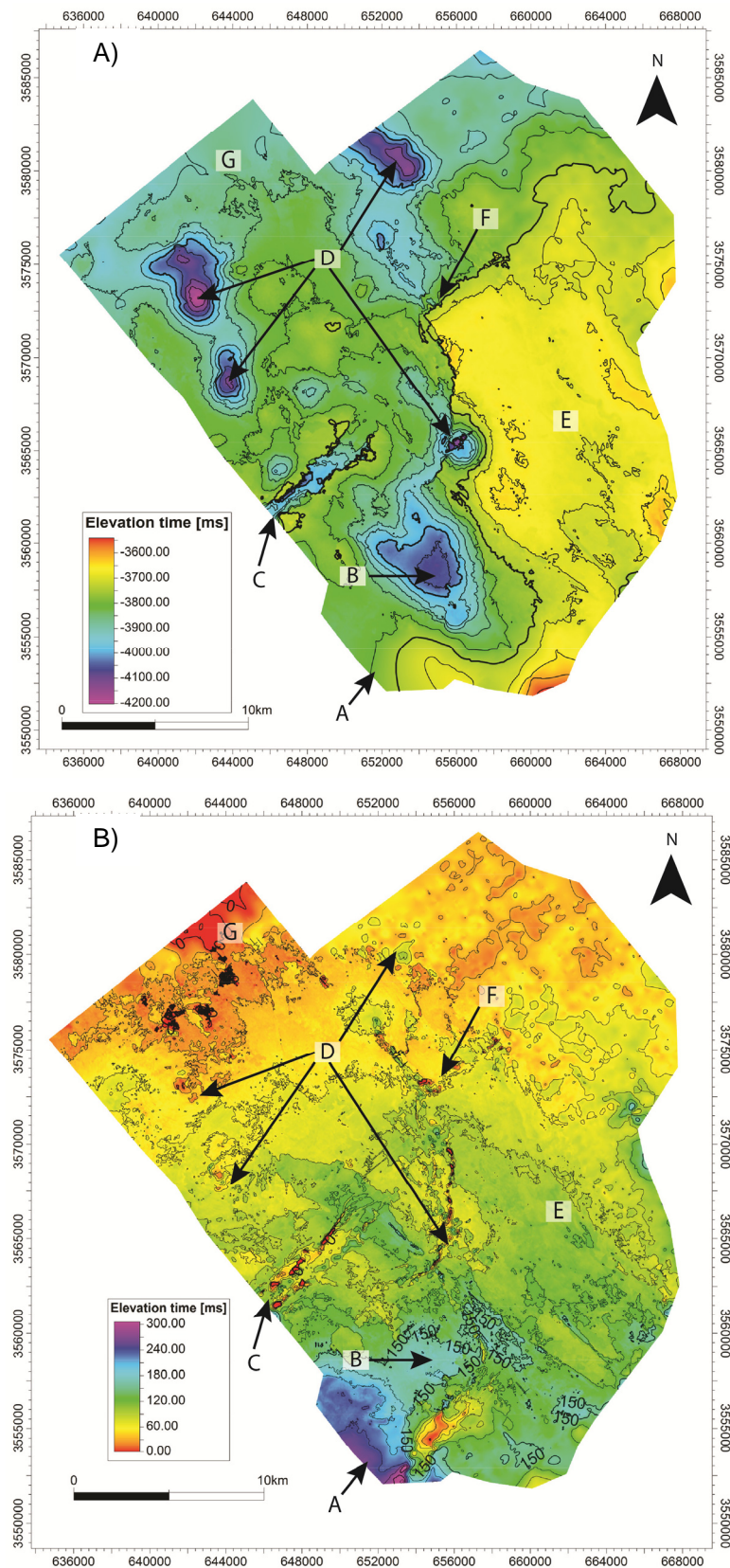


**Fig. 3.2C.** Seismic cross-section which is connecting two previous arbitrary lines showing the main fault, the minibasin and the underlying salt below the five seismic units. Bold line in the map is the location of this arbitrary line.

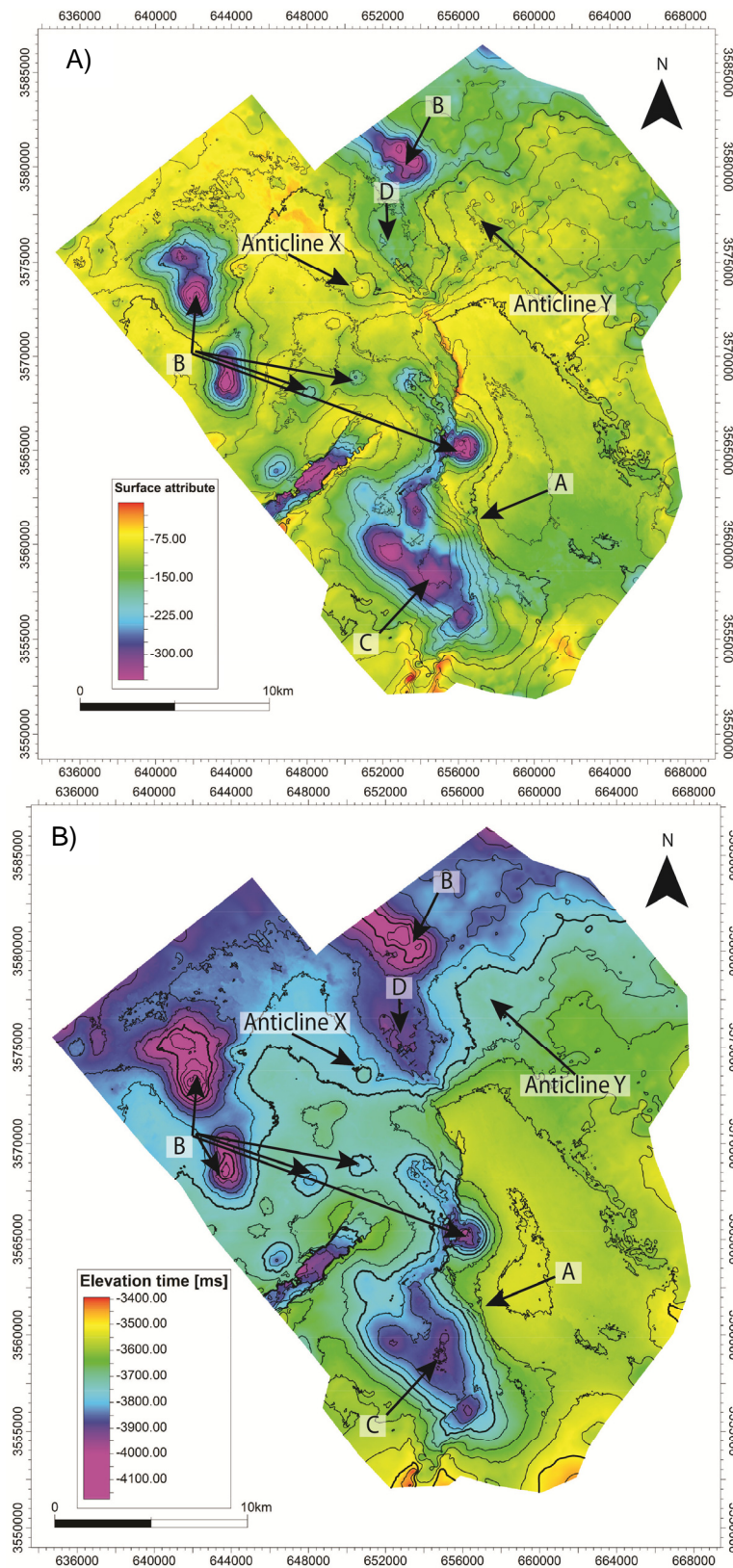


**Fig. 3.3.** A: Map of Top Pliocene (TWT) displaying base of the SU1. B: Isochron map showing thickness distribution of the SU1

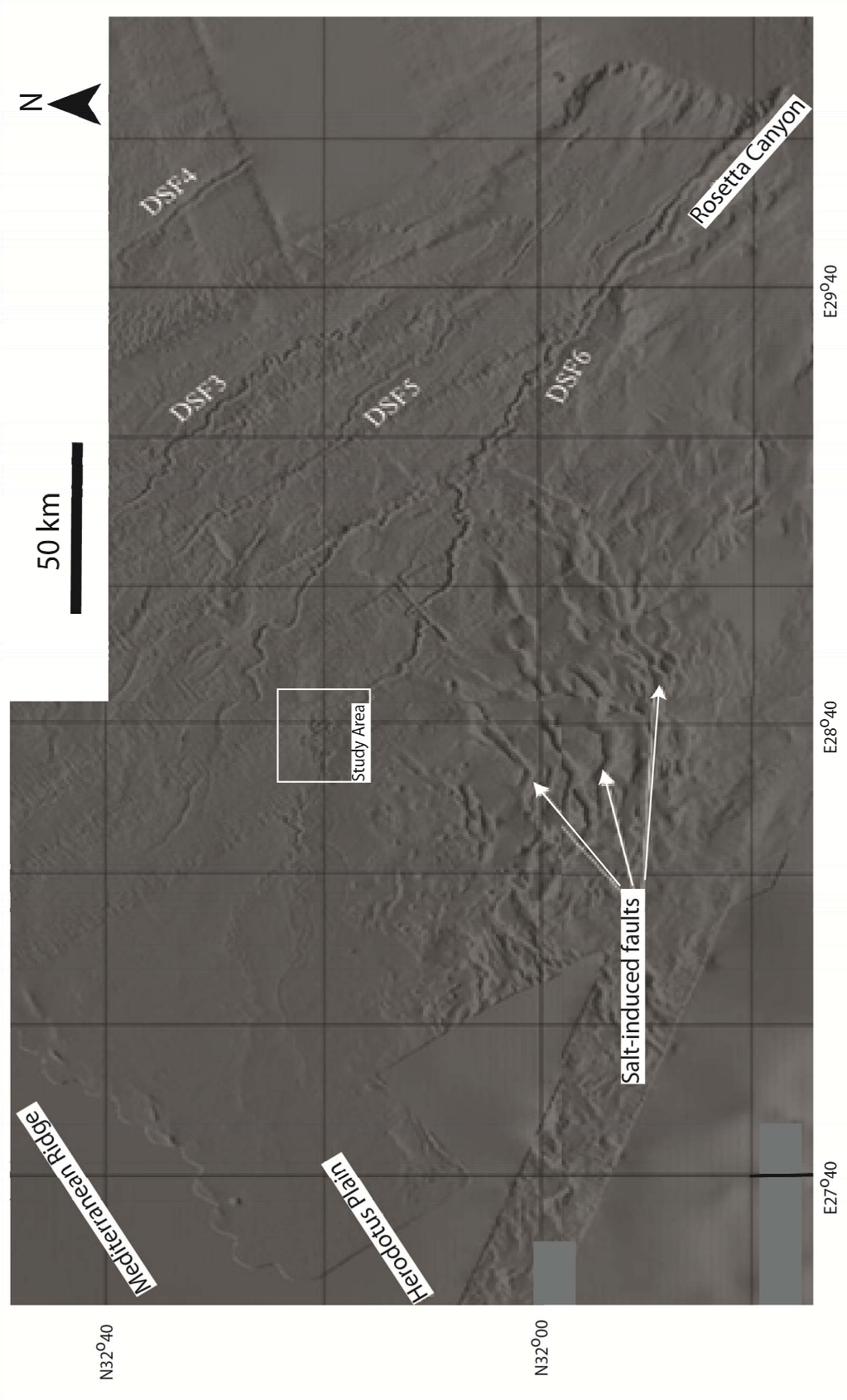




**Fig. 3.4.** A: Map of K horizon (TWT) displaying base of the SU2. B: Isochron map showing thickness distribution of the SU2.



**Fig. 3.5.** A: Map of L horizon (TWT) showing base of the SU3. Note the depression showed in dark colour related to mud diapirs and minibasin development in the southern part. B: Isochron map showing thickness distribution of the SU3



**Fig. 3.6.** Map showing Bathymetry of the western part of the Eastern Mediterranean. Note the location of channel DSF6 and its relative position with the study area. (Migeon et al., 2010).



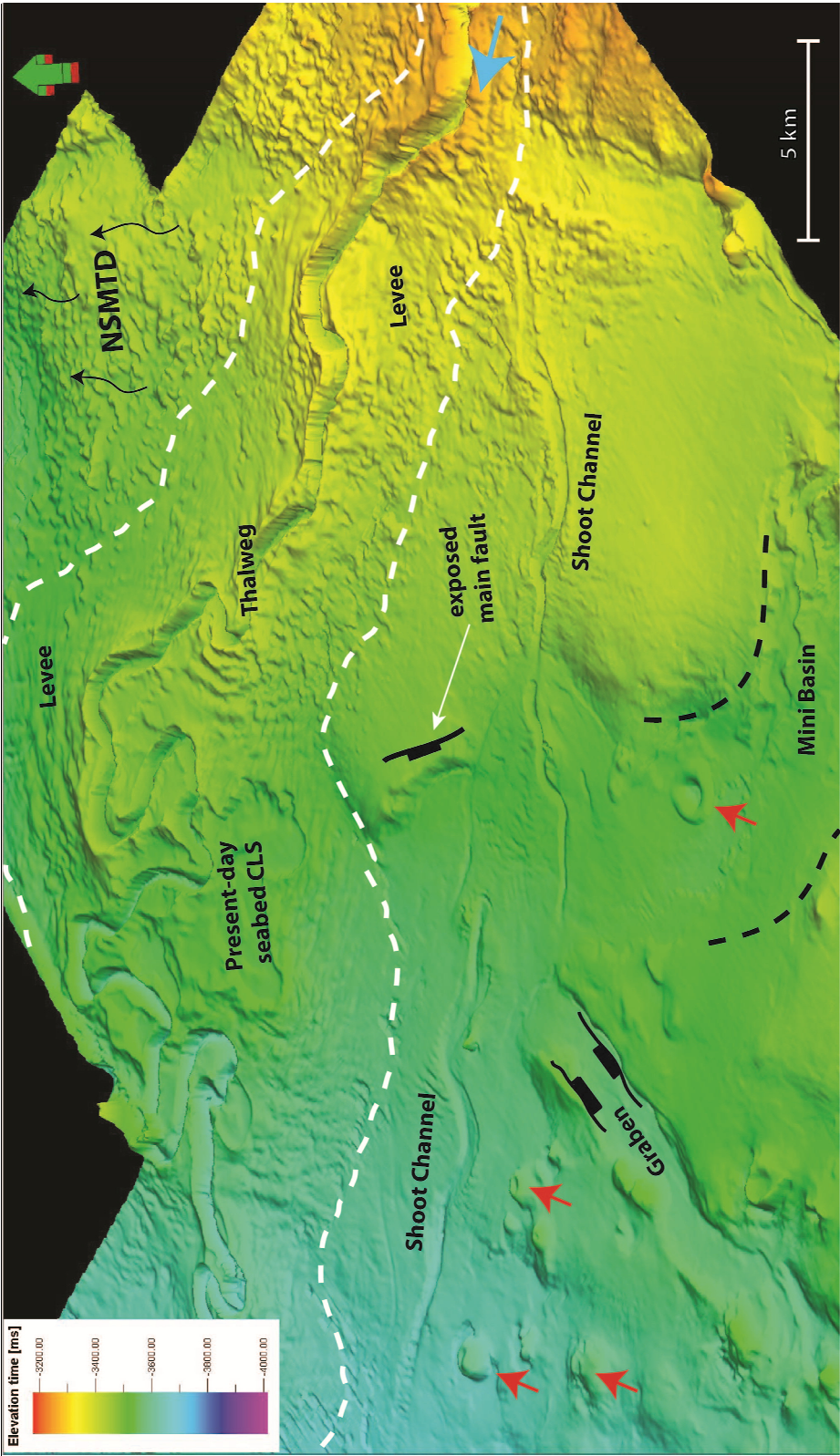
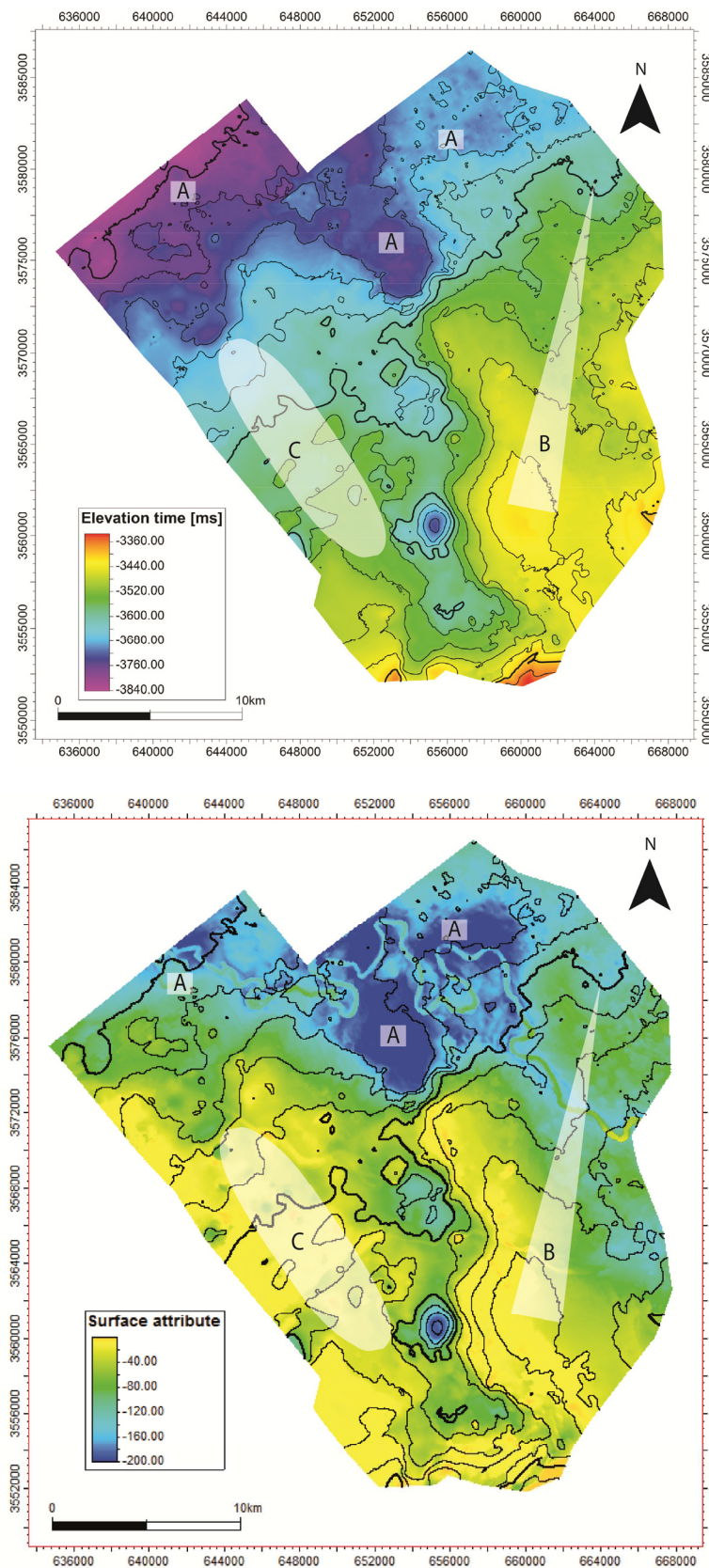
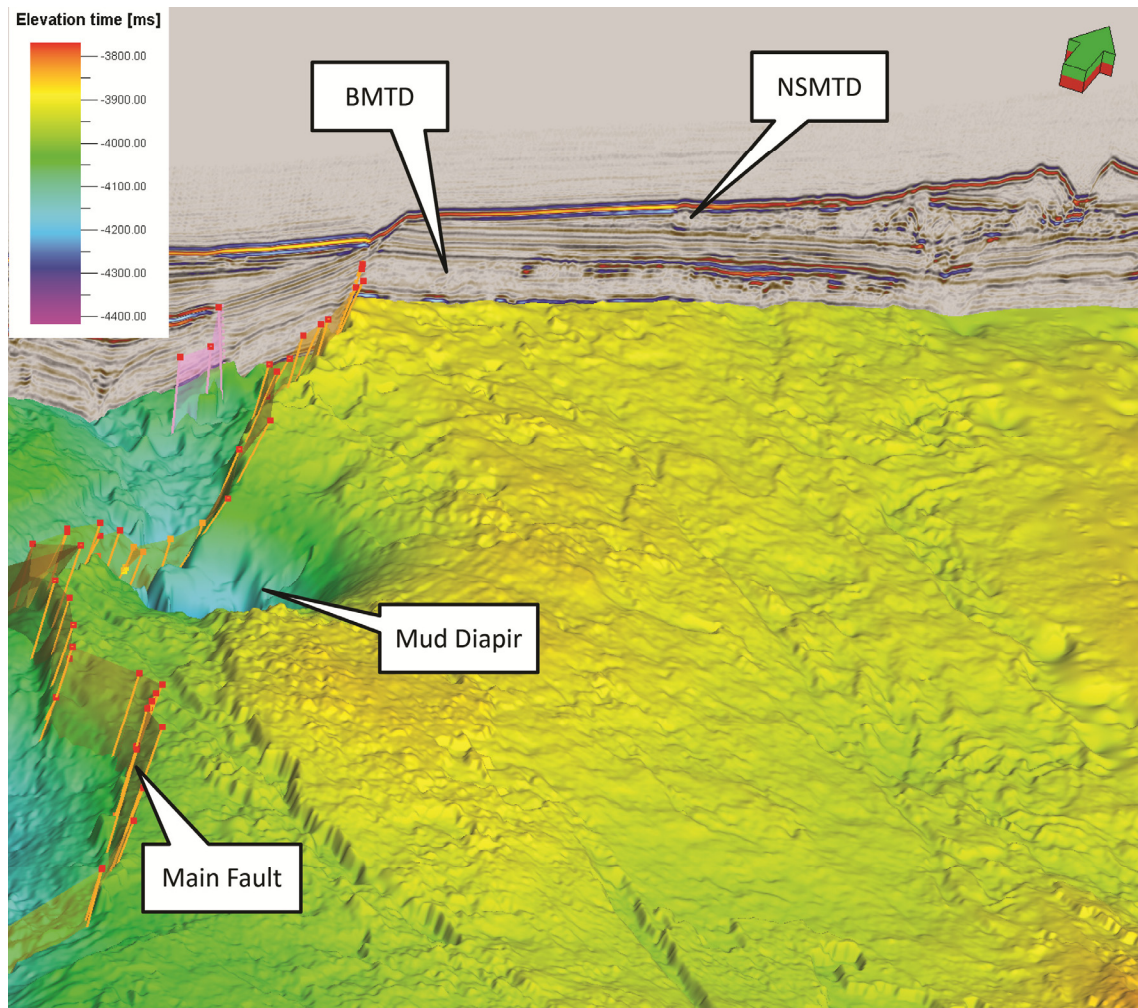


Fig. 3.7. Map above showing current seabed morphology. The red arrows are pointing the mud diapirs location and morphology in the surface. The blue arrow indicates the flow direction of seabed channel-levee. The NSMTD morphology can be traced on the seafloor as the black arrows showing the direction of its flow. The sight is obliquely looking to the north. The direction of present-day channel-levee system is to the northwest following regional slope.



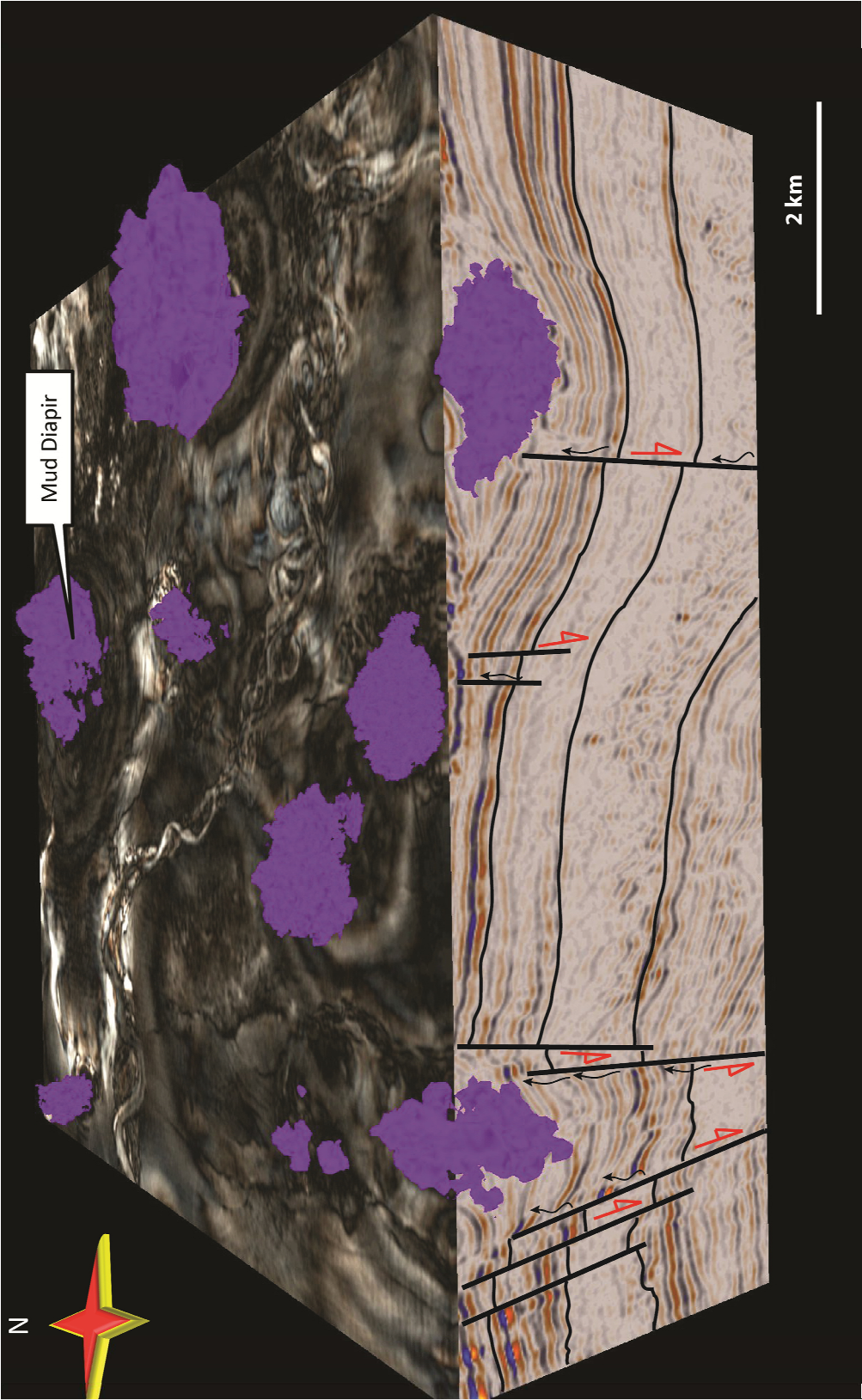


**Fig. 3.8.** A: TWT map of M horizon showing general deepening to north. B: Isochron map showing thickness distribution of SU4 between M horizon and seafloor horizon

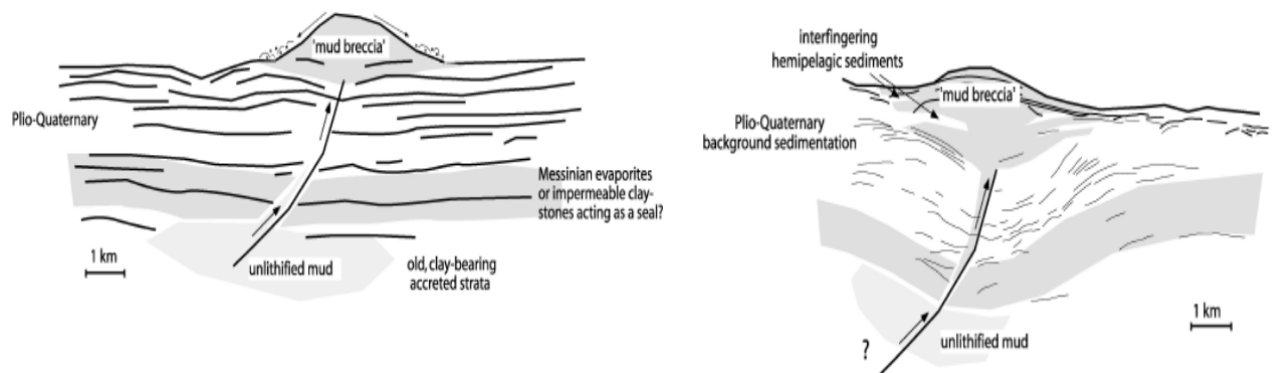


**Fig. 3.9.** Map above showing base of SU2. Note thickness decreasing of NSMTD to the main fault. A round-like depression in the figure refers to mud diapirs. The sight is obliquely looking to the north.





**Fig 3.10.** Picture above displaying mud diapirs (purple color) in the study area and its position to the CLS A which is showed in RGB colour blend map. Red arrow is indicated the fault movement. Black arrow showing the inferred mud diapirs migration pathways.



**Fig. 3.11.** Model above showing the migration pathways of mud diapirs (Modified from Kopf, 2002)

### 3.3. Seismic Geomorphology

The morphology of channel-levee system and mass transport deposit is described in this sub-chapter. High-resolution 3D seismic study combined with spectrally decomposed and colour-blended seismic volume visualization provides an opportunity to examine the morphology of subsurface deposits. Seismic geomorphology has been found to be useful tools for understanding the detailed architectural development and variation of submarine channel. The channel-levee systems that are described here show different morphology that can be related to the process involved as well as the local slope tectonic settings. Sinuosity degree, thalweg incision depth, isochron thickness and channel gradient is quantified to aid understanding of the processes controlling the morphology and evolution of channel-levee systems.

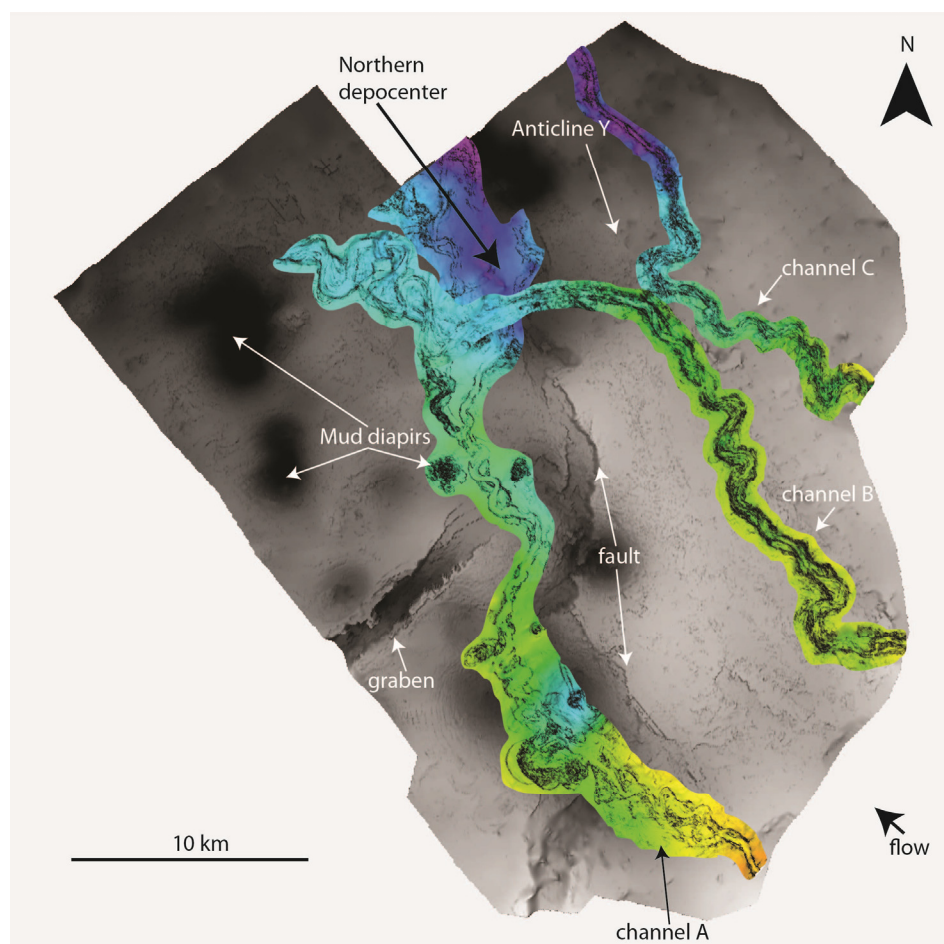
Three main channel-levee systems labelled A, B, and C, are recognised within the study area (Fig. 3.12). Each channel-levee system provides an opportunity to quantify the morphology systems over distances of 10's km and to attempt to understand the factors controlling them. CLS A provides an example of the interaction of channel-levee system with minibasin growth due to faults in the east and also development of channel avulsion in the lower reach. Abundant mud diapirs are thought to influence the levee morphology of CLS A. CLS B gives an insight into morphology variation in the upper, middle, and lower reach. The opportunity to relate channel-levee system architectural changes related to sinuosity and slope profile is offered by examining CLS C. Mass transport deposit will be described in the last sub-chapter to understand the internal morphology and depositional style. The interaction and development of channel-levee systems and MTD within the study area is investigated to gain a clearer understanding of gravity-related deposits within continental margins.

#### 3.3.1. Channel-levee system A

The course of CLS A is influenced by a series of faults growth and mud diapirs (Fig. 3.14). The whole CLS A which is captured within the study area is about 32 km with a varying degree of sinuosity along the course. As described in the previous chapter, CLS A constitutes 3 main reaches: the upper, middle, and lower reach respectively (Fig. 3.14).

The upper reach is characterized by HAR channel-fill (SF1a) and low amplitude levee deposit (SF2). The system displays low sinuosity ( $<1.1$ ) or can be considered effectively a straight channel (Fig. 3.16). From channel thickness distribution (Fig. 3.13b), the upper reach shows relatively the same thickness variation alongside the channel-levee system. The CLS A shows a U-shaped cross-section and deep channel-fill incision with an average of 60 ms TWT or 95 m (Fig 15a). The channel-fill thickness exhibits relatively the same thickness

along way down the reach (Fig. 3.16). Average levee thickness is about 38 ms TWT or 60.8 m with levee thickness decreasing but showing increase in width.



**Fig. 3.12.** Combined TWT and variance amplitude map showing all channel-levee systems within the study area. The distal reach of channel A is lower than channel B. Black colour indicates deeper topography.

The middle reach consists of a proximal and a distal part with a channel length of 10 km and 9 km respectively. The proximal part of the middle reach is characterized by stacked CLS A within minibasin setting, whereas the distal part is identified as a single CLS A with high incision (Fig 3.14). The mud diapirs are commonly occurred in the middle reach where salt-related faults are abundant. Its distribution is shown in a black colour in the variance attribute maps (Fig 3.14) and as a significant increase in thickness in the isochron thickness map (Fig 3.13a).

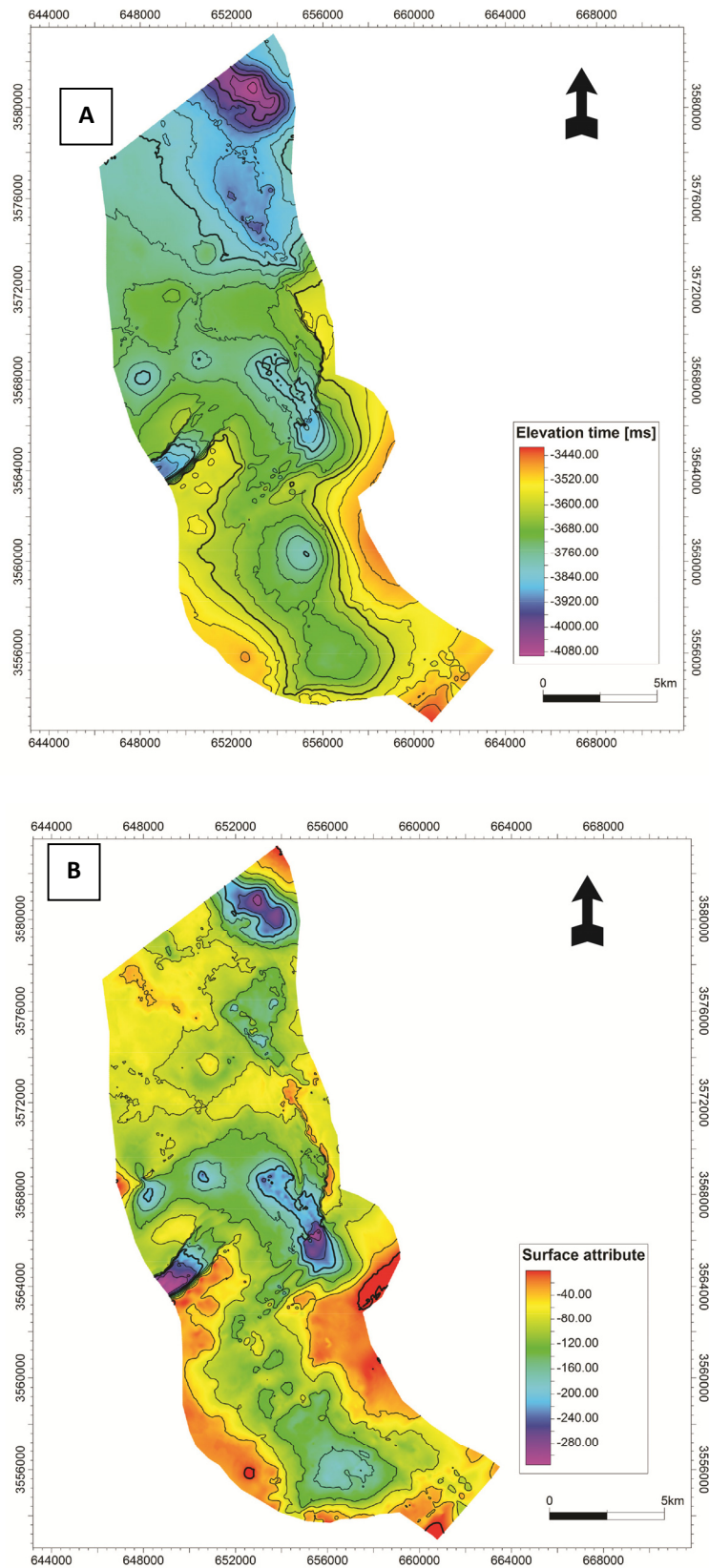
The onset of minibasin starts at km 4 and has a dimension of about 8 km long and 4 km wide (Fig. 3.16). In amplitude and RGB colour blend attribute maps, only in this particular reach the CLS A shows a meandering growth with a range of sinuosity of 1.7 to 2.2 (Fig. 3.18). The CLS is observed to laterally and aggradationally migrate eastwards towards the

fault zone (Fig. 3.15B). Channel-fill within this part constitutes low to medium amplitude reflection and occasional HARs (SF1a). The thalweg incision profile within this reach is steep at the beginning and then followed by a gentle profile in the centre of the minibasin. Levee morphology exhibits generally asymmetric development, wider in the west (up to 2 km with a height of c. 40 m) and narrower towards the east or even eroded by the overlying CLS A (Fig. 3.16, Fig. 3.15B). At km 13, the CLS A had completely fulfilled the minibasin and entered a steep slope profile (Fig 3.16). This point marks the end of the proximal part of the middle reach.

CLS A within the distal part of the middle reach exhibits a different architectural style from the proximal part. The first 4 km has a low sinuosity degree (1.1) and only a single channel development with a minor lateral migration (Fig 15C). SF1a dominates the infill along the whole length within the distally middle reach. The levee architecture shows an increasing thickness of up to 100 m and internal layering of SF2. The next 5 km of CLS A constitutes SF1a with a higher sinuosity (1.2-1.4) and a thicker channel with evidence of aggradation (Fig. 3.16). The levee system exhibits increase in width with a significant thickness increase on the eastern side due to fault growth in the east (Fig. 3.16, Fig.3.17). Mud diapirs development appears to have disturbed the levee architectural style (Fig. 3.17). The levee's internal morphology exhibits a folded layering to the mud diapirs suggesting the channel-levee system has developed before the deposition of mud diapirs (Clark and Cartwright, 2011)

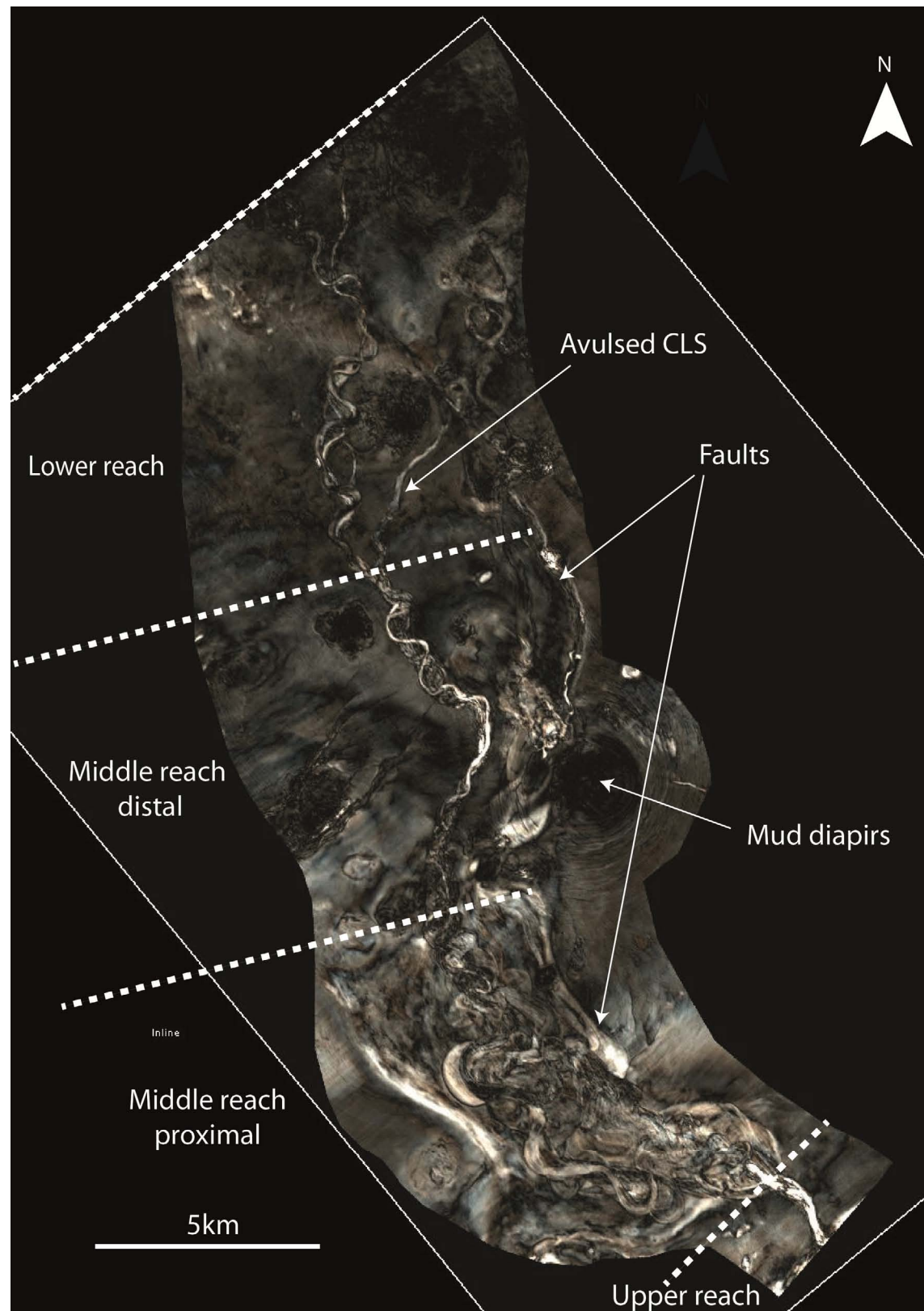
The lower reach of CLS A starts at km 22 and marks the most distal part of the study area. Right at this point the CLS A avulsed to the east and created a new channel-levee system. The avulsion point of the CLS A coincides with the position of anticline 1 (Fig. 3.15D). From the thickness map, it can be observed that the anticline is thin over its crest while the sequence containing the CLSs flanking the anticline displays increasing in thickness (Fig.3.13B). The avulsion channel is characterized by a gradual change from low to high gradients and thus, the channel-levee system shows effectively straight channel (Fig. 3.14, Fig. 3.16). It is composed of SF1a and exhibits a narrow U-shaped channel with a deep incision (Fig. 3.15E). The levee width within this part drops to c. 500 m on both sides with an average thickness about 50 m. The main CLS A in the western part within the lower reach is approximately 10 km and has a fairly low gradient with evidence of aggradation (Fig. 3.16). The CLS shows dominantly SF1a with a range of sinuosity (1.2-1.7). The levee width shows an overall decrease along the course down to 250 m with a thickness of about 30 m.



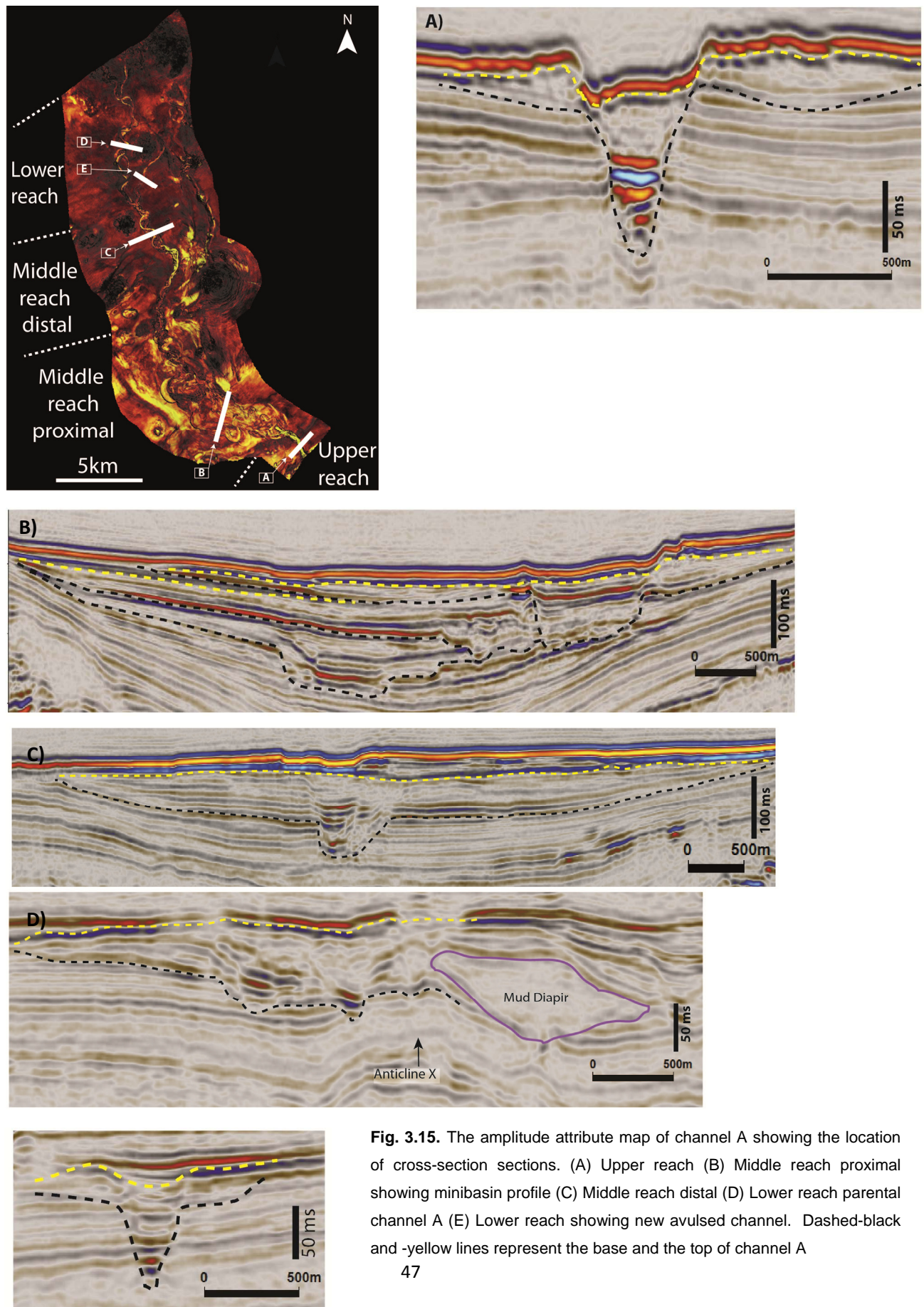


**Fig. 3.13.** (A) Map showing base of channel A (TWT). (B) Thickness map of channel A

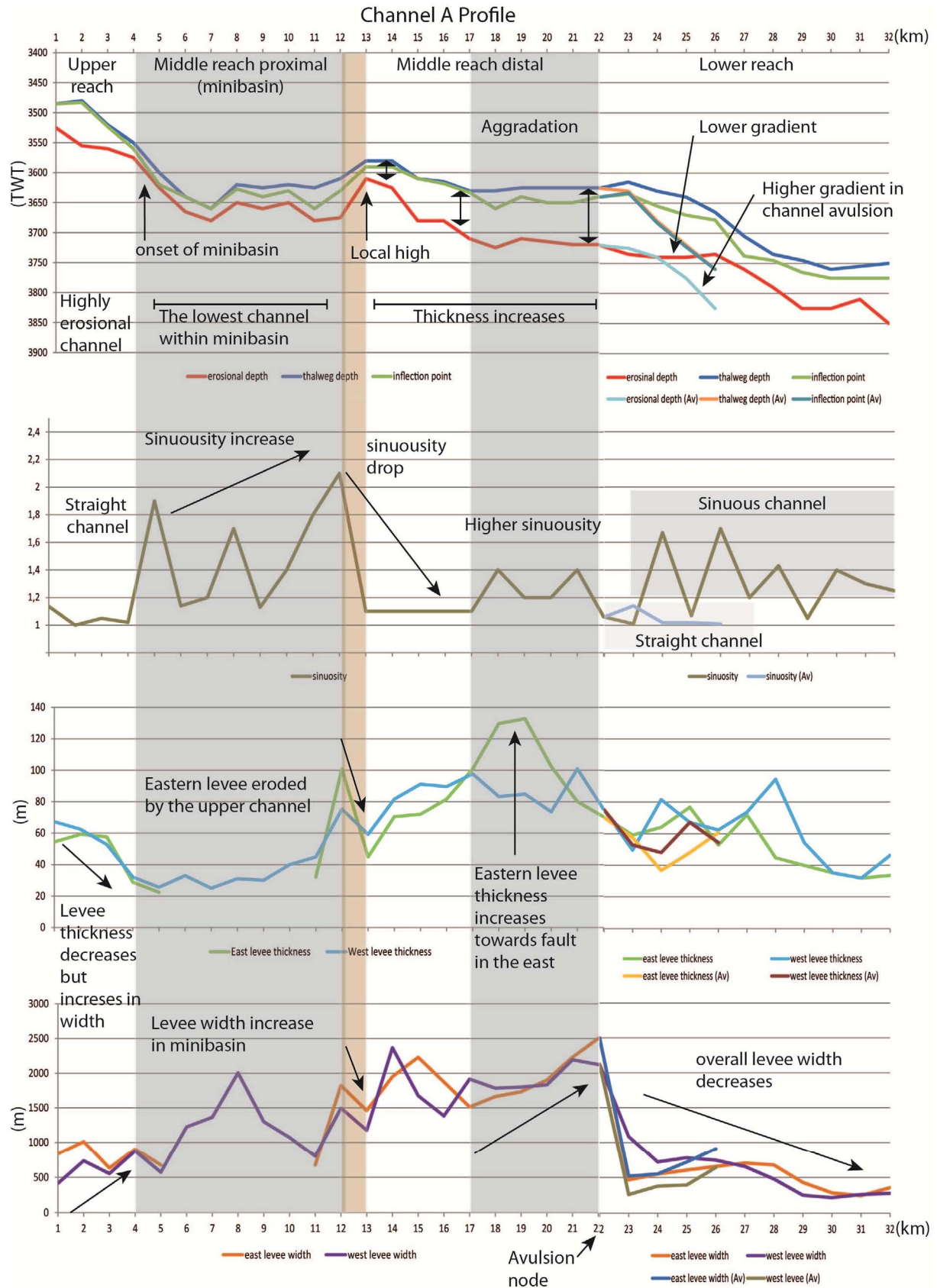




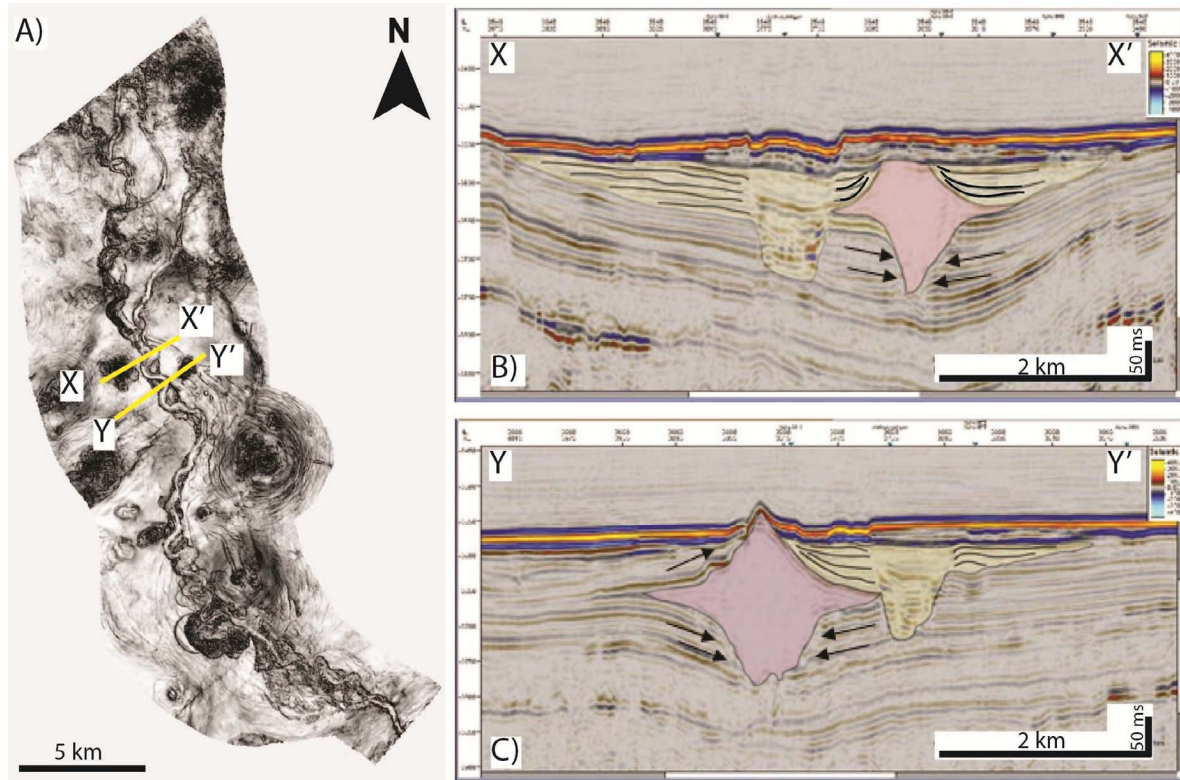
**Fig. 3. 14.** RGB colour blend attributes map of channel-levee system A.







**Fig. 3.16.** Chart showing channel A profile. See text for details.



**Fig. 3.17.** A: Variance attribute map of Channel A. Note the location of seismic lines.

B and C: Cross-section showing example of channel-levee system interaction with mud diapirs.

### 3.3.1.1. Channel-levee system development within the minibasin

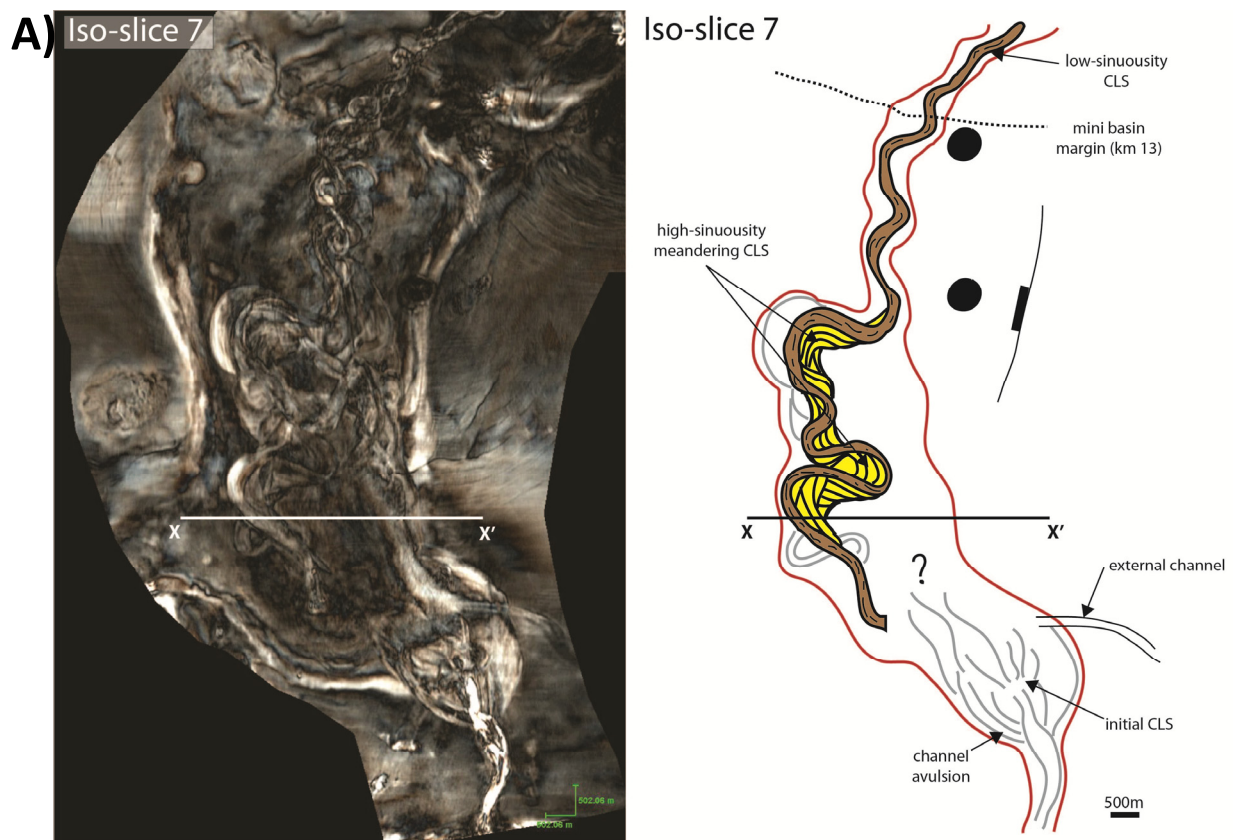
The proximal part of the middle reach comprises a minibasin that is formed as a result of fault growth in the eastern side. The CLS A development can be examined using iso-slice techniques in RGB colour blend attributes cubes. From top to base horizon, CLS A package is divided into 8 horizons to see morphology changes within the minibasin. The isoslices used in this study were chosen based on the clarity to visualize CLS architectural and development on colour blend maps.

In iso-slice 7, the CLS A initially shows complex amalgamated channel elements. This part is characterized by relatively straight to anastomosing channel. It is probably related to change in slope gradient prior to the minibasin which is marked the transition from initial channel incision to more depositional system (Fig.3.18A). Similar development has been found in other channel-levee system in offshore Nile delta and is thought to represent a period of relatively high-frequency gravity-flow deposition (Cross, et al., 2009).

Although the continuation is slightly unclear within iso-slice 7 view, the main channel-levee system starts to be developed and laterally migrated. Further downslope, the channel displays meandering with evidence of lateral accretion package (LAP) signature (Fig. 3.18A). As the channel approaches the minibasin margin, the sinuosity increases and follows the

channel-levee system architectural changing into an effectively straight channel (Fig 3.16). In iso-slice 6, the continuation of CLS A is more visible (Fig. 3.18B). In seismic cross-section, the levee is found to be thinning away from channel axis or occasionally onlapping to the minibasin margin (see Fig. 3.15B).

The CLS A kept its meander within the centre of the minibasin and is appeared to shift towards the east approaching the fault zone suggests that the growth of CLS A is significantly developed in the western side of minibasin (Fig.3.18C). An external channel is appeared to supply sediment from outside the minibasin and developed a frontal splays with finger-like morphology (Fig. 3.18C). Iso-slice 2 represents the final part of the CLS A development. The CLS A is obviously migrated to the eastern part of the minibasin adjacent to the fault zone (Fig. 3.18D). This last interval of CLS A is characterized by high sinuosity but is shown significantly reducing the meandering level.



**Fig. 3.18.** Maps showing RGB colour blend attribute maps and the interpretations.

Iso-slice 7 and iso-slice 6 is the lower most iso-slice providing the clearest image to be interpreted.

Iso-slice 4 and 2 is the next upper slice within the minibasin. (see Fig.3.19 to see the seismic cross-section)



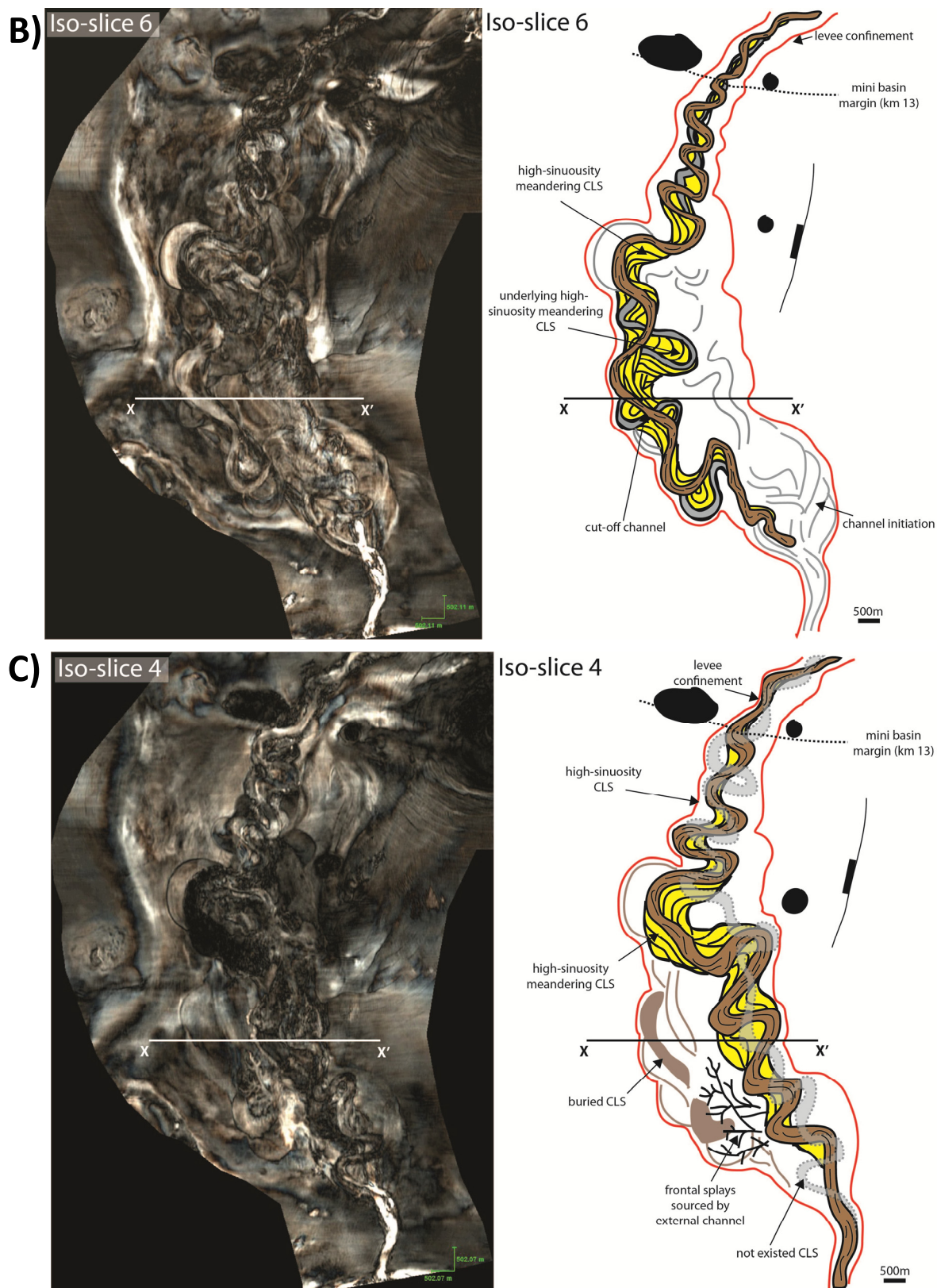


Fig. 3.18 (Continued)

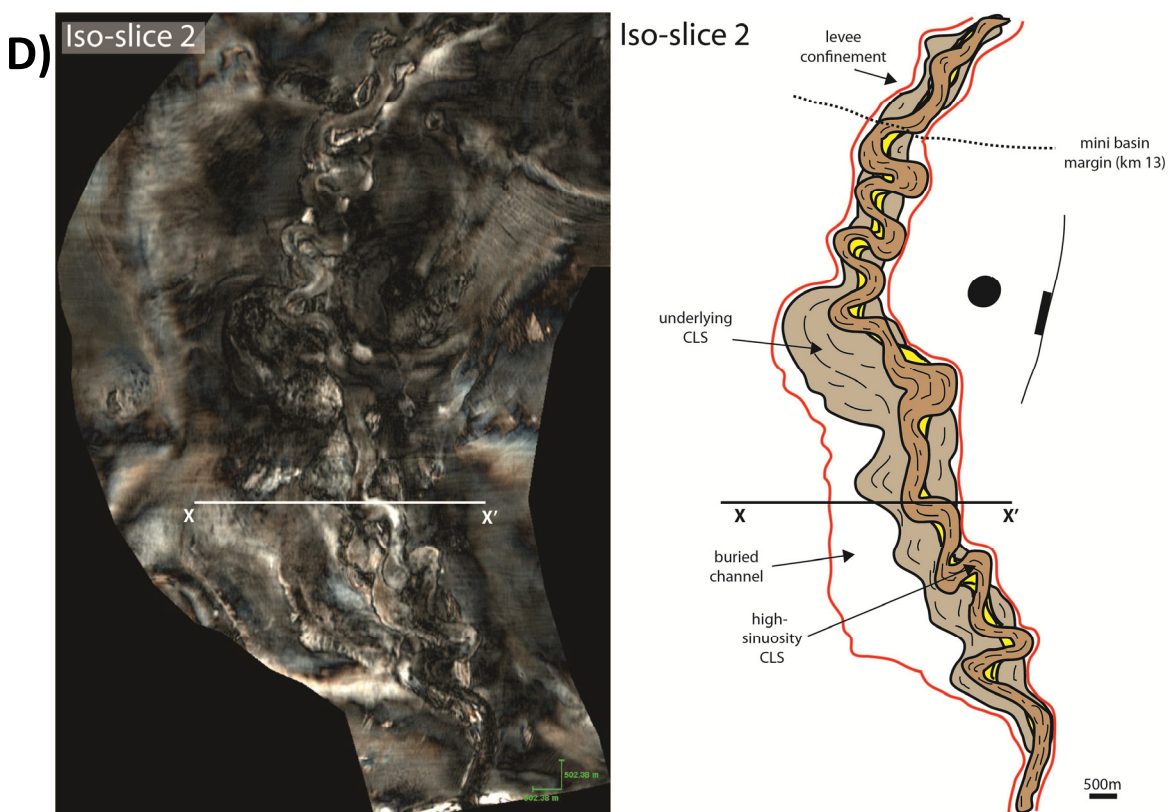
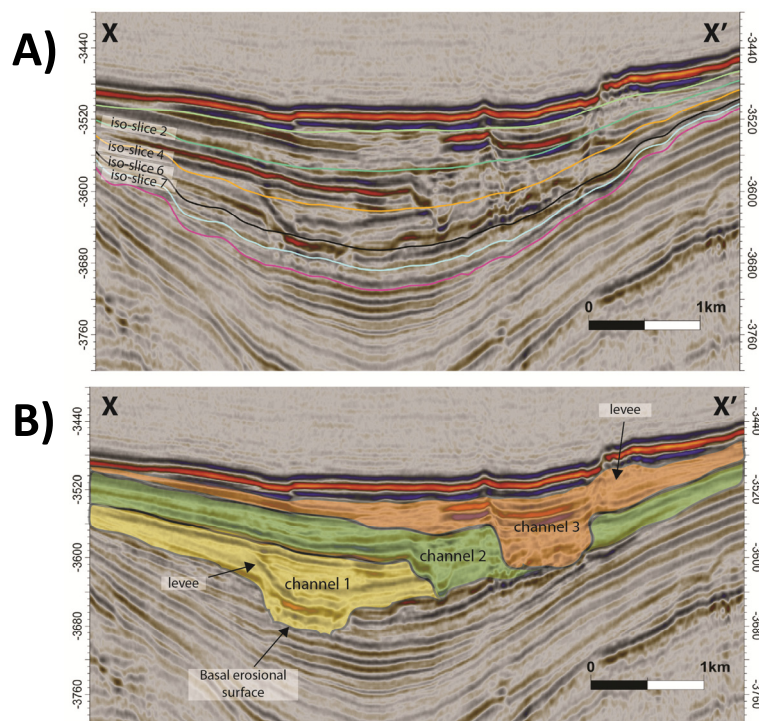


Fig. 3.18 (Continued)



**Fig. 3.19.** (A) Seismic cross section showing position of iso-slice 7, 6, 4, and 2. (B) Figure showing channel-levee system A development within the minibasin and thalweg lateral and upwards migration.



### 3.3.2. Channel-levee system B

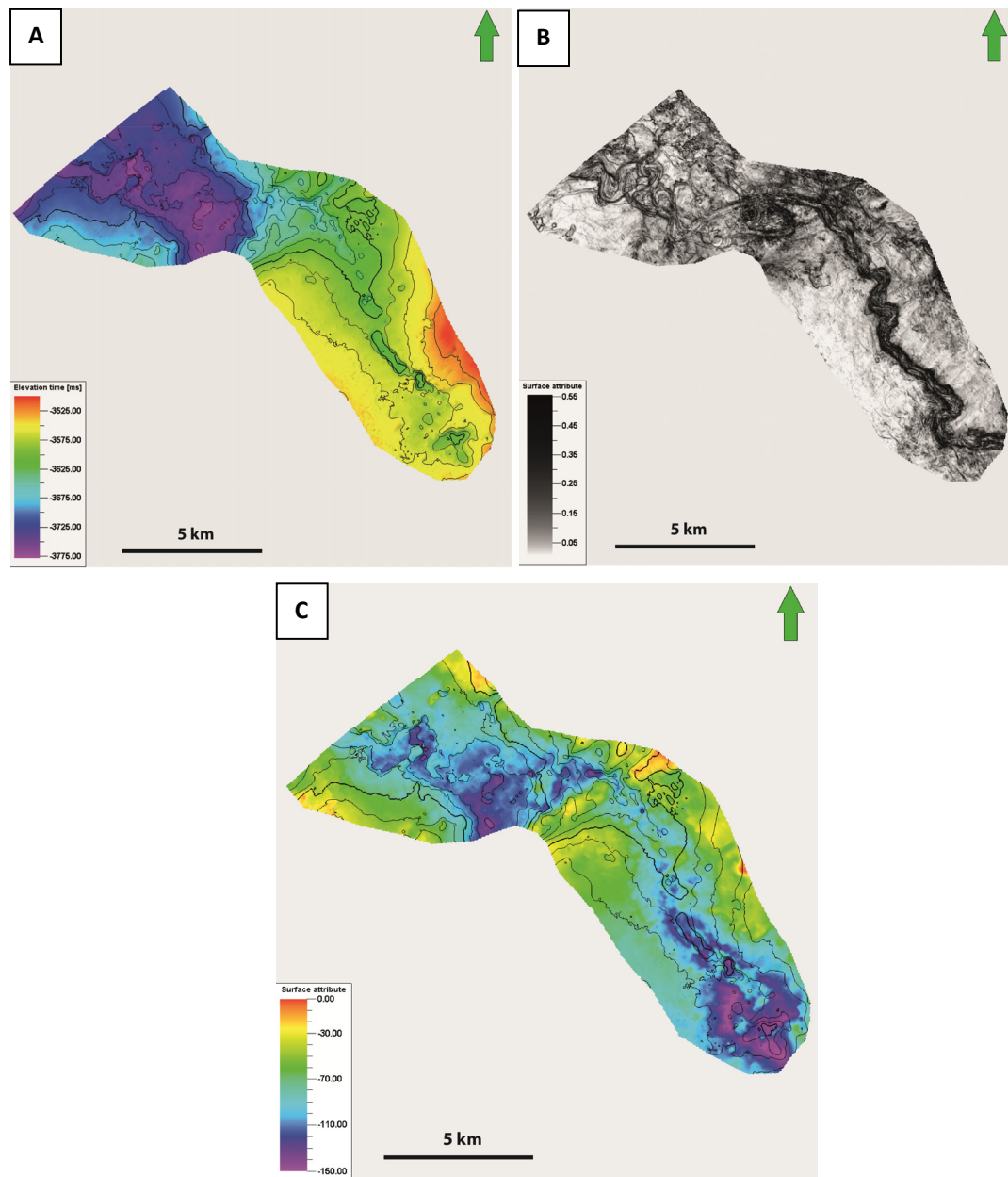
The CLS B comprises of three main reaches: the upper, middle, and lower reach of approximately 32 km and shows various degrees of sinuosity with an average of 1.4. The upper reach marks the first 17 km and exhibits occasional moderate sinuosity (up to 1.6) in relatively gentle slope gradient (Figs. 3.22, 3.23). The channel-fill thickness decreases along the course with evidence of a high incision profile (Fig. 3.21A-C, Fig. 22). The channel B has eroded the underlying fan lobe deposits (SU3) and marked obvious changes from SF3 to SF1b. The variance attribute map illustrates a darker colour within this erosional fairway suggesting a deep incision and a highly erosive channel that is confirmed by a significant gap between the inflection point and the erosional depth along way down the course (Fig. 22, Fig 3.21B). The near-seabed MTD (NSMTD) is overlain the upper part of this channel-levee system and has thus resulted in an interference with the levee system. Accordingly, it is not very easy to observe its morphology. This NSMTD has occasionally reduced the levee thickness or even eroded the levee entirely (Fig. 22).

High amplitude packages (HARPs) are significantly found in the lower part of the inner bend levee and occasionally occurred as minor deposit in the outer bend levee (Fig 3.21C). Levee measurement exhibits a variation in thickness and width distribution along the upper reach of CLS B due to its sinuosity variation. The increase in sinuosity is commonly followed by an increase in levee thickness in the outer bend of CLS and shows asymmetrical width which is slightly narrower in the inner bend (3.21C). The inner bend levee thickness is an average of 70 m and the outer bend levee may reach up to 100 m.

The middle reach starts from the 17 km to the next 5 km of CLS B and exhibits an effectively straight channel (Fig 3.22). The CLS B is located in a steep slope gradient as shown in TWT map as significant different in depth colour (Fig. 18A). Higher topography is laid in the southwest and in the north of CLS B which generates a major bend of CLS towards the northwest (Fig. 3.21D). The channel inflection point between thalweg and the erosional depth within the channel profile graph shows major changes, which suggests a transition from degradational to aggradational channel-levee system. This transition affects the channel-levee system architectural style and the morphology and displays key changes from dominantly cut into older stratigraphy to constructional levee development fulfilling the depositional accommodation space (Fig. 3.21A,E, and G). The present-day channel-levee system has overlain the CLS B in the northern depocenter suggesting preferential of both channel-levee systems to be deposited in a depressed area (3.21D).

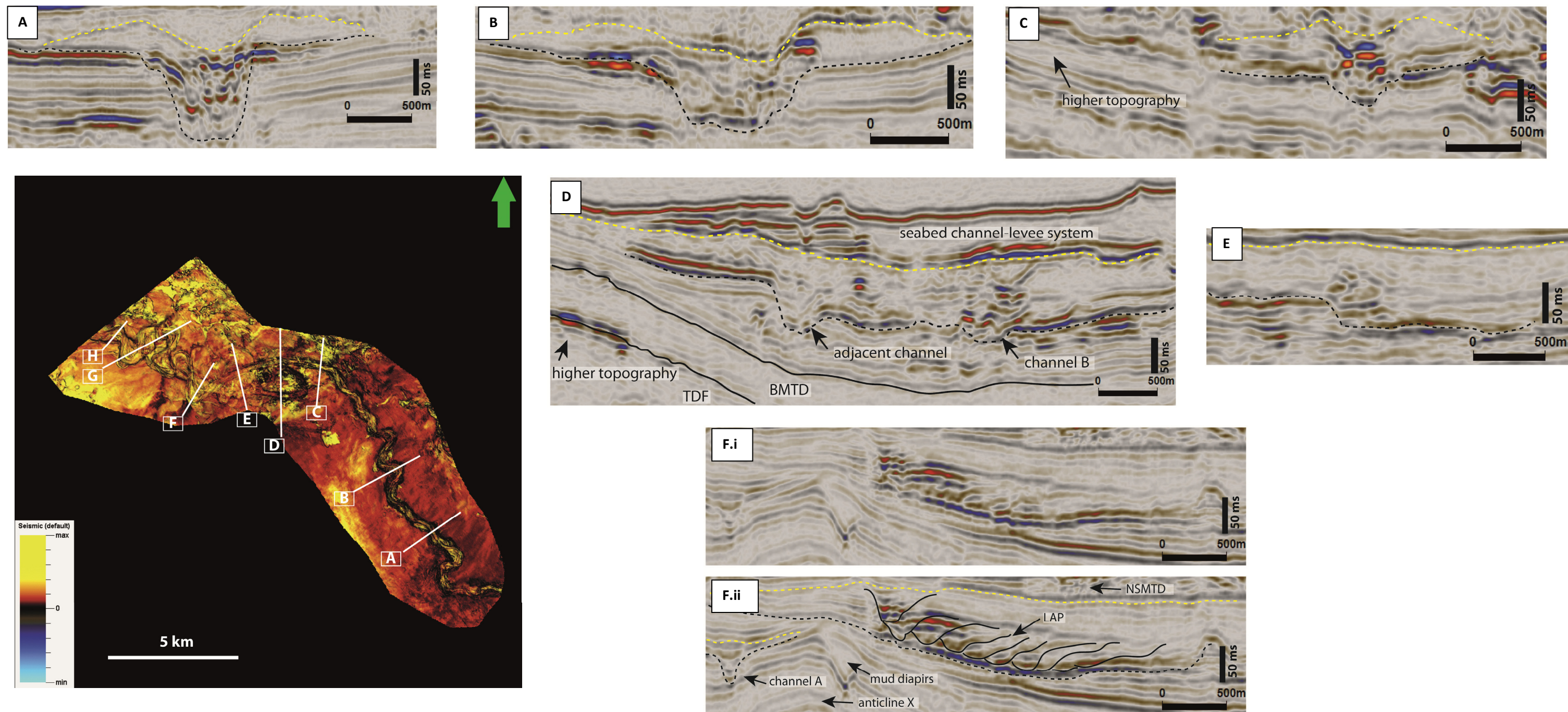
The CLS B from km 22 to the end range within the study area shows high meandering with evidence of lateral and aggradational migration (Fig.21 F-H). The sinuosity degree marks the highest value (2.4) of all the reaches within the CLS B. At the beginning of

this reach, the sinuosity increases and the channel system starts to meander as the base of CLS shows relatively flat topography. The channel erosional and thalweg depth display relatively similar thicknesses along way down its course (Fig. 3.22). This depositional style suggests that this lower reach is characterized by more aggradational rather than erosional channel-levee system (Fig 3.21F-H). Lateral accretion package can be found within this reach suggesting highly meandering CLS (Fig 3.21F, G, and H). The levee system is followed the channel growth and built aggradationally in the upper part of sinuous channel development (Fig 3.21G).

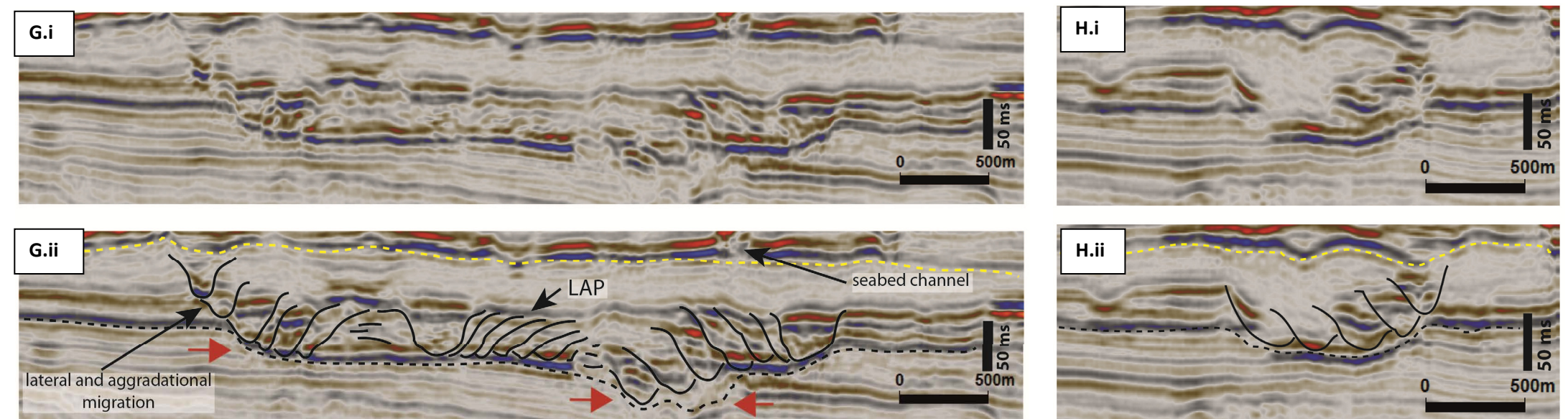


**Fig. 3.20.** (A) Map showing the base of channel B. (B) Variance attribute maps (C) Isochron thickness map

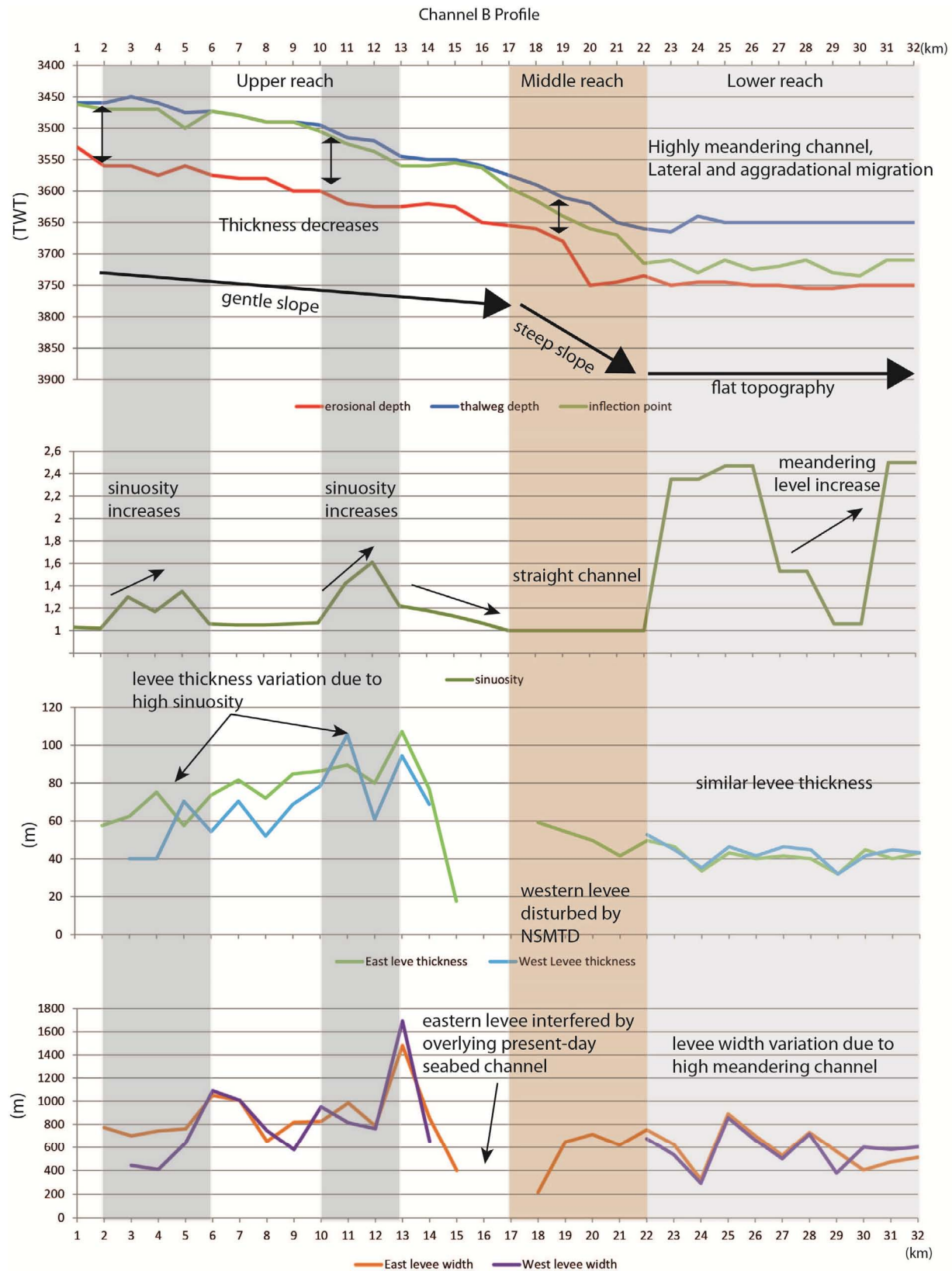




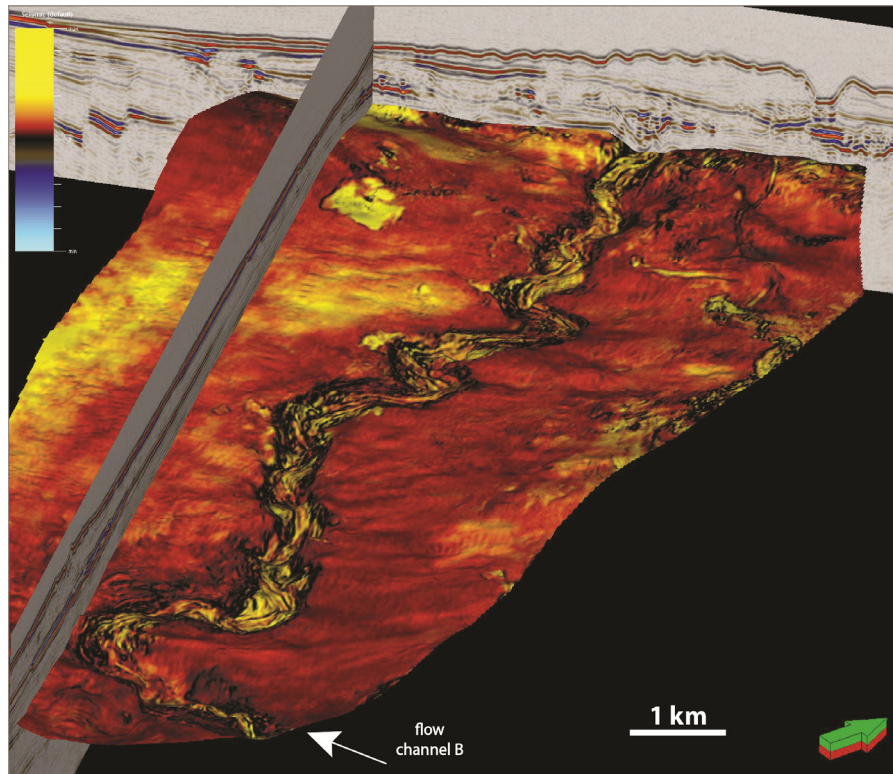
**Fig. 3.21.** RMS amplitude attribute map 50 ms above base of channel B. (A) Upper reach. (B) Upper reach cross-section showing increase of levee thickness in outer bend. (C) Middle reach. (D) Middle reach of channel B influenced by the higher topography. (E) Middle reach cross-section showing transition of channel B before forming sinuous (F) Uninterpreted and interpreted distal reach showing lateral accretion packages. Anticline X and mud diapirs lie below the channel B. (G) Uninterpreted and interpreted distal reach showing lateral and aggradational migration of channel B in relatively flat topography. (H) Uninterpreted and interpreted cross-section showing the most distal reach of channel B in the study area.







3.22. Chart showing channel B profile. See text for details.



**Fig. 3.23.** RMS attributes extraction 50ms above base of channel B combine with variance attributes showing channel B in the upper reach. Green arrow is pointing to the north.

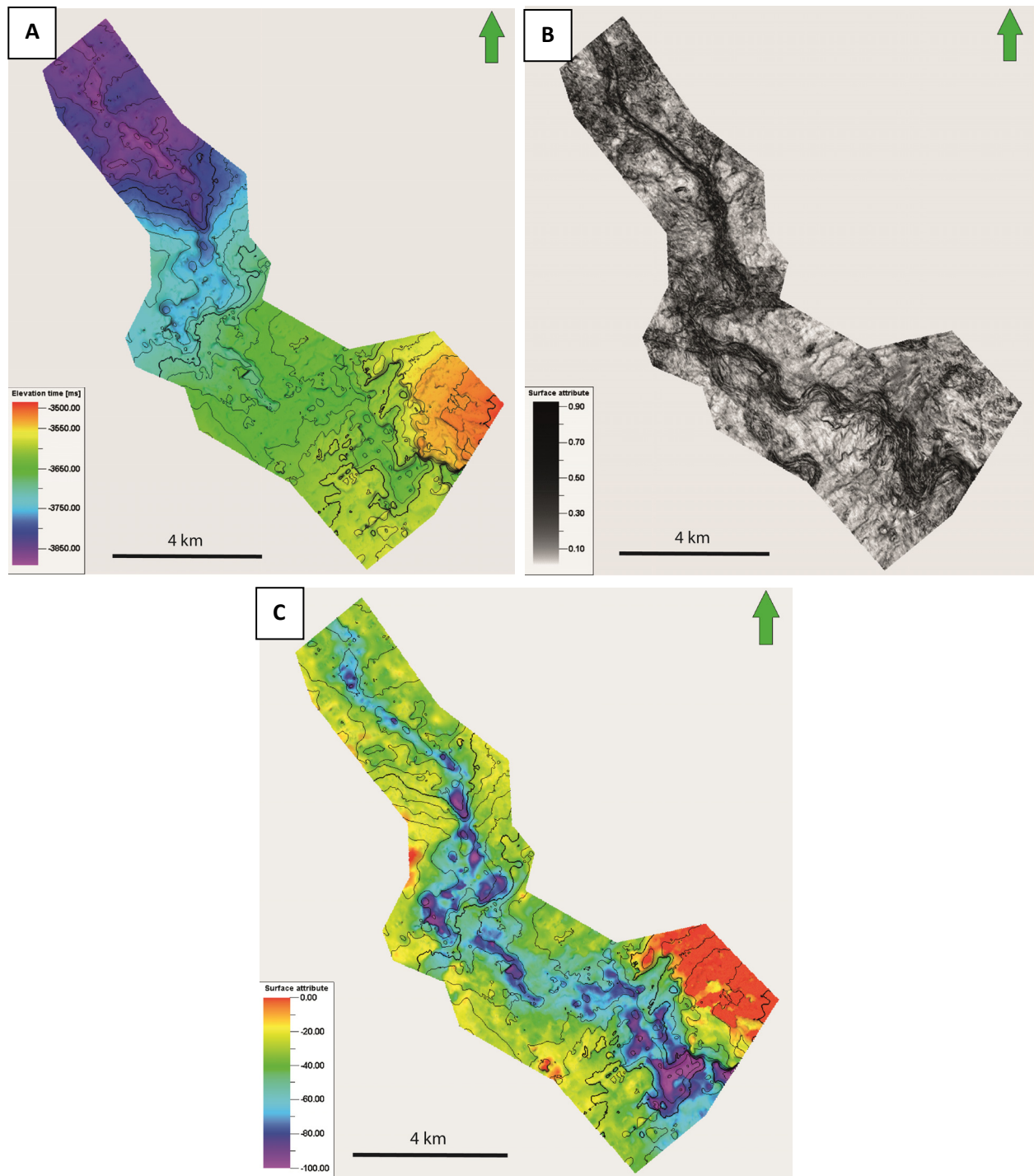
### 3.3.3. Channel-levee system C

The CLS C has a length of 19 km with an average sinuosity of 1.18. The sinuous part of CLS C is laid on a gentle slope profile for the first 11 km (Fig. 3.26). Within this part, the CLS shows dominantly SF1a and SF1b and largely confined by constructional levees. The inflection point in the channel C profile suggests that this reach is characterized by both erosional and aggradational CLS (Fig. 3.26). The levee morphology displays wide distribution away from channel axis and exhibits relatively symmetrical development. The average levee thickness is about 60 m and the width c. 950 m. The CLS C is located slightly below the CLS B on the west side at km 8 (Fig. 3.27). At the contact of these two CLS, the channel axis of CLS B has eroded the left-hand side of levee system C resulting in a shorter width levee (Fig 3.25B). In the inner bend of CLS C, HARP is found at the base of the levee in the immediate adjacent to the channel axis.

The channel thickness shows general reduction towards km 9 (Fig 3.25A and B). To the east part, the thickness map displays the thinnest area (red colour) indicating the development of an underlying CLS juxtaposition relative to CLS C (Fig. 3.25A). The base of levee system A has overtopped the levee from this external channel resulted a slightly tilted levee system A.

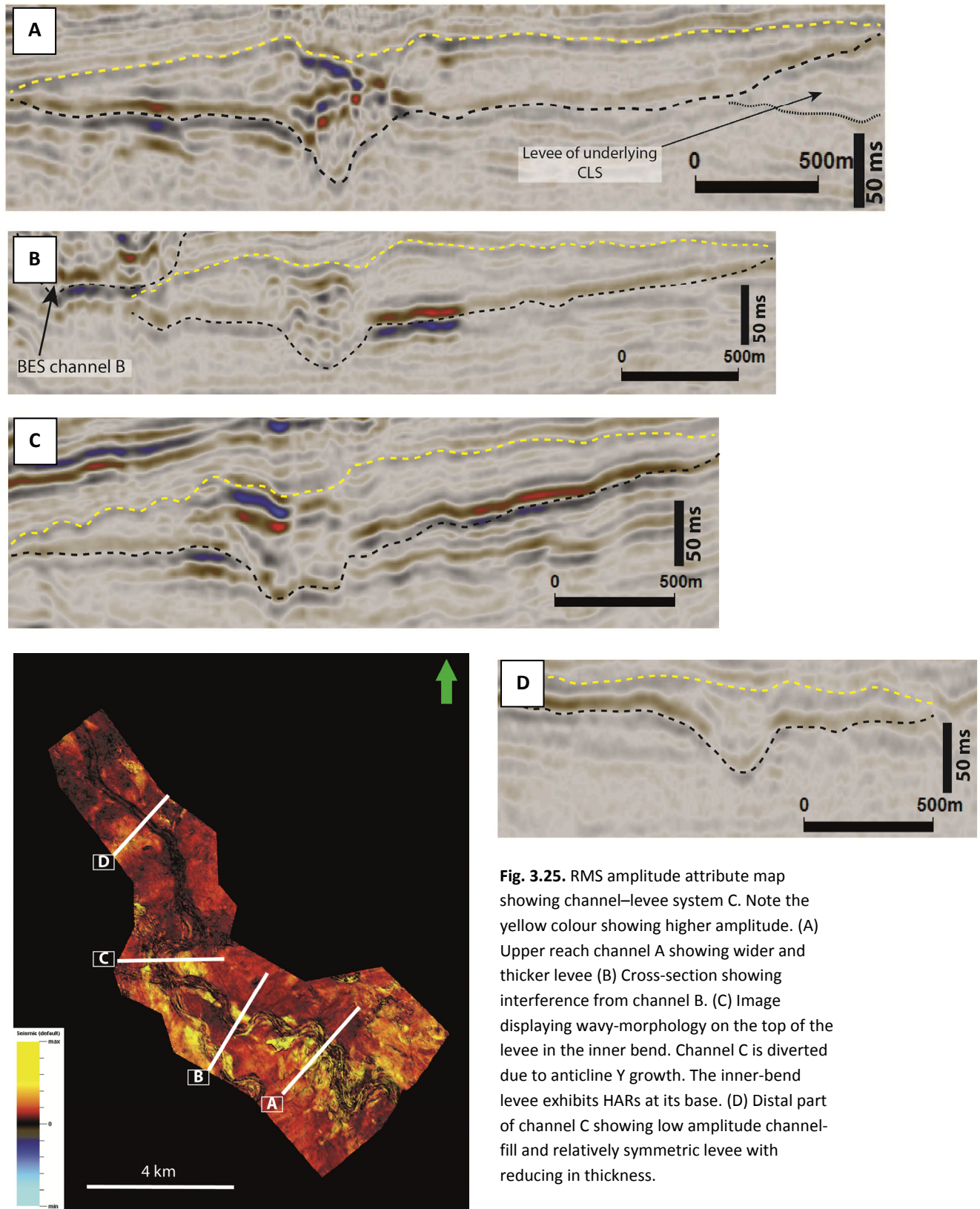
As the CLS C approaches km 9, the channel shows a significant diversion towards the east to avoid anticline Y (Fig. 3.27, see discussion chapter). The outer bend levee is relatively thicker and narrower with wavy-like structures on the top (Fig. 3.25C). The opposite side shows a wider levee thinning away from the channel axis. The channel fill is characterized by significant HARs in the outer bend side within the U-shaped channel axis (Fig. 3.25C). Layered HARP is also found at the base of the levee system in the inner bend within this area. This HARP is thought to be developed as a result of equilibrium flow that generate inner-bend deposit (Kane et al., 2008)

The next km 11 to the end of CLS C exhibits a low sinuosity ( $<1.1$ ) to an effectively straight channel (Fig. 3.26, Fig. 3.25B). The CLS C within this reach is laid on a relatively steep slope profile where channel thalweg and erosional depth has a relatively similar thickness downslope (Fig 3.25A). The levee thickness as well as the levee width exhibits a general decrease down the system. Channel-fill displays a slightly homogenous lower amplitude reflection compared to that commonly found in SF1a with evidence of a moderate incision rate (Fig 3.25D).



**Fig. 3.24.** (A) Map showing base of channel C (TWT) (B) Variance attribute map (C) Isochron thickness map





**Fig. 3.25.** RMS amplitude attribute map showing channel–levee system C. Note the yellow colour showing higher amplitude. (A) Upper reach channel A showing wider and thicker levee (B) Cross-section showing interference from channel B. (C) Image displaying wavy-morphology on the top of the levee in the inner bend. Channel C is diverted due to anticline Y growth. The inner-bend levee exhibits HARs at its base. (D) Distal part of channel C showing low amplitude channel-fill and relatively symmetric levee with reducing in thickness.

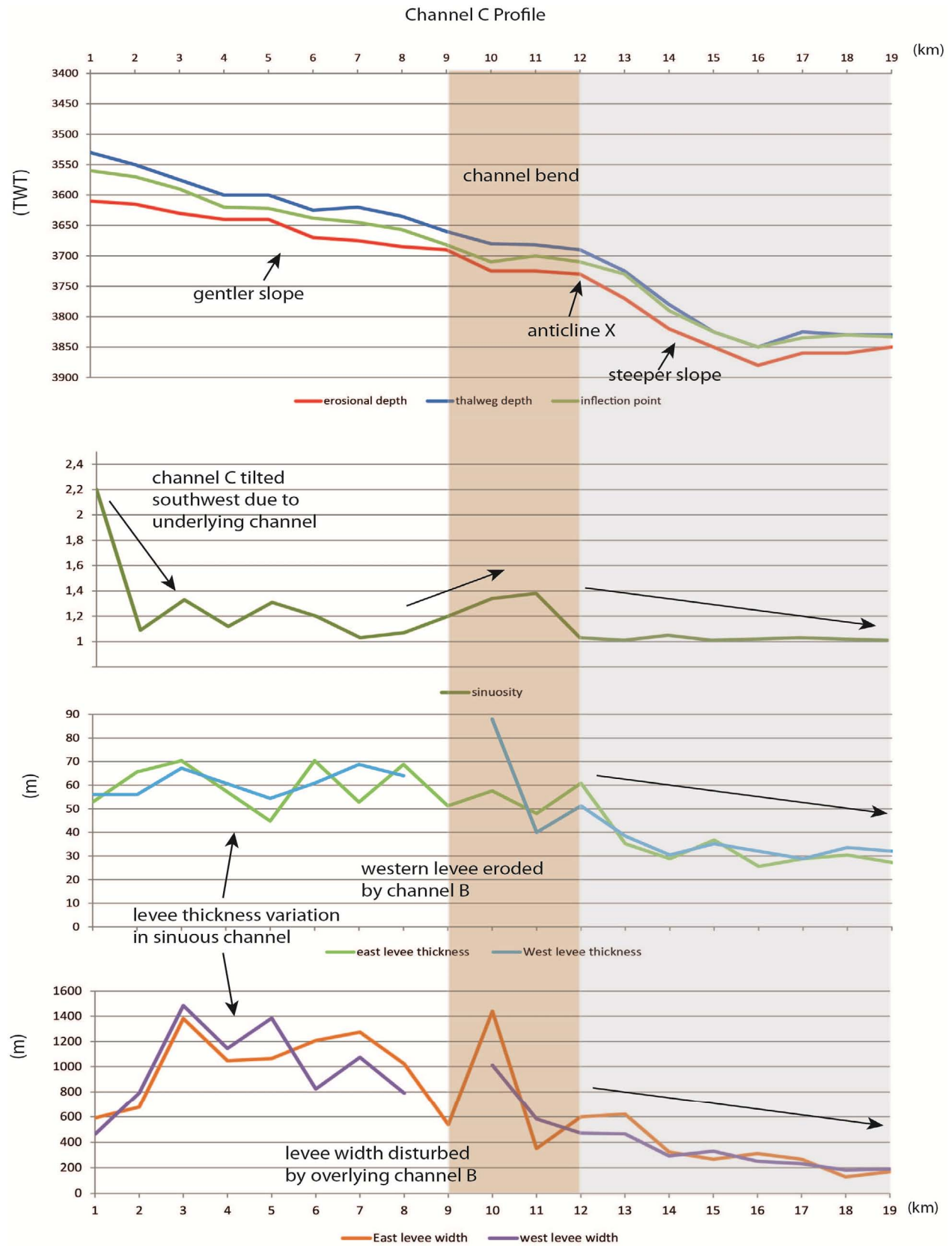
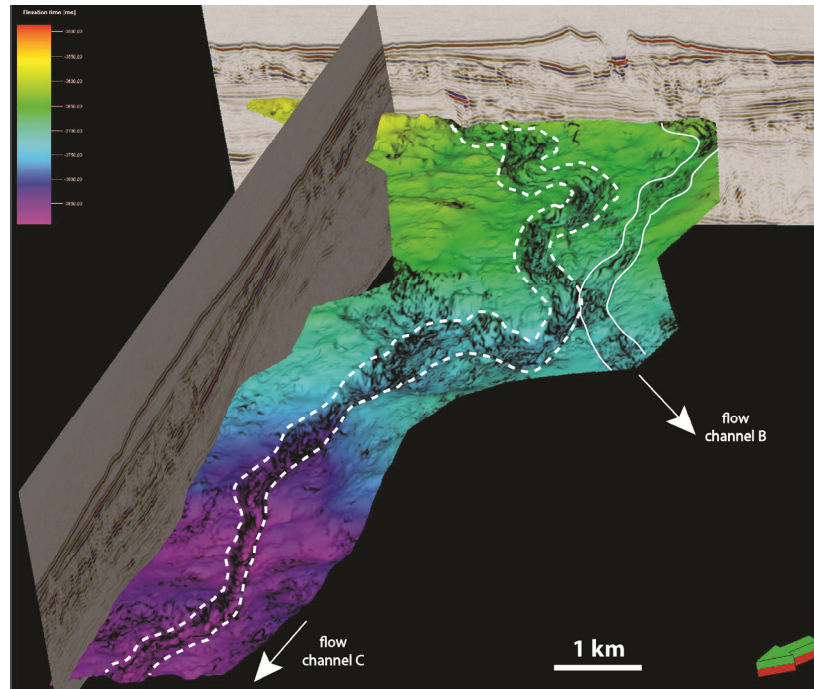


Fig. 3.26. (A) Map showing profile channel C. See text for details.



**Fig. 3.27.** TWT map combines with variance attribute map of base channel C showing diversion of channel B and C. Green arrow is pointing to the north.

### 3.4. Mass Transport Deposit and Splays

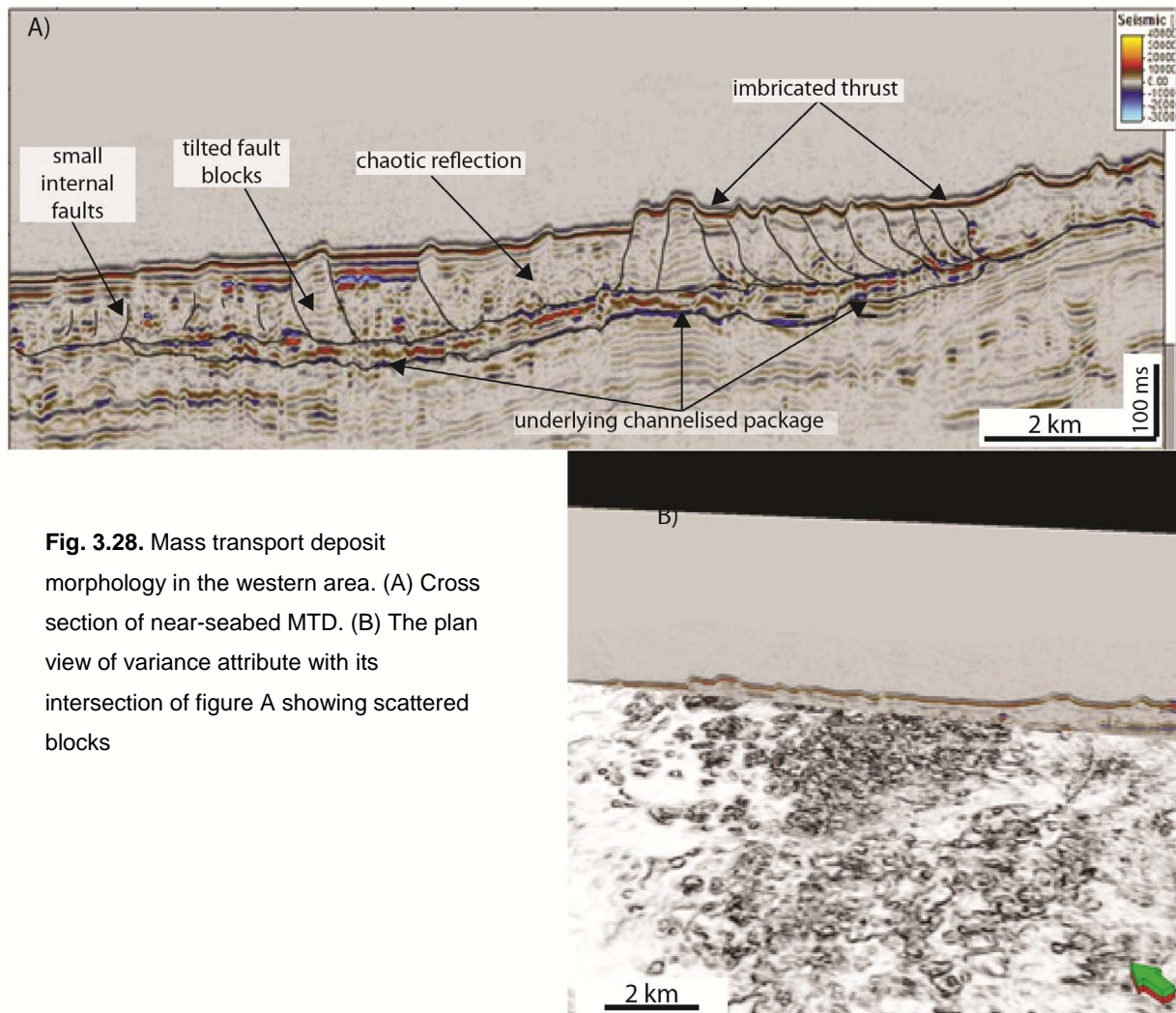
Mass transport deposit within the study area consists of the near-seabed MTD (NSMTD), Buried MTD (BSMTD), and transparent debris flow (TDF) which show a dominantly chaotic reflection of SF3 (Table 1) (Fig. 3.28A). The NSMTD displays various internal features commonly showing steeply tilted packages separated by landward dipping discontinuities. These highly deformed reflectors are interpreted as tilted fault blocks, imbricated thrusts, and small internal faults (Fig. 3.28A). These structures are likely formed under compression as the direction of the NSMTD flow towards the north. In variance attribute map, the NSMTD show rough surface and patchy blocks (Fig. 3.28B). This surface is interpreted as a result of remobilized sediment. At the base of NSMTD, the HARPs are occasionally observed and interpreted as local channelized lobes. As the HARPs are found on the top of SU3, it is probably a continuation of upper packages of fan lobe deposit.

The BMTD and TDF exhibit a similar chaotic reflection throughout the entire study area and show no significant internal structures (Fig. 3.1). In the RGB blend attribute map, the BMTD exhibits some scouring signatures or slope striations in the eastern part (Fig. 3.30, see subchapter 3.2.2). Similar striations have been observed in the Angolan margin by Gee et al., (2007) and are thought to be developed as a result from erosive turbidity current or mass

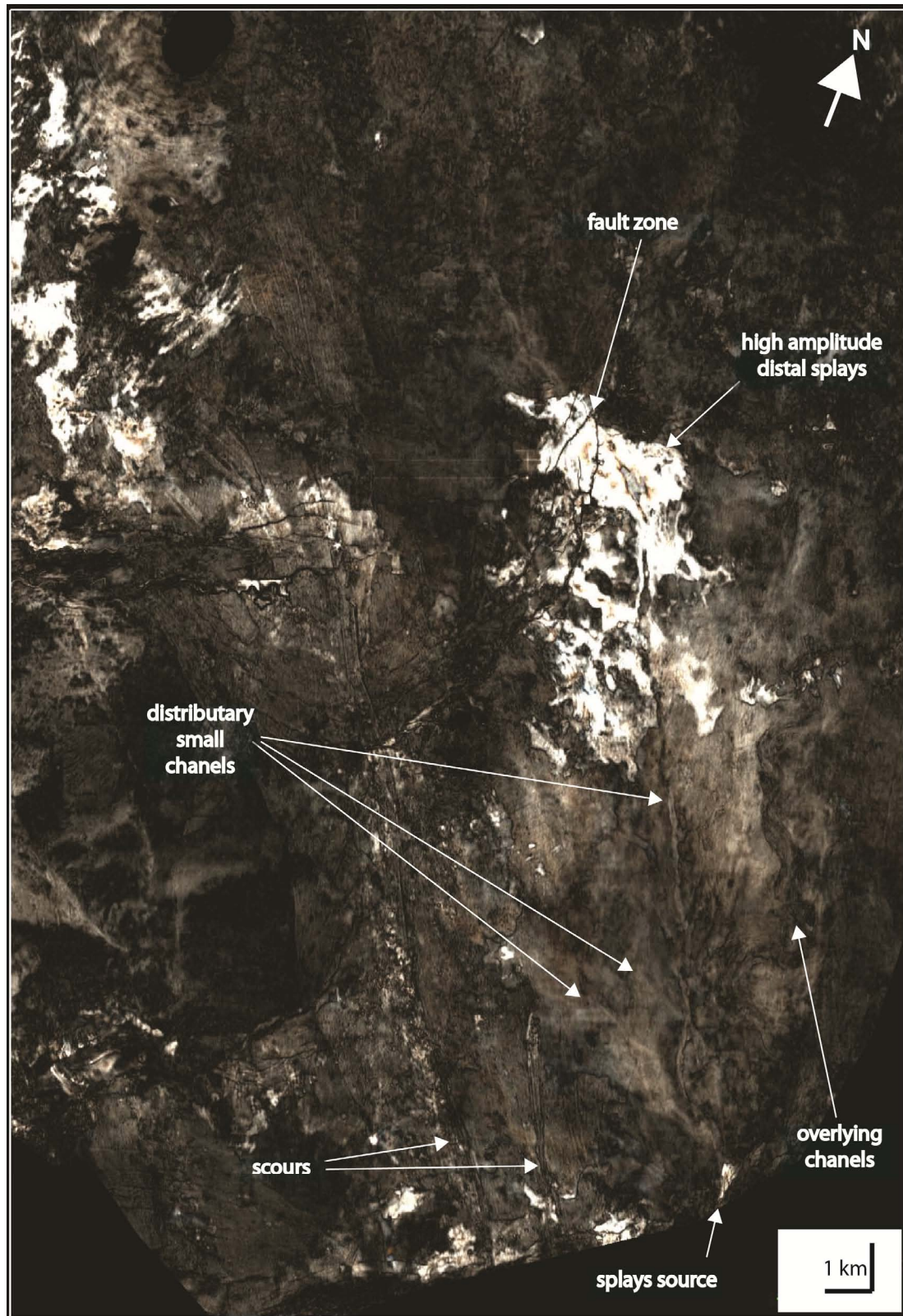


wasting. In the western part, wavy-like structures are found and are interpreted as a result of high deformation of SU3 (Fig. 3.30)

In RGB colour blend attributes map of the K horizon, a sheet-like HARP is observed locally in between BMTD and TDF (Fig 3.29). The dimensions of this feature can reach c. 17 km in length and 10 km in width and exhibits a finger-like form which is indicated as development of distributary small channels. This feature has apparently been sourced up from a single channel in the upper slope rather than feed up from a levee break. This feature can therefore be interpreted as frontal splays, as suggested by Posamentier (2003) which are formed at the end of a main channel and have a wider dimension than crevasse splays. This frontal is commonly observed in deep water settings (Posamentier and Kolla, 2003).

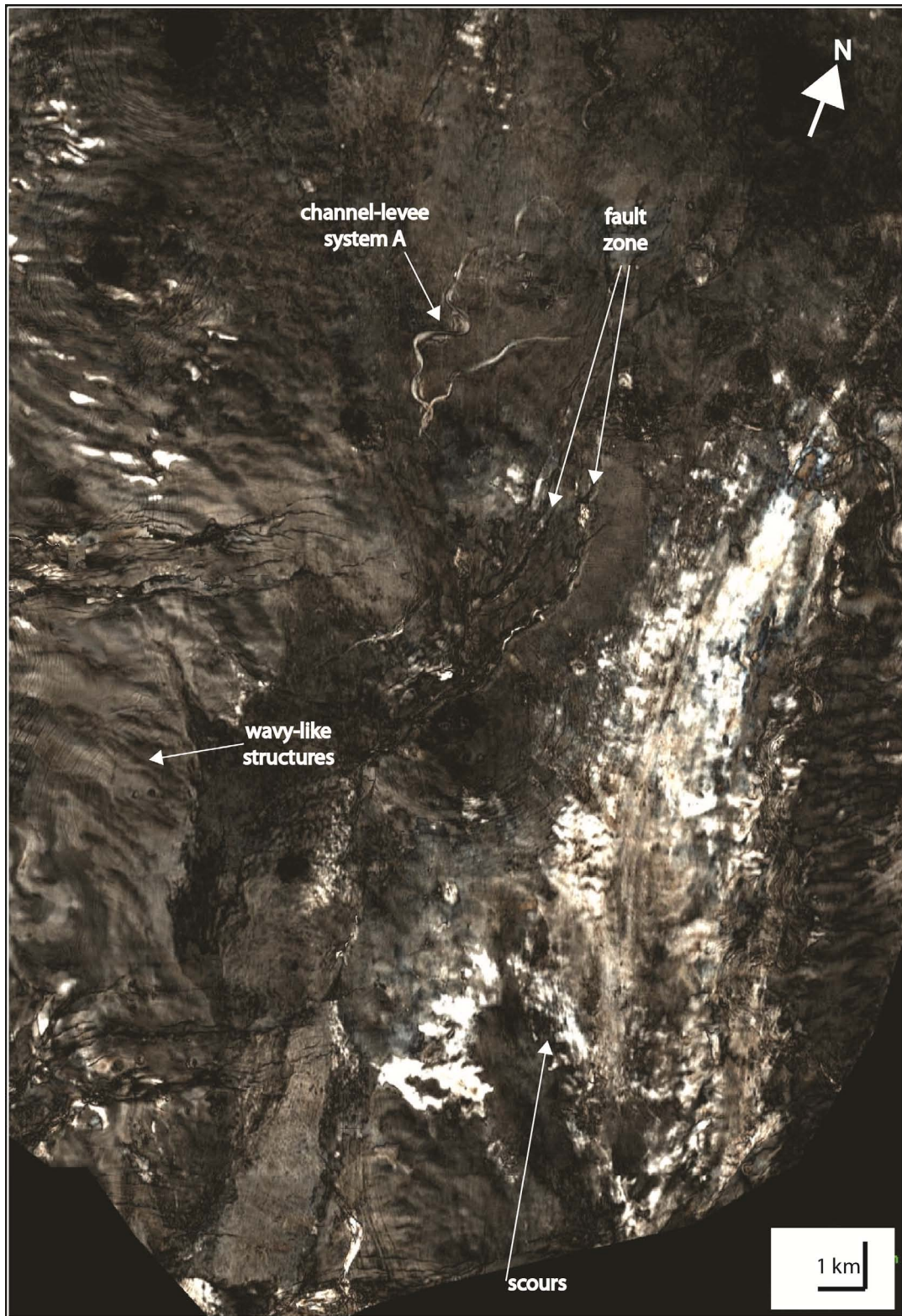


**Fig. 3.28.** Mass transport deposit morphology in the western area. (A) Cross section of near-seabed MTD. (B) The plan view of variance attribute with its intersection of figure A showing scattered blocks



**Fig. 3.29.** RGB blend image of K horizon base showing frontal splay morphology with distributary small channels.





**Fig. 3.30.** RGB blend image of L horizon showing HAR striations.

## 4. DISCUSSION

This chapter discusses the development of the five seismic units and the aspects of the submarine channel-levee system development. The first part of this chapter focuses on the structural control for the stacking pattern of the five seismic units in the study area. The second part discusses the development of sinuosity within channel-levee system. In the third part, the processes and architecture variations of channel avulsion are discussed. The final part of this chapter will discuss the structural controls on channel geometry and channel elements morphology.

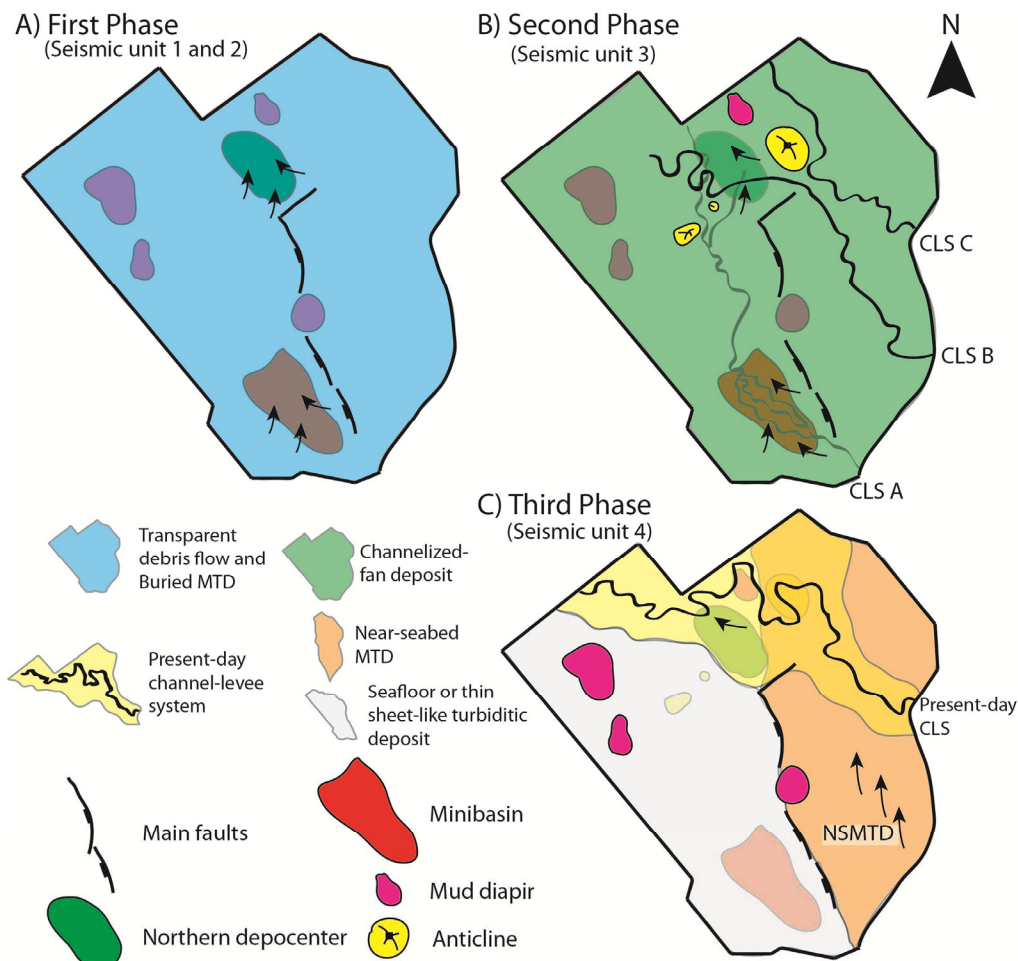
### 4.1. Structural controls of seismic units development

The investigation of temporal and spatial relationship of five seismic units within the study area offers an insight into seismic stratigraphy development in a salt-related slope setting. The response of submarine gravity-driven deposit to structural changes is revealed by variations in their architecture and distribution (Gee and Gawthorpe, 2006; Mayall et al., 2010; Prather, 2003). The seismic units stacking pattern provides information of the overall evolution of the Pleistocene to present-day depositional system. Active salt tectonic and its associated faults have generated high and low topography and may have affected preferential sediment deposition (e.g. anticline X, Y, Z, and minibasin).

Arbitrary lines along the hanging wall, footwall and crossing the main fault were generated in this study (Fig. 3.2A, B, and C). They show that salt has withdrawn within the minibasin and the northern depocenter. The salt movement towards the major footwall of the main fault may have activated the main fault which can be observed from the significant TWT difference between the hanging wall and footwall of the main fault. The TWT value of top salt in the footwall wall is approximately 3850 ms whereas in the hanging wall it shows a maximum of 4400 ms. Therefore, this salt movement has highly affected the accumulation of main structural growth and seismic units within the study area.

The early phase of early Pleistocene strata is characterized by the initial development of the minibasin and the northern depocenter as inferred from the thickness variation of SU1 (Figs. 3.3B, 4.1A). This implies a preferential deposition of SU1 to fill the negative bathymetries. The increasing thickness in the adjacent hanging wall of the main fault system suggests that this fault was active during the early Pleistocene period. Anticline X, Y, and Z might not have been formed during this phase as the thickness of SU1 shows no significant variation around these structures. A similar pattern is observed in the major structures within the SU2 interval except for the northern depocenter. The thickness map of SU2 on the northern depocenter shows a gradual thinning (Fig 3.4B). This suggests that

either the northern depocenter development was slower than the NSMTD accumulation or that the northern depocenter was filled with the pinchout of this unit (Fig. 3.2B)



**Fig. 4.1.** Schematic figures showing development of each phase in the study area.

The pre-existing relief of the early phase seismic units controlled the depositional accumulation and architecture of the subsequent gravity flow of SU3. The second phase is characterized by deposition of the channelized-fan deposit of SU 3, the continuous growth of the main fault and the northern depocenter, and the development of the anticlines (Fig. 4.1B). As can be inferred from the thickness increases in the immediate hanging wall of the fault, the main fault grew significantly during this period (Fig. 3.5). The minibasin shows a significant thickness as a result of CLS A development, whereas the northern depocenter is filled with thick fan lobe deposit which contains the newly avulsed CLS A and the CLS B. This implies that the preferential deposition of channel-levee systems to fill the accommodation space. The thickness differences around the flanks of the anticlines

suggests that all the anticlines grew in this period and affected the channel-levee systems pathways (see sub-chapter 4.3)

These stacking patterns allow us to infer the channel-levee system's relative timing development. CLS C, which is located in the lowest part of the fan deposit, is thought to be the oldest channel-levee system in the study area. The interaction of CLS A and B in the seismic cross-section and the location of new avulsed CLS A below the CLS B imply that the CLS A is relatively older than the CLS B. The CLS C formed in the eastern part of the study area during the early phase of SU3 development following the regional slope trend to the north-west. The CLS A was developed sub-parallel to the main fault as a response to the significant accommodation space available within the minibasin and intense main fault activity before it eventually filled the northern depocenter. The youngest CLS B was formed in the central part of the study area to maintain high sediment supply from the upper slope and filled the accommodation space in the northern western area as a result of a compensational stacking pattern.

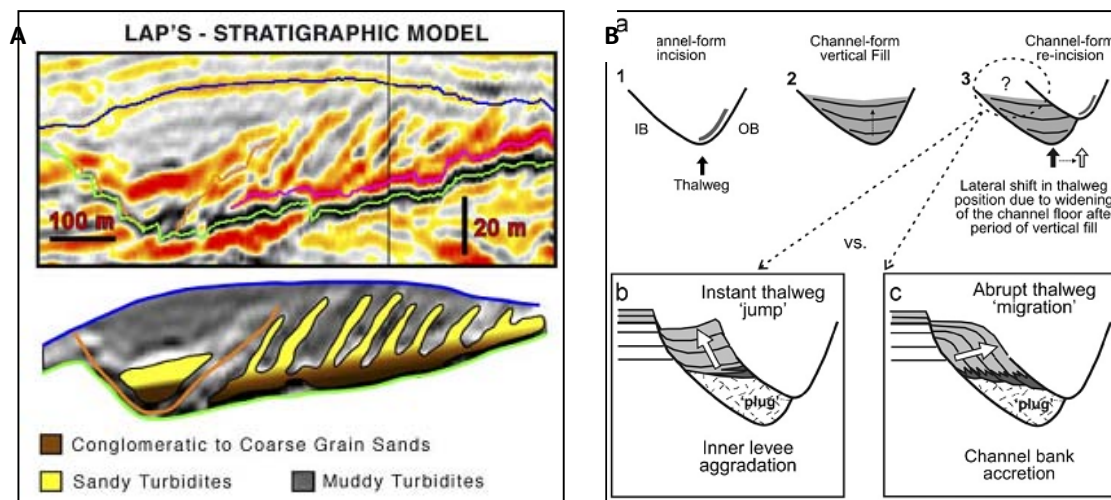
Mud diapirs (SU5) are commonly located in the in the north western part of the study area. The thickness maps of SU1 and SU2 show only negligible changes in the location where the SU5 appears. In contrast, the thickness map of SU3 shows significant thickness changes in the location of SU5, which indicate their existence within this interval. As described in sub-chapter 3.3.5, this unit shows an upward migration of fluid-rich deposit through faults. However, analysis of the interaction of SU5 with channel-levee system suggests that this unit had no influences during SU3 deposition but highly deformed the present-day morphology of the system (Figs. 4.9, 4.10). This implies that the majority of SU5 development is occurred during the third phase of the succession except the one adjacent to CLS C (Fig. 4.1 C).

The third phase of the seismic unit stacking pattern is characterized by the development of present-day channel-levee system and the near-seabed MTD (SU4) and deposition of major mud diapirs (SU5) (Fig. 4.1C). The Near-seabed MTD fills the accommodation space in the eastern area towards the north-east as a result of tilted footwall of the main fault (see sub-chapter 3.2.4). Eventually, the present-day channel-levee system succession covered the NSMD before the system developed significant sinuosity during the filling of the northern depocenter and bent towards the northwest following the regional slope (Fig. 3.8). The development of mud diapirs are significantly affected the seabed morphology in the central and the north-west area as shown as cone-like features on the present-day seafloor (Fig. 4.1C). The main fault growth may still be active as the SU4 thickness increases in the immediate hanging wall of the fault. It is inferred that these fills were deposited as a sediment accumulation to heal the locally depressed bathymetry (Prather, 2003; Steffens et al., 2004).



## 4.2. Sinuous submarine channel-levee system

Previous detailed studies of high resolution 3D seismic imagery have revealed a range of architectural elements associated with sinuous submarine channels, such as channel-fill deposit (SF1), levee (SF2), and lateral accretion packages (LAPs) which may vary during channel evolution (Abreu et al., 2003). Submarine channels are known to adjust their planform geometry to response to changes in flow parameters and topographic variations (Deptuck et al., 2003; Kane et al., 2008; Kolla et al., 2007; Peakall et al., 2000). During its evolution, this can be observed as lateral and vertical aggradation with evidence of significant meander development (Figs. 4.3, and 4.4)



**Fig. 4.2.** A: LAP's model proposed by Abreu et al. (2003) and their interpretation for the lithology. B: Plug-and-cut model by Deptuck et al. (2007). Two alternative mechanisms for plug-and-cut model after vertical fill period in point 2. Box b: Development of inner levee aggradation to keep pace with instant thalweg 'jump'. Box c: Slightly gradual thalweg migration with development of lateral accretion and vertical inner levee aggradation. IB: inner bend, OB: outer bend.

Sinuous submarine channel with meandering development is observed in the lower reach of CLS B (Fig. 4.3). Within the inner side of meandering segment in CLS B, a series of shingled reflection packages are observed and are interpreted as LAPs (Fig. 4.4 Box B). These LAPs are commonly followed by lateral and vertical aggradation at the final meandering development. Therefore, meandering development in CLS B is observed as a series of LAPs development and a combination of lateral and aggradational migration (Fig. 4.4).

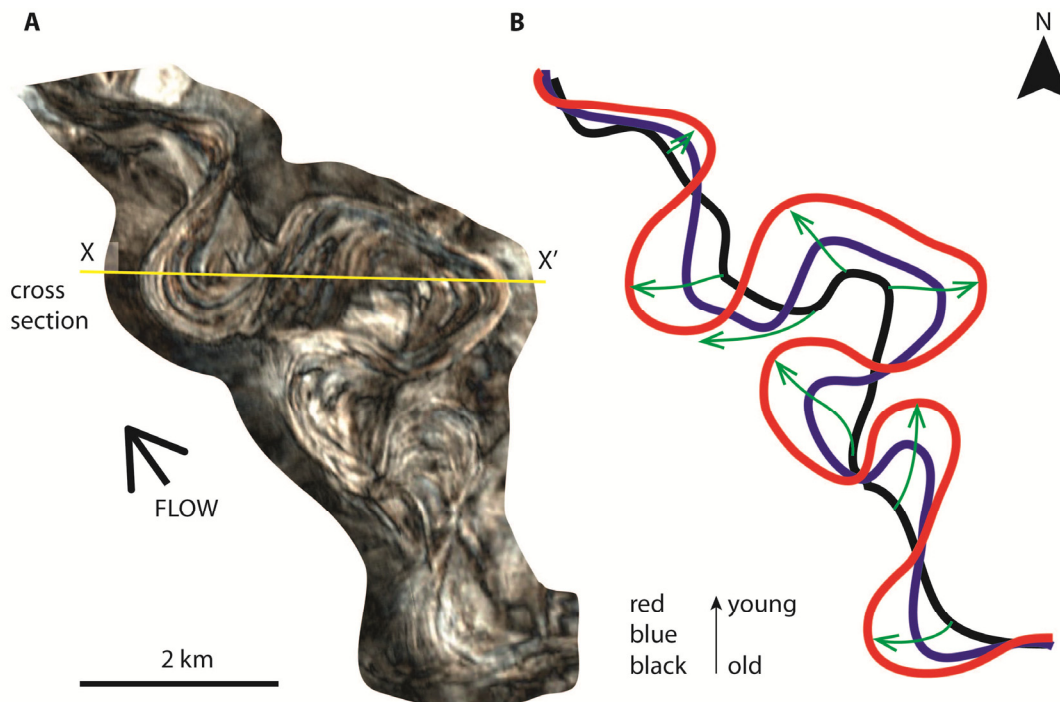
Meander development could also be observed in the CLS A in the proximally middle reach. It can be imaged using iso-slice method on RGB colour-blend attribute map which also shows LAPs (Fig. 3.18). However, LAPs could not be easily distinguished



morphologically in seismic cross-section, probably due to interruption by abundant underlying and overlying mud diaprism development (Figs. 3.10 and 3.19)

Lateral accretion packages are proposed by Abreu et al. (2003) for a continuous lateral migration of channel thalweg during channel evolution which show an overall declining base of the channel thalweg (Fig. 4.2). This ideal feature is commonly characterized by deposition of accretion of sediments in the inner side of the channel bend and erosion in the outer side of the channel (Deptuck et al., 2007; Janocko et al., 2012; Kolla et al., 2007; Mayall et al., 2006). These LAPs commonly occur as the channel experiences a continuous and gradual lateral swing and sweep (i.e. downdip migration).

LAPs do not necessarily show a gradually declining package towards the last thalweg position of the channel due to systematic erosion as the proposed model (Fig. 4.1A). Instead, at the end of LAPs, it commonly shows relatively similar or slightly inclining packages (Fig. 4.2 Box B and C). This might be due to a gradual change in flow types from less-energetic flows that occurred frequently and lasted for a short period of time to a combination of low-to-high energy flows (Kolla et al., 2007).

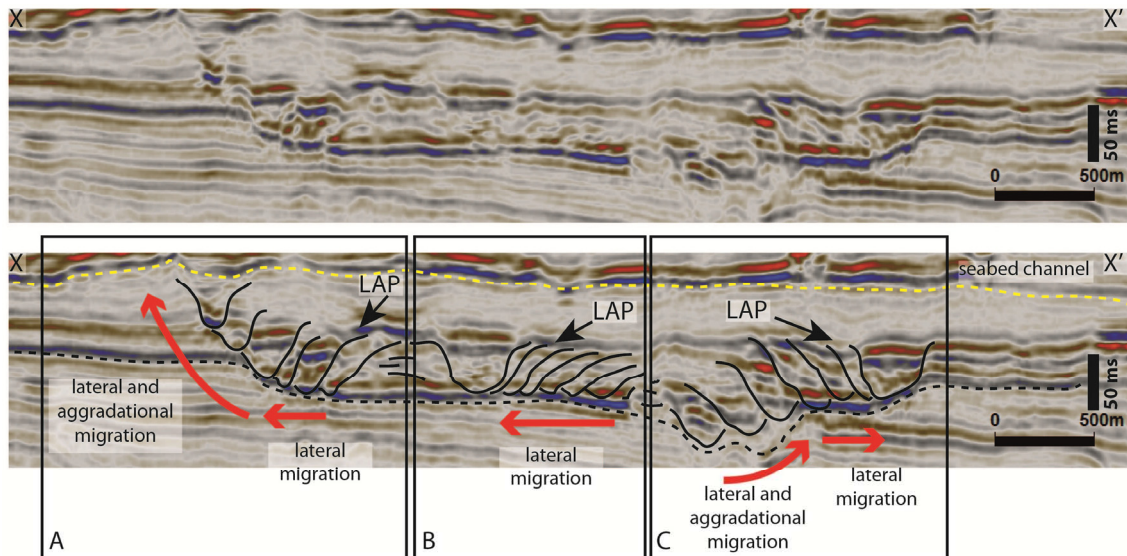


**Fig. 4.3.** A: LAPs are shown in RGB colour blend attribute map B: the interpretation of channel development. Green arrows reflect the meander-loop direction.

Kane et al., (2008) noted a significant control of submarine channel on outer bend and inner bend deposition which represents a change of equilibrium and disequilibrium flow type that marks the fundamental difference between a fluvial and a deepwater system.

However, the growth of significant meander within CLS B is interpreted as a result of a dominant equilibrium flow rather than disequilibrium. In this segment, equilibrium flow may increase channel sinuosity and significantly develop deposition in the inner-bend and limit deposition in the outer bend.

Similar lateral accretion features have been documented in other submarine channel-levee systems. These include those characterized by meander-loop migration (Posamentier, 2003) and downstream and upstream translation (Janocko et al., 2012). Abundant examples of channel migration (lateral migration and/or vertical aggradation) have been documented from channel-levee complex consisting of stacking channel-levee systems which is commonly confined by two master bounding levees (Catterall et al., 2010; Deptuck et al., 2007; Kane and Hodgson, 2011; Mayall et al., 2006).



**Fig. 4.4.** A: Lower segment of sinuous channel B showing lateral migration followed by lateral and aggradational migration. B: LAPs within channel B. C: Upper segment of sinuous channel B showing lateral and aggradational migration followed by lateral migration. See the location in Fig. 4.3

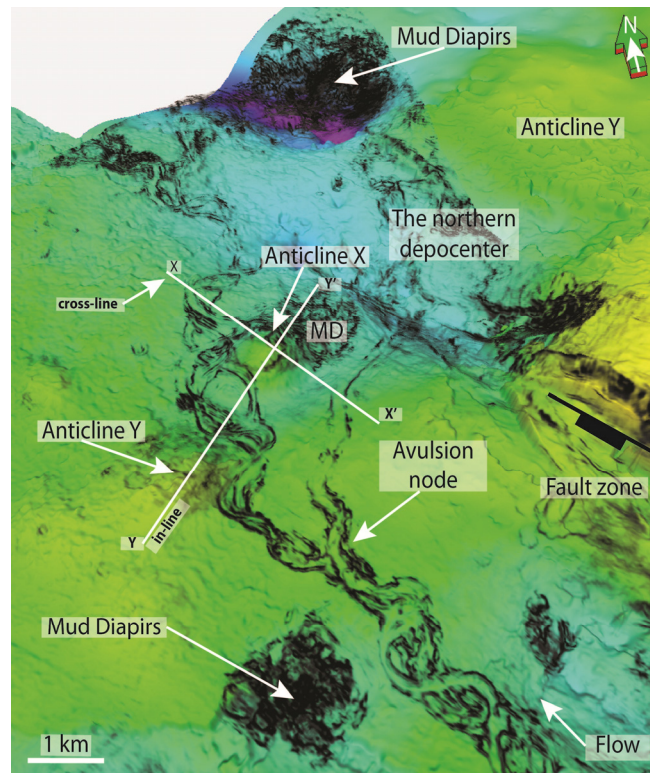
Lateral and vertical migrations in CLS B were due to plug-and-cut process by Deptuck et al. (2007) where channel B shifts are occurred in response to vertical fill (plugging) of underlying thalweg that may shift the subsequent thalweg (Figs. 4.2B and 4.4). However, it is difficult to observe the inner levee geometry to define the specific scheme involved in thalweg shift (Fig.4.2B Box A and B). The plug-and-cut processes in sinuous development of CLS B have a correlation between flows parameter and pre-existing channel morphology which can lead to a variation in thalweg direction.

The meander development in CLS B shows different accretion packages. In the upper segment (Fig. 4.3 Box C), it shows dominantly lateral and vertical aggradation

followed by lateral migration whereas in the lower part (Fig. 4.3 Box A), it exhibits lateral migration followed by lateral and vertical aggradation. This spatial and temporal variation may be explained by the nature of turbidity current that varies through time in terms of erosion, transport, and sedimentation within channel (Babonneau et al., 2002). This may suggest the change from a more deposition flow in during early phase of meander to a more bypassing flow and followed by subsequent depositional flow at the last phase of meandering development (Fig. 4.3 Box A, B, C) (Kolla et al., 2007).

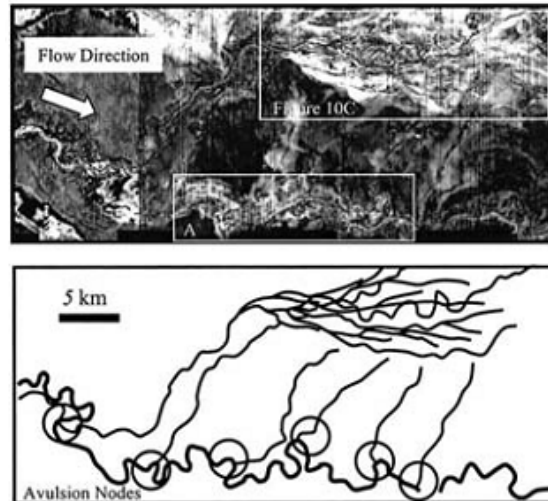
### 4.3. Channel avulsion

Channel avulsion is a mechanism where significant turbidity current outpaces the levee stability and is commonly associated with differential local bathymetry gradient (Babonneau et al., 2002; Pirmez, 1994). In the margin that separates the middle and lower reach of CLS A, a channel avulsion point is observed (Fig. 4.5). The new CLS A showed a steeper channel-axis gradient than the parent CLS and is marked with a deep thalweg incision and narrow channel relief along its course (Figs. 3.22 and 4.5). It is thought that this avulsion was a response to a local gradient change combined with enough high flow energy to breach the levee to form a new erosional fairway.



**Fig. 4.5.** Variance attribute shadow of distal reach of CLS A on the TWT map of SU3. Darker colour means deeper topography. Note the channel avulsion point, the position of the local structures, and seismic line for Fig 4.9 (in-line) and Fig. 4.10 (cross-line).

Avulsion in submarine CLS is observed at various locations such as deepwater Zaire, Brazil and, Gulf of Mexico (Babonneau et al., 2002; Lopez, 2001; Posamentier, 2003). In the Amazon, the development of HARPs commonly takes place at the base of a new channel and are followed by subsequent channel entrenchment with levee build up (Lopez, 2001).



**Fig. 4.6.** Channel avulsion example from CLS in Gulf of Mexico (Posamentier, 2003).

The Joshua CLS in the Gulf of Mexico experienced several avulsions along its length due to differential compaction of the underlying bathymetry and thus created a tilt that triggered the channel avulsion (Fig. 4.6). Frontal splays are features that are commonly observed at the end of a new avulsed channel (Posamentier, 2003). However, in this case, neither HARPs nor frontal splays have been observed within the study area. Across the Amazon CLS avulsion point, HARPs were observed in regions with an abrupt change in slope degree, and therefore the channel characteristic is inferred to be more deposition rather than erosion. In contrast, CLS A avulsion point is occurred by a gradual change from low gradient to high gradient, which may suggest that the new channel will maintain the equilibrium profile by eroding the underlying unit (Fig. 4.5). Hence such HARPs are not found.

#### **4.4. Structural influence on submarine channel-levee system**

Submarine channel architecture records changes in geological settings related to regional or local structural variations as well as changes in the nature of sediment gravity flows (volume, rheology and composition). The interaction between channel-levee system behaviour and slope morphology in many deepwater settings around the world has been described in many studies (Clark and Cartwright, 2009; Gee and Gawthorpe, 2006; Gee et al., 2007; Mayall et al., 2010; Wood and Mize-Spansky, 2009). In addition, the deepwater Nile delta has complex

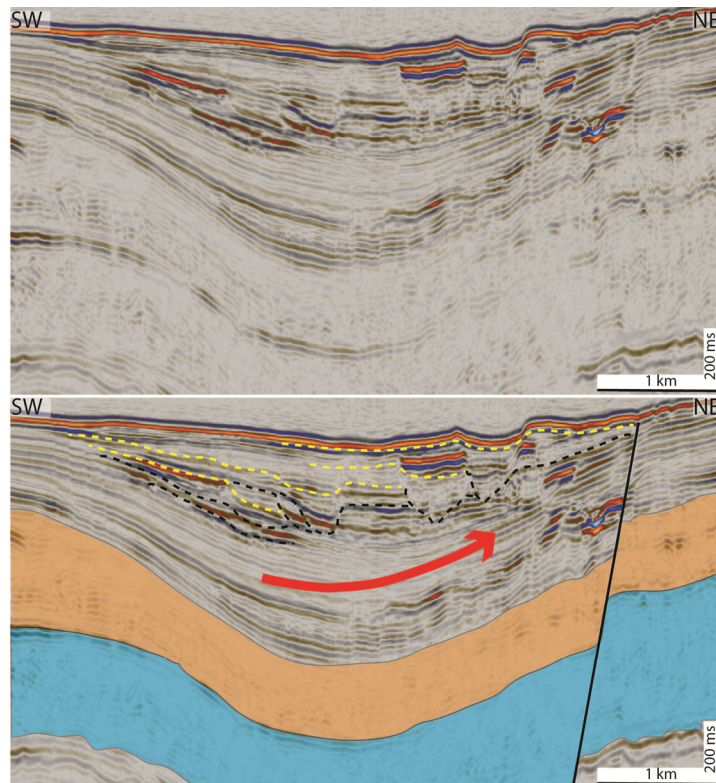


structural settings related to underlying Messinian mobile substrate (Aal et al., 2000; Cross et al., 2006; Loncke et al., 2006; Tari et al., 2012)

This chapter provides analysis of channel-levee system morphology response to the development of structurally induced topography. However, there are two major structure orientations within the study area that are systematically effected the channel-levee system pathways (see Fig. 4.3): structures parallel/sub-parallel to channel-levee system (e.g. the eastern fault that influenced CLS A architecture and morphology in the minibasin confinement) and structures relatively perpendicular to CLS (e.g. anticline X and Y along with examples from the local slope variation along CLSs course).

#### 4.4.1. Case I: Fault growth influence to channel-levee system

The Iso-slicing method on RGB colour blend attributes map has successfully mapped the CLS A gradual shift towards the eastern fault striking sub-parallel to the CLS (sub-chapter 3.1.1) (Fig 4.7). The early phase of sinuous channel development in the north-western area, which is related to the inactive period of the main fault, suggests a continuously high sediment influx from the upper reach and a relatively long duration of accommodation space filling.

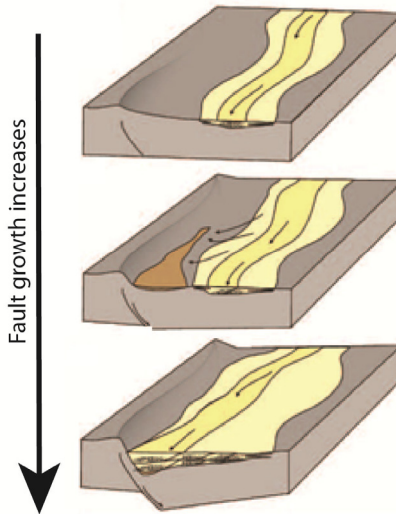


**Fig. 4.7.** Cross-section showing the main fault and channel A within the minibasin. Red arrow shows direction of channel shift towards the main fault. Yellow- and black-dashed line represents top and base of channel.



The subsequent phase shows CLS A shift towards the eastern fault. Thus, it is inferred that the growth rates of the eastern fault kept pace with sedimentation supply rates. Figure 4.8 shows a similar setting and process in Waddington Fell quarry, UK, as described by Kane et al. (2010). The channelized turbidity current may potentially overspill into the accommodation space generated by the fault growth.

The minibasin development in the study area may not be related to the fill-and-spill process of Prather (2003) with example from Nigeria. The Nigerian intraslope basin shows no major control by fault and is generated as a ponded accommodation space available in above-grade slope (Prather, 2003). He explained that the turbidity current behaviour at the entry point of the interslope basin may trigger hydraulic jumps associated with abrupt change in gradient. This promotes the development of sheet-like sands and ponded lobes with distributary channels during the basin filling.

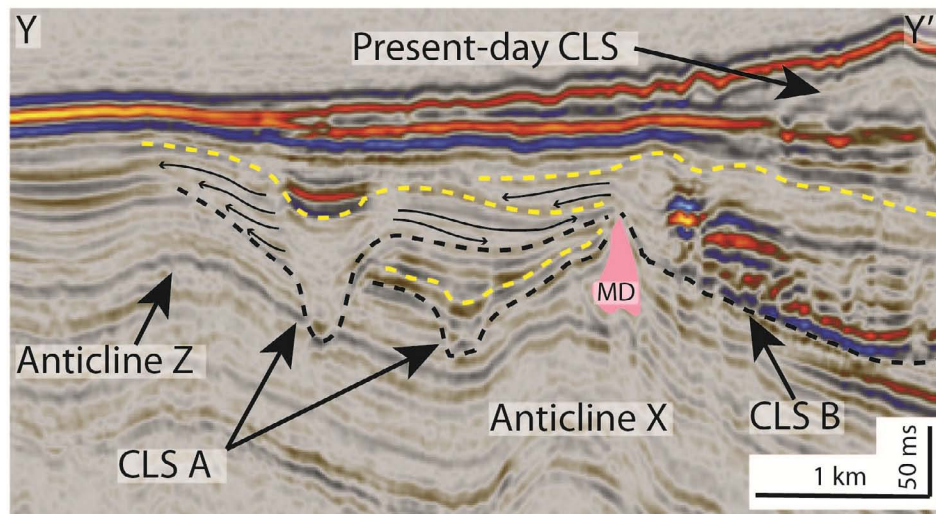


**Fig. 4.8.** Minibasin model, example from Waddington Fell quarry, UK showing the channel shift towards the fault (modified from Kane et al, 2010)

In the case of CLS A, the minibasin was not generated as in the case from Nigeria where the intraslope basin was initially characterized by significant accommodation space and depocenter depth. Here, the minibasin was formed as a result of gradual fault growth in association with salt withdrawal and therefore a stacked channel-levee system migration towards the eastern fault could be developed in response to a continuous slope sediment supply (Figs. 3.18 and 3.19).

#### 4.4.2. Case II: Channel-levee system response to anticlines and mud diapirs

Bathymetry setting is highly affected by underlying salt and associated local structural variation and this may impact CLS morphology. Timing relationship between structures and CLS is important for examining CLS behaviour (Clark and Cartwright, 2011; Mayall et al., 2010). The effects of deformation of the underlying substrates on channel development can be examined by analysing CLS architectural variation along the structure (e.g. levee internal geometry) and CLS pathway on planform attribute map. CLS A shows a significant bend when approaching anticline Z but maintains its course when approaching anticline X (Fig. 4.6). It is inferred that both anticlines may have affected CLS A although anticline Z may generated higher impact than anticline X. In the cross-sectional view, for the same seismic event, anticline Z is located slightly higher than anticline X and it is thought that CLS A had enough erosive power to overcome the rate of growth of anticline X (Fig. 4.9). The eastern levee internal geometry of CLS A displays systematic tilted reflections towards the active anticline Y and, therefore can be interpreted as coeval structure deformation with CLS development (Fig. 4.9).



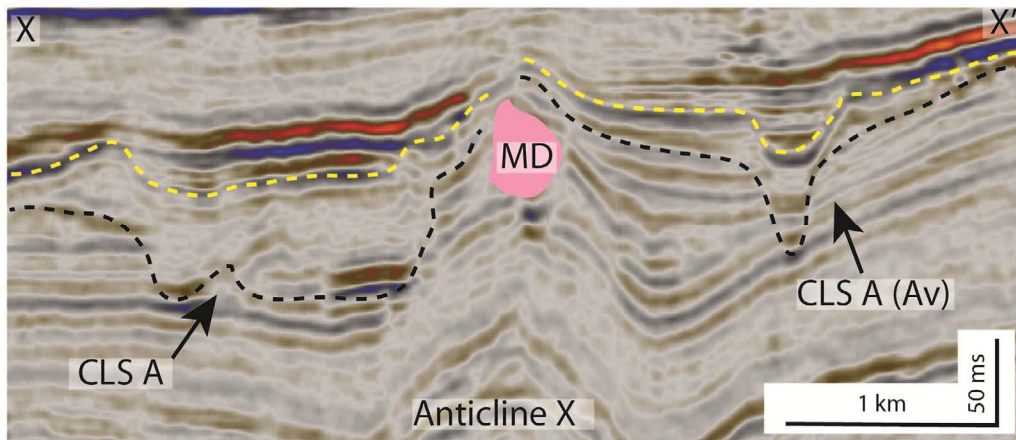
**Fig. 4.9.** Interaction of CL A, CLS B, anticline X and mud diaper (MD) in-line cross-section.

See the location in Fig. 4.5

LAP is commonly a product of channel lateral migration with no major influence from adjacent structures. The steeply inclined LAP of CLS B toward the anticline X is a rare example and can hardly be explained by such a theory (Fig. 4.9). Clark and Cartwright (2009) distinguished four major behaviours when CLS interact with structures, either active or pre-existing structures: diversion, confinement, deflection and blocking. Channel-levee system with a relatively less erosive power tends to avoid the structure whereas CLS with a high enough erosive power will cut through the structures (Mayall et al., 2010). Channel-

levee system B with such a meandering signature is less likely to flow up-dip to the anticline X. It is therefore inferred that the anticline X had formed prior the development of CLS B.

The levee stacking patterns of both CLS A and B display folded levee packages overtop the mud diapir (Fig.4.9). It is interpreted that the mud diapir grew after both CLSs had been deposited. The levee of CLS B is observed to onlap onto the CLS A's levee and this suggests that CLS A is older than CLS B. A similar observation is valid for the avulsion channel of CLS A in seismic cross-section and it is interpreted that the mud diapir is a post-channel deformation (Fig. 4.10).



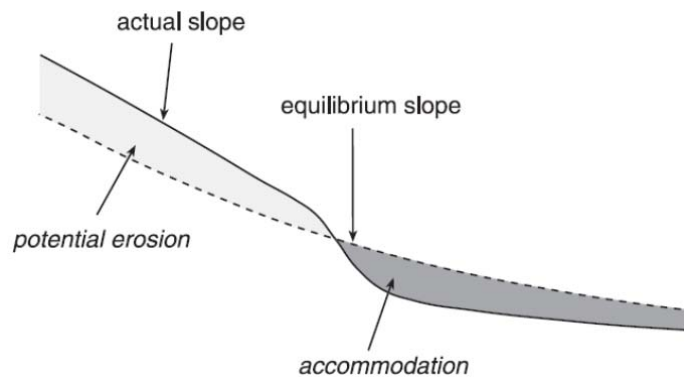
**Fig. 4.10.** Cross-section of cross-line through anticline X and mud diapir (MD). See the location in Fig. 4.5

Diversion is a channel response to a non-active structure which is represented by channel migration to avoid the structure whereas deflection is defined as channel migration around the growing structure with evidence of a systematic shift toward the dip-side of structures (Clark and Cartwright, 2009). Moreover, Mayall et al. (2010) documents three main factors that may influence CLS interaction with structures: (i) size, shape and orientation of the structures, (ii) timing relationship between structures with CLS, and (iii) erosional power of the channel. In the lower part of CLS B and C, anticline Y is thought to be the reason for the sideways migration (diversion) of both channels flanking the anticline (Fig. 4.6). This may imply that both channel-levee systems have relatively lower erosive power to cut through the anticline. A similar case of CLSs in Angola is reported by Gee and Gawthorpe (2006) and Mayall et al. (2010) with various examples of salt wall dimension and orientation. In an example where a channel encounters such a long perpendicular structure (e.g. an elongated salt wall), it may migrate along the structures and may bend through an exit point to continue transport the sediment downslope.

#### 4.5. Slope gradient profile linked to development of channel-levee systems

Channelized turbidity current may undergo changes in flow parameters (e.g. flow density, thickness and composition) and dynamic control on slope morphology that may be represented in a slope equilibrium diagram (Kneller, 2003; Peakall et al., 2000; Samuel et al., 2003). Erosion is more likely to occur where the slope gradient profile is higher than the base of channel floor and deposition will fill the accommodation, when slope profile is lower than the theoretical equilibrium profile (Fig. 4.11). This concept has been used to analyze channel-levee systems development and particularly to examine relative erosive and the depositional phase of channel evolution (Babonneau et al., 2002; Catterall et al., 2010; McHargue et al., 2011).

Channel-levee systems in the study area show similar characteristic with Niger CLS of Deptuck et al., (2007) where channel is observed to be more erosive and exhibits less sinuosity in steeper gradient and vice-versa. Channel-levee systems locally show more erosive in KM 1-4 and KM 22-26 of CLS A (Avulsed channel) (Fig. 3.16) and in KM12-19 of CLS C (Fig. 3.26). It is inferred that higher efficiency flow may govern the erosive segment within channel development (Kneller, 2003).



**Fig. 4.11.** Equilibrium profile (Samuel et al., 2003)

The whole system of CLS B profile provides an example that is closely related to the ideal equilibrium profile proposed by Samuel et al. (2003) (Fig. 3.21). In KM 17-22, as CLS B exits the equilibrium point that marks a transition from overall erosion to deposition, CLS B starts to meander in order to progressively readjust its profile (Fig. 3.21). This implies a change in flow properties from higher to lower efficiency flow (Kneller, 2003). CLS B tends to preserve the equilibrium profile by rapidly developing its meander pattern when it experiences a change in slope gradient and accommodation space (Flood and Damuth, 1987; Peakall et al., 2000).



## 5. CONCLUSION

Salt-related slope setting and their associated structures have significantly contributed to the morphology variations of submarine channel-levee systems and the stratal stacking patterns of seismic units from the Pleistocene to present-day in the western Nile Deep Sea Fan (NDSF).

The following conclusions can be drawn:

- Five seismic facies (SF) have been observed based on seismic reflection characters: channel and channel-fills deposits (SF1a and 1b); levee deposits (SF2); mass transport deposits (SF3); fan-lobe deposits (SF4); and mud diapirs (SF5).
- Five seismic units (SU) have been distinguished within the studied interval: transparent debris flow (TDF) (SU1); buried mass transport deposit (BMTD) (SU2); channelized-fan deposits (SU3); present-day channel-levee system and near-seabed mass transport deposit (NSMTD) (SU4); and mud diapirs (SU5).
- Seismic stratigraphy interpretation has successfully revealed the spatial and temporal development of three main development phases in the study area. The first phase during the early Pleistocene is characterized by deposition of SU1 and SU2 which are the transparent debris flow and buried-MTD respectively. They filled available accommodation space during this interval following the growth of the main fault, the early development of the minibasin, and the northern depocenter. The second phase is marked by the deposition of channelized-fan deposit (SU3). The third phase is characterized by the development of the near-seabed MTD and the present-day channel-levee system (SU4) and the significant growth of mud diapirs (SU5). The near-seabed MTD shows a particular depositional trend towards the north east suggesting a local submarine gravity-failure development. The present-day channel-levee system development following regional slope marked the end of succession in the study area.
- Three submarine channel-levee systems in the study area have been successfully quantified by direct interpretation in high resolution 3D seismic data combined with spectrally decomposed seismic visualization. Channel-levee system development is related to slope equilibrium profile suggesting overall erosion in the upper slope and deposition in the lower slope. Increases in sinuosity, which in turn resulted in channel aggradation, are related to decreases in channel axis gradient. Sinuous channel is successfully characterized in terms of their development. Significant accretion packages are observed in association with lateral and vertical channel migration.

- Levee development shows an overall decrease in thickness and width downslope. This element exhibits architectural variation that response to local structural changes (e.g the main fault). Channel avulsion is thought to be correlated with flow energy and slope setting and commonly observed as an effective straight channel flowing through a steep gradient.
- Pre-existing slope bathymetry is observed to have a strong impact on morphology variation along channel-levee systems. Faults and anticlines are observed to impact the channel-levee system deposition. The erosive ability of flow and the rate of structural growth influence the preferential deposition of subsequent channel path.
- This study of the near-seafloor turbiditic system is useful to predict the same deposit in the reservoir level with commonly lower seismic resolution. Thus, it provides analogues to describe turbiditic reservoir architecture and understand its distribution. Finally, this study improves the understanding of tectonostratigraphy in the western NDSF and contributes to further hydrocarbon exploration in the region.

## REFERENCES

- Aal, A.A., El Barkooky, A., Gerrits, M., Meyer, H., Schwander, M. and Zaki, H., 2000. Tectonic evolution of the Eastern Mediterranean Basin and its significance for hydrocarbon prospectivity in the ultradeepwater of the Nile Delta. *The Leading Edge*, 19(10): 1086-1102.
- Abreu, V., Sullivan, M., Pirmez, C. and Mohrig, D., 2003. Lateral accretion packages (LAPs): an important reservoir element in deep water sinuous channels. *Marine and Petroleum Geology*, 20(6): 631-648.
- Anderson, R.N., Boulanger, A. and Initiative, L.E., 2009. Prospectivity of the Ultra-Deepwater Gulf of Mexico. Lean Energy initiative, Lamont-Doherty Earth Observatory, Columbia University–Palisades, New York, 10964.
- Babonneau, N., Savoye, B., Cremer, M. and Klein, B., 2002. Morphology and architecture of the present canyon and channel system of the Zaire deep-sea fan. *Marine and Petroleum Geology*, 19(4): 445-467.
- Boucher, P.J., Dolson, J.C., Siok, J. and Heppard, P.D., 2004. Key Challenges to Realizing Full Potential in an Emerging Giant Gas Province: Nile Delta/Mediterranean Offshore, Deep Water, Egypt.
- Bouma, A.H., Kuenen, P.H. and Shepard, F.P., 1962. Sedimentology of some flysch deposits: a graphic approach to facies interpretation, 168. Elsevier Amsterdam.
- Brun, J.P. and Fort, X., 2011. Salt tectonics at passive margins: Geology versus models. *Marine and Petroleum Geology*, 28(6): 1123-1145.
- Camerlenghi, A., Cita, M., Hieke, W. and Ricchiuto, T., 1992. Geological evidence for mud diapirism on the Mediterranean Ridge accretionary complex. *Earth and Planetary Science Letters*, 109(3): 493-504.
- Catterall, V., Redfern, J., Gawthorpe, R., Hansen, D. and Thomas, M., 2010. Architectural style and quantification of a submarine channel–levee system located in a structurally complex area: offshore Nile Delta. *Journal of Sedimentary Research*, 80(11): 991-1017.
- Chakraborty, A. and Okaya, D., 1995. Frequency-time decomposition of seismic data using wavelet-based methods. *Geophysics*, 60(6): 1906-1916.
- Clark, I.R. and Cartwright, J.A., 2009. Interactions between submarine channel systems and deformation in deepwater fold belts: Examples from the Levant Basin, Eastern Mediterranean sea. *Marine and Petroleum Geology*, 26(8): 1465-1482.
- Clark, I.R. and Cartwright, J.A., 2011. Key controls on submarine channel development in structurally active settings. *Marine and Petroleum Geology*, 28(7): 1333-1349.
- Cross, N.E., Cunningham, A., Cook, R.J., Taha, A., Esmaie, E. and El Swidan, N., 2009. Three-dimensional seismic geomorphology of a deep-water slope-channel system: The Sequoia field, offshore west Nile Delta, Egypt. *AAPG bulletin*, 93(8): 1063-1086.
- Damuth, J.E. and Flood, R.D., 1983. Morphology, sedimentation processes, and growth pattern of the Amazon deep-sea fan. *Geo-Marine Letters*, 3(2): 109-117.
- De Ruig, M.J. and Hubbard, S.M., 2006. Seismic facies and reservoir characteristics of a deep-marine channel belt in the Molasse foreland basin, Puchkirchen Formation, Austria. *AAPG bulletin*, 90(5): 735-752.
- Deptuck, M.E., Steffens, G.S., Barton, M. and Pirmez, C., 2003. Architecture and evolution of upper fan channel-belts on the Niger Delta slope and in the Arabian Sea. *Marine and Petroleum Geology*, 20(6): 649-676.
- Deptuck, M.E., Sylvester, Z., Pirmez, C. and O'Byrne, C., 2007. Migration–aggradation history and 3-D seismic geomorphology of submarine channels in the Pleistocene Benin-major Canyon, western Niger Delta slope. *Marine and Petroleum Geology*, 24(6): 406-433.
- Dewey, F., van der Meulen, M. and Whitfield, P., 2006. Using dual-azimuth data to image below salt domes. first break: 55.
- Dolson, J., Boucher, P., Siok, J. and Heppard, P., 2005. Key challenges to realizing full potential in an emerging giant gas province: Nile Delta/Mediterranean offshore, deep water, Egypt,

- Geological Society, London, Petroleum Geology Conference series. Geological Society of London, pp. 607-624.
- Ducassou, E., Migeon, S., Mulder, T., Murat, A., Capotondi, L., Bernasconi, S.M. and Mascle, J., 2009. Evolution of the Nile deep-sea turbidite system during the Late Quaternary: influence of climate change on fan sedimentation. *Sedimentology*, 56(7): 2061-2090.
- Feseker, T., Brown, K.R., Blanchet, C., Scholz, F., Nuzzo, M., Reitz, A., Schmidt, M. and Hensen, C., 2010. Active mud volcanoes on the upper slope of the western Nile deep-sea fan—first results from the P362/2 cruise of R/V Poseidon. *Geo-Marine Letters*, 30(3): 169-186.
- Flood, R.D. and Damuth, J.E., 1987. Quantitative characteristics of sinuous distributary channels on the Amazon deep-sea fan. *Geological Society of America Bulletin*, 98(6): 728-738.
- Fort, X., Brun, J.P. and Chauvel, F., 2004. Salt tectonics on the Angolan margin, synsedimentary deformation processes. *AAPG bulletin*, 88(11): 1523-1544.
- Garcia, S.F.M., Letouzey, J., Rudkiewicz, J.L., Danderfer Filho, A. and Frizon de Lamotte, D., 2012. Structural modeling based on sequential restoration of gravitational salt deformation in the Santos Basin (Brazil). *Marine and Petroleum Geology*.
- Gardner, M.H., Borer, J.M., Melick, J.J., Mavilla, N., Dechesne, M. and Wagerle, R.N., 2003. Stratigraphic process-response model for submarine channels and related features from studies of Permian Brushy Canyon outcrops, West Texas. *Marine and Petroleum Geology*, 20(6): 757-787.
- Garziglia, S., Migeon, S., Ducassou, E., Loncke, L. and Mascle, J., 2008. Mass-transport deposits on the Rosetta province (NW Nile deep-sea turbidite system, Egyptian margin): Characteristics, distribution, and potential causal processes. *Marine Geology*, 250(3): 180-198.
- Gee, M. and Gawthorpe, R., 2006. Submarine channels controlled by salt tectonics: Examples from 3D seismic data offshore Angola. *Marine and Petroleum Geology*, 23(4): 443-458.
- Gee, M., Gawthorpe, R., Bakke, K. and Friedmann, S., 2007. Seismic geomorphology and evolution of submarine channels from the Angolan continental margin. *Journal of Sedimentary Research*, 77(5): 433-446.
- Gemmer, L., Beaumont, C. and Ings, S.J., 2005. Dynamic modelling of passive margin salt tectonics: effects of water loading, sediment properties and sedimentation patterns. *Basin Research*, 17(3): 383-402.
- Gomes, P.O., Kilsdonk, B., Minken, J., Grow, T. and Barragan, R., 2009. The outer high of the Santos Basin, Southern São Paulo Plateau, Brazil: pre-salt exploration outbreak, paleogeographic setting, and evolution of the syn-rift structures. *American Association of Petroleum Geologists Search and Discovery Article*, 10193.
- Henderson, J., Purves, S.J., Fisher, G. and Leppard, C., 2008. Delineation of geological elements from RGB color blending of seismic attribute volumes. *The Leading Edge*, 27(3): 342-350.
- Hsü, K., Ryan, W. and Cita, M., 1973. Late Miocene desiccation of the Mediterranean. *Nature*, 242(5395): 240-244.
- Huang, Y., Lin, D., Bai, B., Roby, S. and Ricardez, C., 2010. Challenges in presalt depth imaging of the deepwater Santos Basin, Brazil. *The Leading Edge*, 29(7): 820-825.
- Hudec, M.R. and Jackson, M., 2007. Terra infirma: Understanding salt tectonics. *Earth-Science Reviews*, 82(1): 1-28.
- Janocko, M., Nemec, W., Henriksen, S. and Warchoř, M., 2012. The diversity of deep-water sinuous channel belts and slope valley-fill complexes. *Marine and Petroleum Geology*.
- Kane, I.A., Catterall, V., McCaffrey, W.D. and Martinsen, O.J., 2010. Submarine channel response to intrabasinal tectonics: The influence of lateral tilt. *AAPG bulletin*, 94(2): 189-219.
- Kane, I.A. and Hodgson, D.M., 2011. Sedimentological criteria to differentiate submarine channel levee subenvironments: exhumed examples from the Rosario Fm.(Upper Cretaceous) of Baja California, Mexico, and the Fort Brown Fm.(Permian), Karoo Basin, S. Africa. *Marine and Petroleum Geology*, 28(3): 807-823.



- Kane, I.A., Kneller, B.C., Dykstra, M., Kassem, A. and McCaffrey, W.D., 2007. Anatomy of a submarine channel–levee: An example from Upper Cretaceous slope sediments, Rosario Formation, Baja California, Mexico. *Marine and Petroleum Geology*, 24(6): 540-563.
- Kane, I.A., McCaffrey, W.D. and Peakall, J., 2008. Controls on sinuosity evolution within submarine channels. *Geology*, 36(4): 287-290.
- Kellner, A., El Khawaga, H., Brink, G., Brink-Larsen, S., Hesham, M., El Saad, H.A., Atef, A., Young, H. and Finlayson, B., 2009. Depositional History of the West Nile Delta–Upper Oligocene to Upper Pliocene. *American Association of Petroleum Geologists Search and Discovery Article*, 30092.
- Kneller, B., 2003. The influence of flow parameters on turbidite slope channel architecture. *Marine and Petroleum Geology*, 20(6): 901-910.
- Kneller, B.C. and Branney, M.J., 1995. Sustained high-density turbidity currents and the deposition of thick massive sands. *Sedimentology*, 42(4): 607-616.
- Kolla, V., Posamentier, H. and Wood, L., 2007. Deep-water and fluvial sinuous channels—Characteristics, similarities and dissimilarities, and modes of formation. *Marine and Petroleum Geology*, 24(6): 388-405.
- Kopf, A.J., 2002. Significance of mud volcanism. *Reviews of Geophysics*, 40(2): 2-1-2-52.
- Leeder, M.R., 2011. Tectonic sedimentology: sediment systems deciphering global to local tectonics. *Sedimentology*, 58(1): 2-56.
- Limonov, A., Woodside, J., Cita, M. and Ivanov, M., 1996. The Mediterranean Ridge and related mud diapirism: a background. *Marine Geology*, 132(1): 7-19.
- Loncke, L., Gaullier, V., Droz, L., Ducassou, E., Migeon, S. and Mascle, J., 2009. Multi-scale slope instabilities along the Nile deep-sea fan, Egyptian margin: A general overview. *Marine and Petroleum Geology*, 26(5): 633-646.
- Loncke, L., Gaullier, V., Mascle, J., Vendeville, B. and Camera, L., 2006. The Nile deep-sea fan: an example of interacting sedimentation, salt tectonics, and inherited subsalt paleotopographic features. *Marine and Petroleum Geology*, 23(3): 297-315.
- Loncke, L., Mascle, J. and Parties, F.S., 2004. Mud volcanoes, gas chimneys, pockmarks and mounds in the Nile deep-sea fan (Eastern Mediterranean): geophysical evidences. *Marine and Petroleum Geology*, 21(6): 669-689.
- Lopez, M., 2001. Architecture and depositional pattern of the Quaternary deep-sea fan of the Amazon. *Marine and Petroleum Geology*, 18(4): 479-486.
- Malaguti, R., Allen, M., Litvin, A. and Gregory, C., 2001. Sub-salt imaging using 3D pre-stack depth migration in the UK Southern North Sea—a case history. *First Break*, 19(5): 253-258.
- Mascle, J., Benkheilil, J., Bellaiche, G., Zitter, T., Woodside, J. and Loncke, L., 2000. Marine geologic evidence for a Levantine-Sinai plate, a new piece of the Mediterranean puzzle. *Geology*, 28(9): 779-782.
- Mayall, M., Jones, E. and Casey, M., 2006. Turbidite channel reservoirs—Key elements in facies prediction and effective development. *Marine and Petroleum Geology*, 23(8): 821-841.
- Mayall, M., Lonergan, L., Bowman, A., James, S., Mills, K., Primmer, T., Pope, D., Rogers, L. and Skeene, R., 2010. The response of turbidite slope channels to growth-induced seabed topography. *AAPG bulletin*, 94(7): 1011-1030.
- McArdle, N. and Ackers, M., 2012. Understanding seismic thin-bed responses using frequency decomposition and RGB blending. *first break*, 30.
- McHargue, T., Pyrcz, M.J., Sullivan, M.D., Clark, J., Fildani, A., Romans, B., Covault, J., Levy, M., Posamentier, H. and Drinkwater, N., 2011. Architecture of turbidite channel systems on the continental slope: patterns and predictions. *Marine and Petroleum Geology*, 28(3): 728-743.
- Migeon, S., Ducassou, E., Le Gonidec, Y., Rouillard, P., Mascle, J. and Revel-Rolland, M., 2010. Lobe construction and sand/mud segregation by turbidity currents and debris flows on the western Nile deep-sea fan (Eastern Mediterranean). *Sedimentary Geology*, 229(3): 124-143.
- Milkov, A., 2000. Worldwide distribution of submarine mud volcanoes and associated gas hydrates. *Marine Geology*, 167(1): 29-42.

- Nemec, W., and Steel, R.J. (1984). Alluvial and coastal conglomerates: their significant features and some comments on gravelly mass-flow deposits. *Canadian Society of Petroleum Geologists Memoir* 10, pp. 1-31.
- Normark, W.R., Posamentier, H. and Mutti, E., 1993. Turbidite systems: state of the art and future directions. *Reviews of Geophysics*, 31(2): 91-116.
- Partyka, G., Gridley, J. and Lopez, J., 1999. Interpretational applications of spectral decomposition in reservoir characterization. *The Leading Edge*, 18(3): 353-360.
- Peakall, J., McCaffrey, B. and Kneller, B., 2000. A process model for the evolution, morphology, and architecture of sinuous submarine channels. *Journal of Sedimentary Research*, 70(3): 434-448.
- Penge, J., Taylor, B., Huckerby, J. and Munns, J., 1993. Extension and salt tectonics in the East Central Graben, Geological Society, London, *Petroleum Geology Conference series*. Geological Society of London, pp. 1197-1209.
- Pettingill, H.S. and Weimer, P., 2002. Worldwide deepwater exploration and production Past, present, and future. *The Leading Edge*, 21(4): 371-376.
- Pickering, K., Coleman, J., Cremer, M., Droz, L., Kohl, B., Normark, W., O'Connell, S., Stow, D. and Meyer-Wright, A., 1986. A high sinuosity, laterally migrating submarine fan channel-levee-overbank: results from DSDP Leg 96 on the Mississippi Fan, Gulf of Mexico. *Marine and petroleum geology*, 3(1): 3-18.
- Pirmez, C., 1994. Growth of a submarine meandering channel-levee system on the Amazon Fan, Columbia University New York,, USA.
- Pirmez, C., Hiscott, R.N. and Kronen, J., 1997. Sandy turbidite successions at the base of channel-levee systems of the Amazon Fan revealed by FMS logs and cores: unraveling the facies architecture of large submarine fans, *Proceedings of the Ocean Drilling Program. Scientific results*. Ocean Drilling Program, pp. 7-33.
- Posamentier, H., Davies, R., Cartwright, J. and Wood, L., 2007. Seismic geomorphology-an overview. *SPECIAL PUBLICATION-GEOLOGICAL SOCIETY OF LONDON*, 277: 1.
- Posamentier, H.W., 2003. Depositional elements associated with a basin floor channel-levee system: case study from the Gulf of Mexico. *Marine and Petroleum Geology*, 20(6): 677-690.
- Posamentier, H.W. and Kolla, V., 2003. Seismic geomorphology and stratigraphy of depositional elements in deep-water settings. *Journal of Sedimentary Research*, 73(3): 367-388.
- Prather, B.E., 2003. Controls on reservoir distribution, architecture and stratigraphic trapping in slope settings. *Marine and Petroleum Geology*, 20(6): 529-545.
- Rowan, M.G., Peel, F.J., Vendeville, B.C. and Gaullier, V., 2012. Salt tectonics at passive margins: Geology versus models—Discussion. *Marine and Petroleum Geology*.
- Ryan, W.B.F., 1978. Messinian badlands on the southeastern margin of the Mediterranean Sea. *Marine Geology*, 27(3): 349-363.
- Samuel, A., Kneller, B., Raslan, S., Sharp, A. and Parsons, C., 2003. Prolific deep-marine slope channels of the Nile Delta, Egypt. *AAPG bulletin*, 87(4): 541-560.
- Sestini, G., 1989. Nile Delta: a review of depositional environments and geological history. Geological Society, London, *Special Publications*, 41(1): 99-127.
- Steffens, G., Shipp, R., Prather, B., Nott, J., Gibson, J. and Winker, C., 2004. The use of near-seafloor 3D seismic data in deepwater exploration and production. Geological Society, London, *Memoirs*, 29(1): 35-43.
- Stow, D.A.V. and Mayall, M., 2000. Deep-water sedimentary systems: New models for the 21st century. *Marine and Petroleum Geology*, 17(2): 125-135.
- Talbot, C., 1993. Spreading of salt structures in the Gulf of Mexico. *Tectonophysics*, 228(3): 151-166.
- Tari, G., Belopolsky, A. and Peace, D., 2012a. Introduction to this special section: The Mediterranean region. *The Leading Edge*, 31(7): 766-767.
- Tari, G., Hussein, H., Novotny, B., Hannke, K. and Kohazy, R., 2012b. Play types of the deep-water Matruh and Herodotus basins, NW Egypt. *Petroleum Geoscience*, 18(4): 443-455.

- Vendeville, B.C., 2005. Salt tectonics driven by sediment progradation: Part I—Mechanics and kinematics. AAPG bulletin, 89(8): 1071-1079.
- Wood, L.J. and Mize-Spansky, K.L., 2009. Quantitative seismic geomorphology of a Quaternary leveed-channel system, offshore eastern Trinidad and Tobago, northeastern South America. AAPG Bulletin, 93(1): 101-125.
- Wu, S., Bally, A.W. and Cramez, C., 1990. Allochthonous salt, structure and stratigraphy of the north-eastern Gulf of Mexico. Part II: Structure. Marine and Petroleum Geology, 7(4): 334-370.
- Wynn, R.B., Cronin, B.T. and Peakall, J., 2007. Sinuous deep-water channels: Genesis, geometry and architecture. Marine and Petroleum Geology, 24(6): 341-387.
- Zitter, T., Huguen, C. and Woodside, J., 2005. Geology of mud volcanoes in the eastern Mediterranean from combined sidescan sonar and submersible surveys. Deep Sea Research Part I: Oceanographic Research Papers, 52(3): 457-475.